

**THE APPLICATION OF ADVANCED COMPUTER MODELS  
TO THE PREDICTION OF SOUND IN ENCLOSED SPACES**

by

Mark John Howarth

This thesis was submitted for the degree of Doctor of Philosophy in the  
Department of Acoustics and Audio Engineering at the University of Salford.

1998

# Contents

1. Introduction . . . . .	- 1 -
2. Background . . . . .	-3-
2.1 Geometrical room acoustics . . . . .	-3-
2.2 Room acoustic computer modelling . . . . .	-4-
2.3 The importance of diffuse reflections . . . . .	-8-
2.4 Computer modelling of diffuse reflections . . . . .	-10-
2.5 Assessment of predictive accuracy . . . . .	-15-
3. Field Measurements . . . . .	-17-
3.1 Description of enclosures . . . . .	-17-
3.2 Measurement procedure . . . . .	-37-
4. The Conventional Hybrid Model . . . . .	-43-
4.1 Description of the computer model . . . . .	-43-
4.2 Accuracy of input data . . . . .	-44-
4.3 Modelling of early reflections . . . . .	-47-
5. Performance of the Hybrid Model . . . . .	-49-
5.1 Assessment of model performance . . . . .	-49-
5.2 Overall prediction of room acoustic parameters . . . . .	-50-
5.3 A more detailed view of predictive accuracy . . . . .	-61-
5.4 Summary of comparisons . . . . .	-83-
6. Development of a New Calculation Procedure . . . . .	-87-
6.1 Specification for a suitable algorithm . . . . .	-87-
6.2 The new 'Hybrid-Markov' model . . . . .	-88-
7. Performance of the Hybrid-Markov Model . . . . .	-95-
7.1 Program operation . . . . .	-95-

7.2 Overview of predictive accuracy .....	-96-
7.3 Were problems encountered with the hybrid method solved? .....	-102-
7.4 Summary of Hybrid-Markov performance .....	-110-
8. Conclusions .....	-112-
9. Further Work .....	-115-
References .....	-117-
Appendix A: Common acoustic parameters for rooms .....	-122-
Appendix B: Hybrid-Markov program listing .....	-125-

# Glossary of symbols

$\star$	Convolution
$\alpha$	Absorption coefficient
$\delta$	Diffusion coefficient
$\delta(s)$	Dirac delta function
$\epsilon_N$	Total energy at step $N$
$\Omega_i$	Solid angle subtended from surface $i$ to receiver
$\Omega_{ik}$	Solid angle subtended from surface $k$ to centre of surface $i$
$\theta_i$	Angle of incident sound ray from surface normal vector
$\theta_r$	Angle of reflected sound ray from surface normal vector
$\theta_{im}$	Angle subtended from element $m$ on surface $i$ to receiver (from surface normal)
$A$	Diagonal matrix of surface reflection coefficients
$A_i$	Area of surface $i$
$A_{im}$	Area of element $m$ on surface $i$
$dS$	Elemental area of a surface
$D^{(N)}$	Vector of diffuse energy from ray tracing on all surfaces at $t = N \bar{t}$
$D_i^{(N)}$	Diffuse energy from ray tracing on surface $i$ at $t = N \bar{t}$
$e^{(N)}$	Vector of energy on all surfaces at $t = N \bar{t}$
$e_i^{(N)}$	Energy on surface $i$ at $t = N \bar{t}$
$E_i$	Individual ray energy incident on surface $i$
$E_{it}$	Energy on surface $i$ at time $t$
$h(s)$	Linear system impulse response
$I_i$	Intensity incident on a surface
$I(r)$	Reflected intensity at distance $r$ from a reflecting surface
$m$	Number of elements on surface
$n$	Number of surfaces in a model
$N$	Markov-chain step number
$N_i$	Number of rays emitted from surface $i$
$N_k$	Number of rays hitting surface $k$
$p_{ik}$	Radiant-exchange transition probability

$P$	Matrix of transition probabilities
$r$	Distance from a reflecting surface
$r_{im}$	Distance from element $m$ on surface $i$ to receiver
$R_{xy}(s)$	Cross-correlation of linear system input and output
$R_{xx}(s)$	Auto-correlation of linear system input
$t$	Time
$\bar{t}$	Markov-chain time step length
$x(s)$	Linear system input
$y(s)$	Linear system output

# Abstract

Computer modelling of acoustics in enclosures has developed into various forms, none of which have yet demonstrated 100% accuracy. This thesis therefore details a study of room acoustic computer modelling. It highlights weaknesses with existing modelling techniques and describes the development and subsequent verification of an improved modelling technique.

The study discovers that for accurate prediction of many common room acoustic parameters diffuse reflections should be accounted for in the modelling of all reflection orders. However, many of the problems encountered in existing techniques are found to be caused by the way these diffuse reflections are modelled.

An improved modelling technique, referred to as a 'Hybrid-Markov' method, is proposed and developed that combines a conventional hybrid method with a radiant-exchange process to model diffuse reflections. Initial verification of the new modelling technique results in similar overall accuracies to existing modelling techniques but solves many of the specific problems discovered. It therefore provides a flexible and robust framework for the future development of computer prediction of sound in enclosed spaces.

# Chapter 1

## Introduction

Since the first computer models of room acoustics of forty years ago<sup>1</sup>, modelling techniques have evolved to a stage where they are currently used by some acousticians as a tool in the design of auditoria. Computer models have an advantage over other design methods in that they are cost effective since they allow the designer considerable flexibility in the design process, where changes in materials or geometry can be tried and tested relatively quickly compared with, for instance, scale modelling techniques. Many modern programs also use their calculations as part of an 'auralization' process to enable listeners to hear simulated room responses. However, despite the increasing complexity of computer models they are still not an 'indispensable tool' for the acoustician. One of the reasons for this is their questionable accuracy.

This was illustrated by a 1995 round-robin survey by Vorländer<sup>2</sup>, in which fourteen computer simulation programs were used to predict several acoustic parameters in a room. Program users were firstly given technical drawings detailing geometrical information along with qualitative descriptions of the materials within the room. Secondary tests were also carried out using identical absorption coefficients in each of the models. The predictions were then compared to measured values from the enclosure

in the 1 kHz octave band. The study concluded that only three of the fourteen computer models produced 'unquestionably reliable predictions'. These three models, however, still produced errors greater than difference limens in at least 50 % of predictions.

To exploit fully the potential advantages of computer modelling in the design of enclosures, the accuracy of predictions therefore needs to be improved. This study addresses this need.

The key objectives of this study are therefore to

- highlight weaknesses with current modelling techniques
- to develop an improved modelling technique.

The investigation methodology is as follows

- a. A literature survey provides information on current computer modelling techniques used and their associated advantages and possible weaknesses
- b. Common room acoustic parameters specified in ISO 3382<sup>3</sup> are measured in eight real enclosures
- c. Predictions of these acoustic parameters in the eight enclosures are made using a computer model, identified in Vorländer's survey as reliable, and are compared with values measured in actual enclosures
- d. Reasons for weaknesses in these predictions are hypothesized and areas for refinement are suggested
- e. A new model is developed and its results are compared to actual measurements and previous predictions.

## Chapter 2

# Background

### 2.1 Geometrical room acoustics

Geometrical modelling of sound propagation is governed by Fermat's principle<sup>4</sup>, which states that every wave propagates from the source to the receiver by way of the fastest path. In the case of room acoustics, sound propagates through air that can be considered as an isotropic, homogeneous medium at rest and the speed of sound can be regarded as constant. This means that sound propagates from the source to the receiver by way of the shortest path; that is, in a straight line or 'ray'<sup>5</sup>.

Geometrical modelling therefore gives us the concept of sound rays, where energy from a sound source is divided into energy packets that propagate in straight lines away from the source. This is directly analogous to the concept of light rays in optics but has important differences which are discussed below. The analogy with light rays is useful since it gives us a way of visualizing reflection, diffraction and refraction of sound rays.

Reflections occur in every enclosed space since at some point a ray will meet a surface where it will at least partially be reflected. Geometric modelling of a reflection assumes

the surface is perfectly smooth and has dimensions far greater than the wavelength of the incident sound. In optics, where wavelengths of visible light range from 0.3 to 0.8  $\mu\text{m}$ , this is always the case but in acoustics wavelengths of audible sound be as long as 17 m, which few surfaces will reflect specularly.

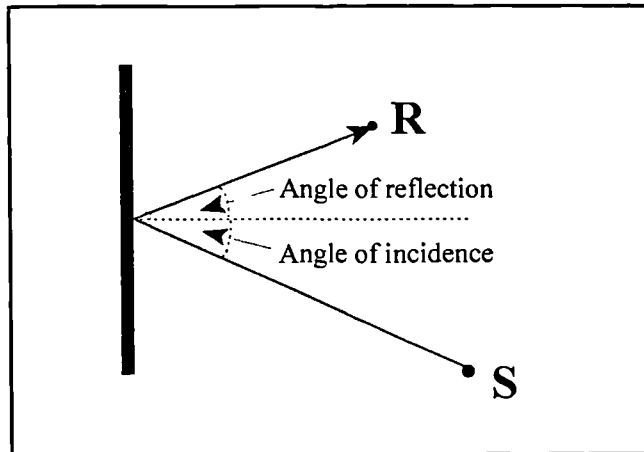


Figure 2.1 Specular reflection from a smooth surface

Where geometric assumptions are not satisfied, diffuse or partially diffuse reflections may occur; these are discussed in section 2.3. Fermat's principle tells us that a ray propagating from a source and reflecting from a surface to a receiver will travel by the quickest route or, since the speed of sound can be taken as constant, by the shortest path. The reflection point is therefore such that the angle of reflection is equal to the angle of incidence. This is referred to as specular reflection and is illustrated in figure 2.1, where sound from source 'S' is reflected from a surface and received at point 'R'.

## 2.2 Room acoustic computer modelling

### 2.2.1 Image-source method

The idea of using image sources to model sound reflections in enclosures was taken from optics, where, just as a plane mirror produces an image of a source of light, a reflecting surface - with dimensions considerable larger than the wavelength of reflecting sound - will produce an image of a source of sound. This essentially means, for calculation purposes, reflecting surfaces can be replaced by image sources. Eyring used this concept in the development of his reverberation time formula in 1930<sup>6</sup> and it was widely known as a technique for calculating reflections in enclosures prior to the advent of computer modelling<sup>7,8,9</sup>. As shown in figure 2.2, the method models reflections by creating image sources on the opposite side of reflecting surfaces. The strength of these image sources is determined by their distance from the initial source and the absorption coefficients of the surfaces concerned. Reflecting surfaces are then effectively considered transparent

and the image sources emit sound directly through them to the receiver.

A computer implementation of the technique was written by Gibbs and Jones<sup>10</sup> to calculate sound pressure levels within enclosures and the method was used to calculate 'echograms' by Santon<sup>11</sup> and predict

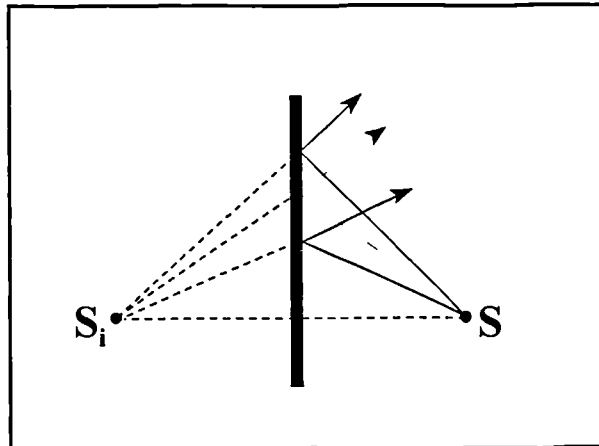


Figure 2.2 Construction of image source,  $S_i$

reverberation times by Allen and Berkley<sup>12</sup>. In 1982, Borish further refined the technique to allow the method to be used for more complex enclosures but noted that the number of image sources required increased exponentially with the desired length of decay<sup>13</sup>. The complexity of models was consequently limited by computation time. Lee and Lee<sup>14</sup> attempted to reduce calculation times by using a coordinate transformation method to eliminate non-visible image sources and therefore reduce the number of image calculations required. Their method also made more efficient use of computer memory, which meant more complex models could be modelled on computers with restrictive memory limitations.

One of the key advantages of the image-source method is that all possible reflection paths are found between source and receiver, which leads to a high time resolution of reflections. While one of its disadvantages is the required long computation time when high-order image sources are desired. Kristiansen, Krokstadt and Follestad<sup>15</sup> therefore developed a method of extrapolating low-order reflections to calculate high-order reflections as a way of speeding up the calculation process.

### 2.2.2 Ray-tracing method

The term 'ray tracing' is used here to represent all energy-particle tracing methods, where energy-particles can be represented by rays, beams, cones or pyramids. The method was first programmed for the modelling of room acoustics in 1958 by Allred and Newhouse<sup>1</sup> and developed by Krokstadt, Strøm and Sørdsdal<sup>16</sup> in 1967. As with the

image-source method, it is based on geometrical acoustics.

In the ray tracing method, energy-particles are emitted from a source and reflected around a modelled enclosure. At each reflection, energy is taken from the particle according to the value of the reflecting surface's absorption coefficient. Particles are then 'collected' at a receiver position where their strengths and arrival times give an approximation of an energy decay after a sound source is switched off.

Ray tracing is more commonly used for modelling room acoustics than the image-source method because it is easier to program<sup>13</sup>, particularly for more complicated enclosure shapes. Its computation time also increases proportionally with the number of reflections modelled<sup>17</sup>, whereas with the image-source method, the computation time increases exponentially with the number of reflections<sup>13</sup>, which means more complex enclosures and longer decay times can be more easily modelled.

A further advantage of the ray-tracing method is that it can take non-specular effects into account. Several authors have therefore modified the method to account for non-specular reflections, these are discussed in section 2.4.

Despite its advantages, the ray-tracing method has two important causes of errors that have been investigated in some depth by Lehnert<sup>18</sup>. These are that there is a limit on the spatial resolution of rays due to computation time limitations and that errors are encountered by the detection of rays because detectors have to have finite dimensions. In 1983, Krokstad, Strøm and Sørsdal gave guidance on the density of rays required for suitable predictions<sup>19</sup>. They noted that with rays emitted every 2° the distance between rays after 100 ms will be 1.18 m, they therefore recommend matching of the number of rays to the dimensions of the enclosure and the surfaces within it.

### 2.2.3 Hybrid models

The term 'hybrid' is used to describe modelling techniques that use a combination of ray tracing and the image-source method. They achieve this by using a ray-tracing algorithm to 'find' image sources, which are then used, as with the conventional image-source method, to radiate directly to the receiver. The problem, in conventional ray tracing, of determining an optimum 'ray-detector' size can therefore be avoided and the locations of image sources can be calculated with greater ease for more complicated enclosures than with the conventional image-source method.

A cone-tracing technique by Maercke and Martin<sup>20,21</sup> used this concept to model early order reflections but because of computer memory limitations, higher order reflections were calculated with a conventional beam tracing algorithm. Their method used cones traced from image sources to determine whether image sources were valid. This eliminated the need to use finite-sized detectors around receivers.

Vorländer<sup>17</sup> developed a technique to calculate complete energy decays by using rays rather than cones to determine image-source locations. This method used ray tracing to determine the visibilities of image-sources and therefore retained the concept of ray detectors around receivers. The errors caused by this were neglected for reductions in computation time.

Naylor<sup>22</sup> used a similar method to Vorländer but only for early order reflections. For later orders diffuse secondary sources, located on surfaces, were used to reduce computation times. Naylor also used rays to determine the visibilities of image sources claiming that the use of cones causes valid images to be disregarded. The use of diffuse secondary sources is discussed further in section 2.4.

## 2.3 The importance of diffuse reflections

A diffuse reflection is one where sound incident on a surface is reflected into a wider solid angle than that of a specular reflection and is therefore not directly accounted for in geometrical modelling of acoustics. This scattering is attributable to wave effects caused by surface roughness, geometry and diffraction.

Diffuse reflections have an important role to play in the acoustics of rooms as they can improve the uniformity of a reverberant field and reduce the risk of areas of poor acoustics within a room<sup>23</sup>. They also create a softer sound<sup>24</sup> and reduce the risk of undesirable echoes by improving the smoothness of the reverberant decay. In a study of surface diffusion by Hodgson<sup>25</sup> it was noted that in rooms with only specularly reflecting surfaces sound decays were non-linear with slopes decreasing with time causing rates of sound decay to be less than that predicted by Eyring's theory, especially in disproportionate rooms. However, in rooms with more diffuse surfaces, sound decays were more linear. Fricke and Haan<sup>26,27</sup> conducted surveys asking musicians and music critics about their preferences for over fifty concert halls and compared these with objective features of the halls. They found that the feature that correlated best with their preferences was the diffusion of interior surfaces. This signifies the importance of accounting for surface diffusion in the design of such enclosures.

Diffuse reflections occur from 'rough' surfaces where the dimensions of the roughness are comparable to the wavelength of the diffused sound. Common sources of diffuse reflections in auditoria are areas of seating, ornamental plasterwork, unfinished brickwork, convex curved surfaces<sup>28</sup> and 'mathematically-designed' diffusors<sup>29,30</sup>.

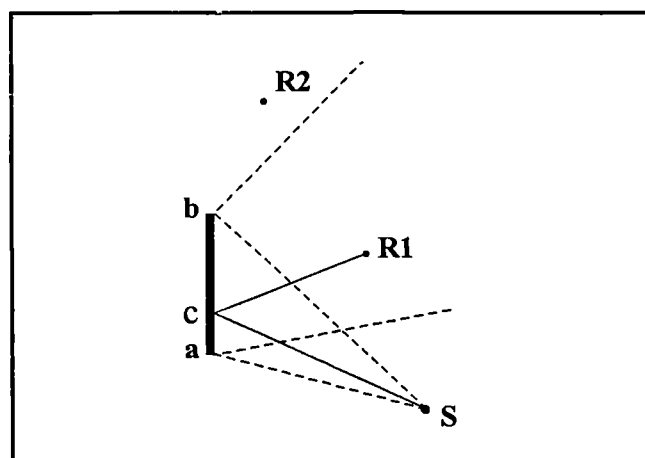


Figure 2.3 Reflections from a smooth surface. S = source, R1,R2 = receivers

One of the effects of diffuse reflections is the spatial spreading of reflected sound energy into non-specular regions. This is best described by considering reflections from a single surface. Figure 2.3 shows a two-dimensional view of rays from a source, S, being reflected

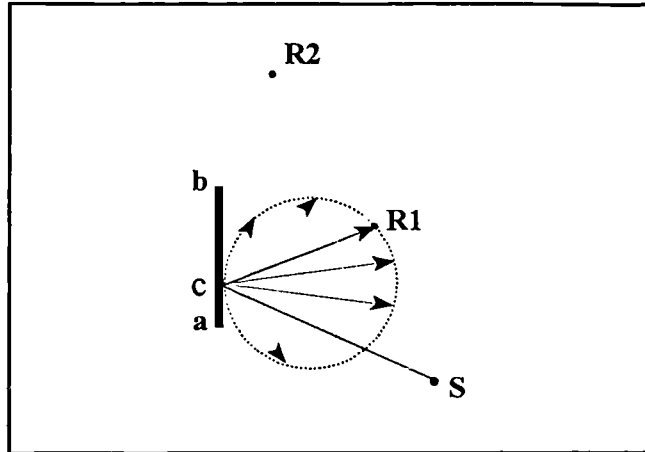


Figure 2.4 Diffuse reflection from a rough surface

specularly from a surface. The region illuminated by these specular reflections is bounded by the paths given by reflections at points a and b. If the source and receivers shown are considered as points, and S radiates to all positions along the reflecting surface, it is clear that only one reflection, at position c, reaches R1. Any receivers outside this illuminated zone, such as R2, receive no energy at all. If this specularly reflecting surface is now replaced by a diffusely reflecting surface, each incident ray, from S, is split by the surface into many weaker rays, reflecting out in a number of directions. Figure 2.4 shows a two-dimensional representation of a completely diffuse reflection from a rough surface. As in optics, this is described by Lambert's cosine law. Let us suppose a group of parallel rays with intensity  $I_i$  strike a surface along a small area  $dS$  at angle  $\theta_i$  from the surface normal, then the reflected intensity  $I(r)$  at angle  $\theta_r$  and distance  $r$  from the surface is given by

$$I(r) = I_i dS \frac{\cos\theta_r \cos\theta_i}{\pi r^2}$$

If the incident angle is constant the received intensity is therefore proportional to the cosine of the reflection angle as represented by the circle in figure 2.4. The surface therefore reflects into all angles in  $2\pi$  space so energy is received at R2. This spatial spreading of energy helps to make the reverberant field more diffuse.

In addition to spatial spreading, amplitude smoothing and temporal smearing makes the

reverberant decay more linear. Energy reflected at position c by the diffusely reflecting surface is still received at R1 but with a lower amplitude than the specularly reflecting surface because incident energy at c is now dispersed in many directions. However, since energy is scattered at all positions along the reflector, energy is now also received at R1 from many other positions at slightly different times. This consequently smooths the reverberant decay at R1 in the time domain.

Diffusers also affect reflections in the frequency domain. With specularly reflecting surfaces reflections can produce a harsh sound equivalent to optical glare<sup>31</sup>. However, with 'fine-scale' diffusers, high frequencies are scattered and decays are smoothed, effectively reducing high-frequency energy from specular reflections. The diffusers therefore act like low-pass filters producing a mellower, softer tone. This is particularly noticeable where few diffusing surfaces are present but becomes less important when diffuse reflections are arriving from many directions<sup>32</sup>.

## **2.4 Computer modelling of diffuse reflections**

In reality very few enclosures have only smooth surfaces that can be modelled specularly. Areas of seating and surfaces that are shaped or textured are common causes of diffuse reflections. It is therefore not surprising to find the need to include the modelling of diffuse reflections for accurate prediction of room acoustic parameters has been recognised by many authors<sup>2,33</sup>. Vorländer noted that the three best programs in his survey all had algorithms that included the modelling of diffuse reflections. An overview of some techniques used to model such reflections is given here.

A 'diffusion coefficient' (sometimes referred to as 'diffusion factor'),  $\delta$ , is often used to describe the fraction of reflected energy diffused by a surface and is therefore defined as the fraction of reflected energy directed non-specularly. If  $\alpha$  is the absorption coefficient of a surface we can say:

$$\text{incident energy} = \text{absorbed energy} + \text{diffused energy} + \text{specular energy}$$

where, incident energy =  $E_i$   
absorbed energy =  $\alpha E_i$   
diffused energy =  $\delta(1 - \alpha) E_i$   
specular energy =  $(1 - \delta)(1 - \alpha) E_i$

With ray-tracing methods, one method of modelling this energy reflected in non-specular directions would be to split rays into many weaker rays at each diffusely reflecting surface<sup>4</sup>. These new weaker rays would then each be traced and split further at each subsequent diffusely reflecting surface. However, this method has been rejected because the exponential increase in rays produced with time would result in long calculation times<sup>34</sup>.

To avoid the exponential increase in rays associated with ray-splitting, Kuttruff and Straßen<sup>35</sup> developed a technique to model diffuse reflections by combining two ray-tracing algorithms: one to model specular reflections and the other to model diffuse reflections. The diffuse reflection algorithm used the diffusion coefficient of a surface to decide whether to re-direct a reflected ray. It worked by assigning a diffusion coefficient between zero (for specular) and one (for completely diffuse) to each room surface. When a ray met that surface a random number between one and zero was generated. This random number was then compared to the surface's diffusion coefficient. If it was greater than the coefficient the ray was reflected specularly. If it was less than the coefficient the ray was either reflected in a random direction or according to a probability function following Lambert's cosine law. This ray was then continued and the procedure was repeated at each subsequent surface creating a stochastic process. Rays were then only registered at the receiver if their last reflection was non-specular. This method is a simple way of reducing the number of rays required but means that the scattering directivity from any diffusely reflecting surface is not defined correctly at any specific moment in time and is only represented when averaged over time. It would be possible to reduce this effect by increasing the number, and hence density, of rays traced but this would extend the required calculation times and counters the reason for the methods use. In addition, to account for frequency dependent scattering, the re-direction ray tracing

algorithm has to be repeated for each frequency band required, which further increases computation time.

Kuttruff and Straßen's re-direction method was developed further by Heinz<sup>36</sup> for auralization purposes. In this method specular reflections were calculated using a high-resolution hybrid method and a low resolution ray tracing was then performed using Kuttruff's method to create a diffuse decay. The specular and diffuse decays were then combined to give an overall energy decay. The calculations required were found to be time consuming so to reduce computation times only early reflection orders were modelled in this manner and the remaining 'reverberant tail' was modelled statistically so its 'gross temporal and spectral behaviour agrees with that of the true decay process'. Heinz indicated that this was only valid for rooms that are 'well-shaped' and that the method should not be considered for flat or long rooms.

In Naylor's method<sup>37</sup> the calculation procedure is divided into two sections. The first calculates early reflections according to geometrical acoustics theory using the conventional hybrid method. The second creates secondary diffuse sources at points where traced rays hit surfaces. These sources then radiate to visible receivers according to Lambert's cosine law (see section 2.3). The two sections are separated by a reflection transition order, so that diffusion is only modelled for reflection orders above this. Naylor developed this approach to predict 'long rich reflection sequences'<sup>22</sup> and considered that the 'pure' hybrid method could not produce these on a personal computer because a finite limit on the number of rays would have to be imposed, which would place an upper limit on the length of an accurate reflectogram obtainable.

Another technique, used by Lam<sup>38</sup>, is to add the diffuse energy from each reflection to a diffuse energy 'pool' and to assume that this decays exponentially according to Sabine's or Eyring's formula. This is simple to implement but partly relies on traditional reverberation time calculations, which for some complicated rooms may be inaccurate. Localised effects within rooms may also be poorly predicted since the diffuse energy is spread evenly throughout the room.

Non-specular reflections were modelled by Gerlach<sup>39</sup> and Kruzins and Fricke<sup>40</sup> by using a radiant-exchange method based on Markov-chain theory. The method was not designed to specifically model diffuse reflections but to predict energy decays in semi-diffuse spaces. In this method energy is distributed from one surface to another at discrete intervals according to a transition probability. Each probability is calculated by dividing the visible solid angle projected onto a receiving surface by the total solid angle visible from the 'emitting' surface. This technique allows the shape of the room and the location of surfaces to influence the diffuse decay at a receiver. Gerlach compared predictions to scale model measurements where different combinations of absorptive and reflective surfaces were used. No diffuse surfaces were used in the model. Predicted results were found to correspond well except when only one wall was absorptive. Kruzins and Fricke used their model to predict sound pressure levels in rooms containing internal barriers. They compared predictions with measurements in scale models and noted that their model did not account for edge diffraction effects and therefore limited comparisons to octave bands above 1 kHz. Predictions were found to correlate well with measured values.

A method that divided surfaces into interconnected nodes was developed by Krämer et al<sup>41</sup> in 1992. This method was similar to the radiant-exchange techniques described above but where surfaces were described by either specular nodes or diffuse nodes. For diffuse nodes energy was re-directed to another randomly-chosen node in a similar manner to Kuttruff's re-direction of rays. No validation of the program's predictions was presented by the authors so it is difficult to determine the accuracy of the technique.

Lewers<sup>42</sup> used a radiant-exchange method in combination with a specular ray-tracing method using triangular beams. Energy was subtracted at surfaces according to a diffusion coefficient and placed in a radiant-exchange procedure. The method was only used to predict reverberation times at a single frequency and computation times were not considered as the program was implemented on a fast mainframe computer. Comparisons were only made with reverberation time predictions using Sabine's formula in a single theoretical enclosure. It is therefore difficult to assess the accuracy of the

technique.

In Borish's development of the image-source method<sup>13</sup> the filtering of specular reflections was proposed as a way of modelling diffuse reflections. This would involve convolution of measured or calculated responses of diffusors with incident sound. However, this approach would not model all aspects of diffuse reflections: the time-smearing effect of diffusion would be modelled but not the spatial scattering of energy. A similar method was proposed by D'Antonio<sup>43</sup>. However, its accuracy cannot be assessed as the technique has not been implemented.

Lehnert and Blauert<sup>34</sup> illustrated how diffuse reflections would be regarded by the image-source method as 'image source clouds' surrounding conventional geometrical image sources. This was suggested by Dalenbäck, Kleiner and Svensson<sup>44</sup> as a way of extending the image-source method to model diffuse reflections. However, they did not implement the method and claimed it would not be able to model all necessary reflection combinations.

In 1995, Dalenbäck introduced a technique for modelling diffuse reflections by splitting of cones/rays at diffuse surfaces<sup>45</sup>. To avoid an exponential increase in calculation times with increasing reflection order, diffuse surfaces were sub-divided into diffuse sub-surfaces referred to as 'patches'. The algorithm then proceeded in stages. In the first stage, cones were specularly traced around an enclosure, at (partially) diffusely reflecting surfaces diffuse energy was subtracted from the cone and stored at the appropriate patch. For the second stage this energy was dispersed by tracing rays from the centre of each patch. As with the first stage when these rays hit diffuse reflecting surfaces, energy was stored in at the appropriate patch. For subsequent stages diffuse energy from the previous stage was traced using rays from the centres of the diffuse patches. The stages continued until a required reflection density was achieved at the receiver. The density of rays traced from the diffuse patches was determined by the reflection time (earlier reflections had a greater density) and by the factor  $(1 - \alpha)\delta$  so that highly diffusing reflective surfaces were modelled in greater detail. Required computation times were not

discussed by the author and no validation against measured data was presented so it is difficult to assess the success of the technique.

## 2.5 Assessment of predictive accuracy

In order to assess the accuracy of models, errors in predicted acoustic parameters were compared to their subjective difference limens. A subjective difference limen (or threshold) is the change in a value that is just perceptible to a percentage of a population. The percentage normally used is 50 % so if errors are within difference limens, more than 50 % of a population would be unlikely to perceive a difference between the predicted value and the actual value, if heard.

Parameter	Difference Limen
Reverberation Time (s)	5%
Sound Strength (dB)	1 dB
Early Decay Time (s)	5%
Deutlichkeit	5%
Clarity Index (dB)	0.5 dB
Centre Time (ms)	10 ms
Lateral Energy Fraction	5%

Table 2.1 Rounded subjective difference limens used in this study

The determination of subjective difference limens is complex because they are dependent upon the stimulus used. In 1958, Seraphim<sup>46</sup> determined that for reverberation times in the range 0.5 s to 2.0 s, a difference limen of approximately 4 % was appropriate. The study asked 500 test subjects to compare decaying band-pass noise signals but determined the quoted difference limen by assessing the differences that 75 % of the subjects could perceive. Cremer and Müller<sup>4</sup> noted that for reverberation times below 0.6 s an absolute difference limen of approximately 0.024 s and that for reverberation

times between 1.5 s and 2.5 s differences of less than 0.1 s were not important. Studies by Reichardt and Schmidt<sup>47,48</sup> in the 1960's resulted in difference limens for individual reflection strengths and delays. However, the only recent research in this area was by Cox, Davies & Lam<sup>49</sup>, who specifically investigated difference limens for commonly used room acoustic parameters. These values were rounded by Vorländer<sup>2</sup>, probably because they were stimulant dependent, and have since been used in this rounded form by other authors<sup>50,51</sup>. These rounded values are shown in table 2.1 and were used to assess the overall accuracy of predictions in this investigation.

## **Chapter 3**

# **Field Measurements**

### **3.1 Description of enclosures**

#### **3.1.1 Overview of enclosures**

Eight enclosures were included in this investigation, two of which had variable acoustics and were studied in two different acoustic configurations. Table 3.1 shows the enclosures used along with their location and assigned reference number. The enclosures are specified by these reference numbers throughout the remainder of this text.

All the enclosures studied are commonly utilised for purposes where the acoustical behaviour of the space is of importance. This included five enclosures where orchestral concerts are performed; two theatres commonly used for drama and amplified music; two lecture theatres; a converted factory space, used for religious gatherings; and a general purpose University hall used for examinations, presentations and concerts. Two of the enclosures were designed as multi-purpose enclosures with variable acoustics. This enabled the prediction of acoustic changes to be assessed.

This varied mix of enclosure types represents the wide range of acoustic conditions

commonly encountered and highlights some of the difficulties encountered in predicting the acoustic behaviour of such diverse conditions.

<b>Enclosure reference</b>	<b>Enclosure name and location</b>
1a	Basingstoke Anvil Hall, Hampshire (concert mode)
1b	Basingstoke Anvil Hall, Hampshire (drama mode)
2	Blackheath Concert Hall, London
3	Covenant Community Church, Manchester
4	Wycombe Swan Theatre, Buckinghamshire
5a	Limerick University Hall, Ireland (lecture mode)
5b	Limerick University Hall, Ireland (concert mode)
6	Maxwell Hall, Salford
7	Royal Albert Hall, London
8	Pennine Theatre, Sheffield

*Table 3.1 Enclosures used in investigation*

### **3.2.1 Enclosure details**

The following pages contain details of the enclosures such as overall dimensions and descriptions of key features. Plans of the enclosures showing measurement positions are also given.

## Enclosure 1

---

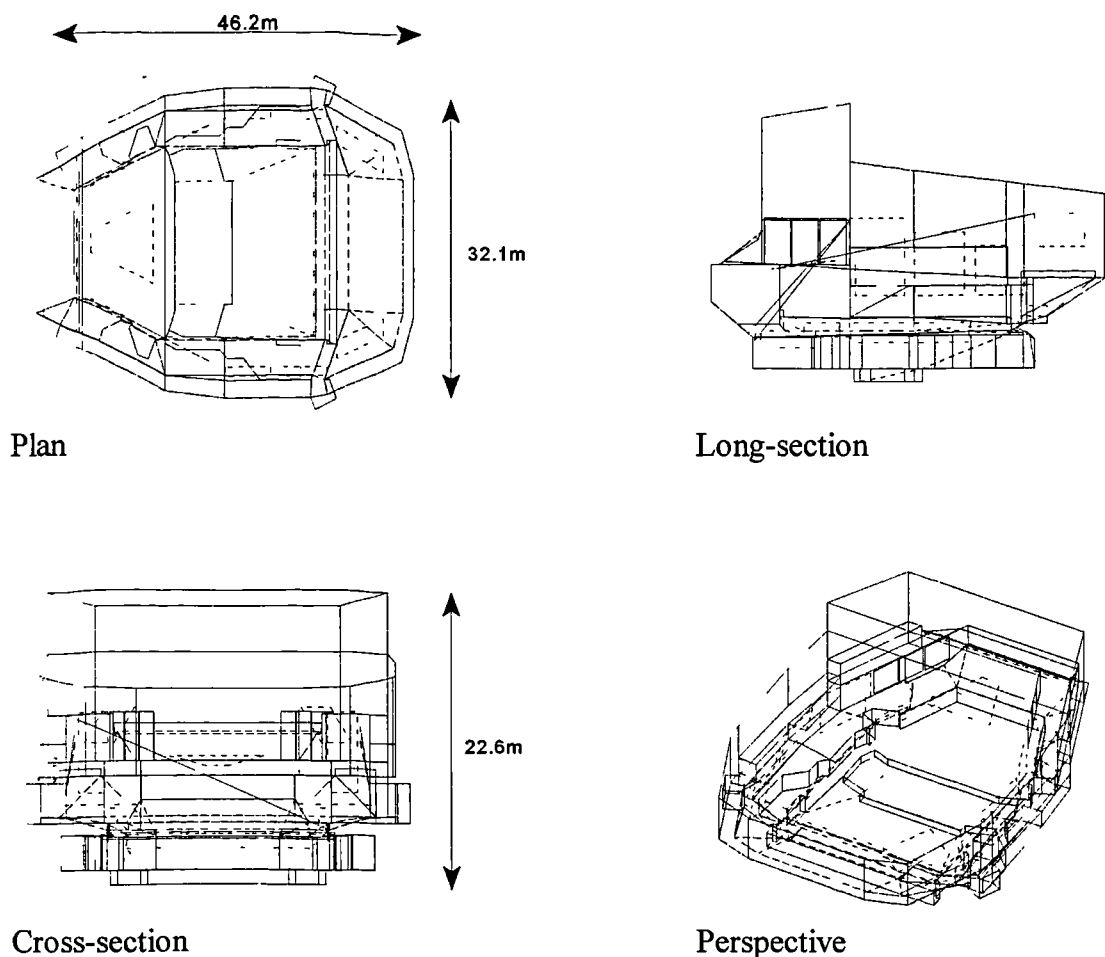


Figure 3.1 Views and overall dimensions of enclosure 1

Seated Capacity (approx) : 1400

Volume (approx) : 15000 m<sup>3</sup>

Reverberation Time at 1 kHz : 1.8 s (drama mode), 1.9 s (concert mode)

Enclosure 1 is commonly used for drama, concerts and sporting events and changes configuration for each occasion. For this study configurations for drama and concerts were investigated. For concerts, absorption is largely provided by cloth-covered seating

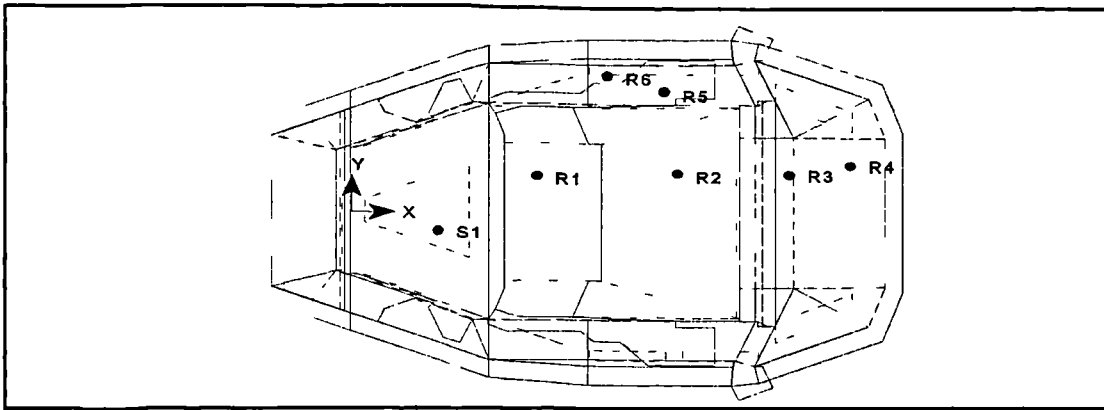


Figure 3.2 Source and receiver positions in enclosure 1

located on the main floor of the auditorium; in the choir area around the stage and along narrow side balconies. The seating in the front section of the main auditorium is bleacher seating that slopes to meet permanent seating at the rear of the enclosure. The side balconies contain four rows of seating. For the drama configuration, curtains are draped around the stage, which hide the choir seating from the auditorium. Similar curtains are draped along the side walls of the enclosure. Curved diffusers approximately 3 m high by 1.5 m wide are hung along the front of the side balconies for all configurations. Additional surface diffusion is provided by profiled wall shapes and the seating areas.

Responses were determined with a source (S1) located on the stage and six receivers located in the auditorium (R1 - R6). The positions of these are shown in figure 3.2. Coordinates of the positions used are presented in table 3.2.

Position	x (m)	y (m)	z (m)
S1 ( <i>stage</i> )	9.60	-1.00	1.70
R1 ( <i>bleachers</i> )	15.15	4.20	0.70
R2 ( <i>bleachers</i> )	24.20	4.20	2.95
R3 ( <i>stalls</i> )	35.10	5.00	6.95
R4 ( <i>stalls</i> )	38.00	6.00	8.35
R5 ( <i>side balcony</i> )	24.20	10.00	4.80
R6 ( <i>side balcony</i> )	19.10	12.00	5.10

Table 3.2 Coordinates of source and receiver positions in enclosure 1

## Enclosure 2

---

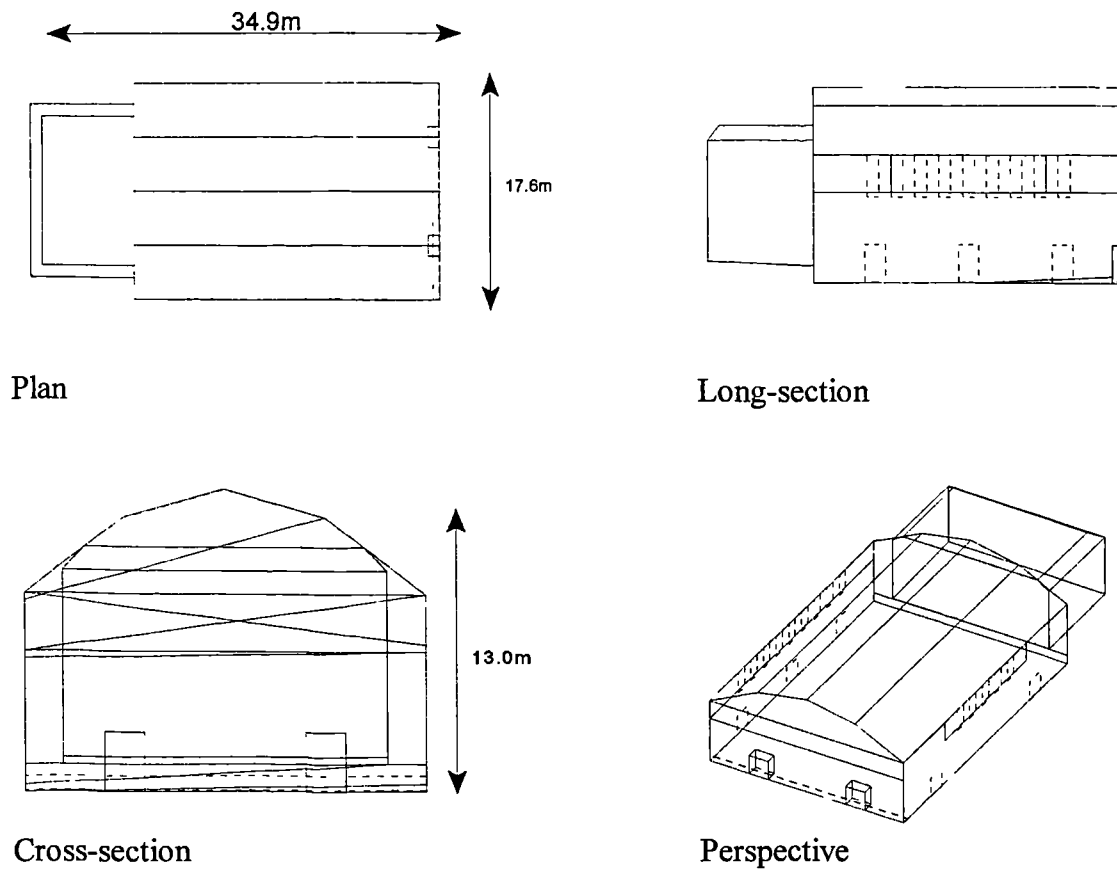


Figure 3.3 Views and overall dimensions of enclosure 2

Seated Capacity (approx) : 600  
Volume (approx) : 6800 m<sup>3</sup>  
Reverberation Time at 1 kHz : 2.6 s

Enclosure 2 is commonly used for classical concerts. During the measurements, absorption was largely provided by heavy curtains covering the back stage wall and part of the rear wall of the main auditorium. During performances additional absorption is provided by the audience but only the unoccupied state was considered in this study. During measurements plastic seating, used during performances, was stacked at the rear

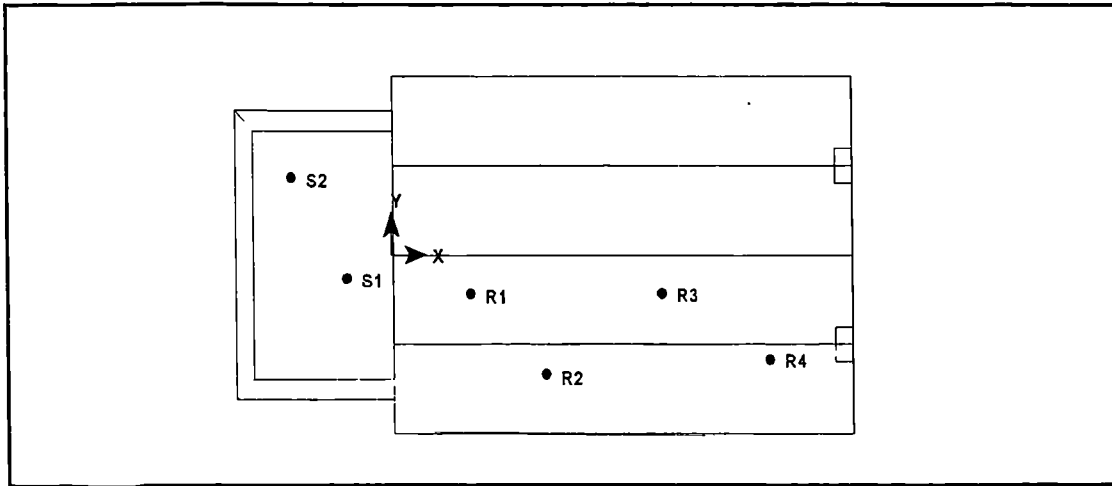


Figure 3.4 Source and receiver positions in enclosure 2

of the hall leaving a clear wooden floor. The walls and barrel-vaulted ceiling were finished with lime plaster on laths. Surface diffusion was provided at high frequencies by ornamental plasterwork on the ceilings and around doorways.

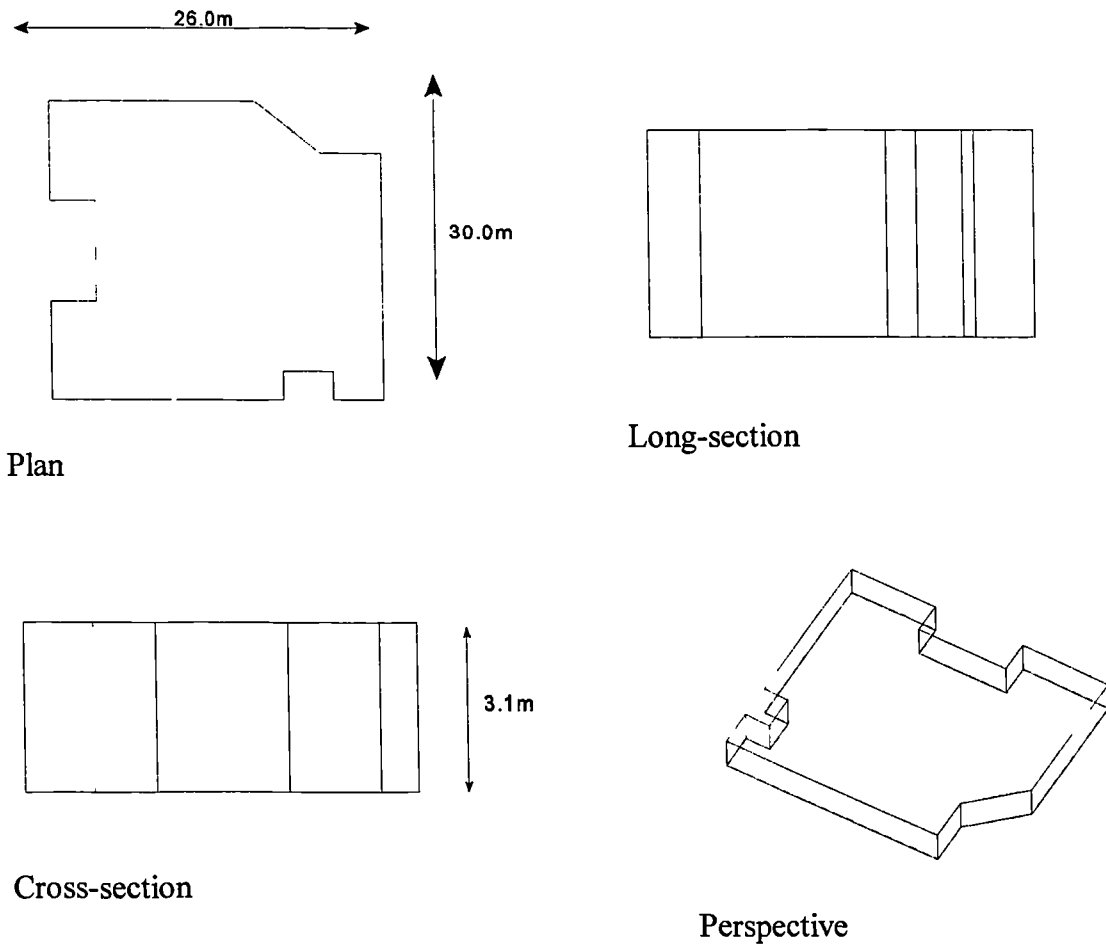
Responses were determined with two sources (S1 and S2) located on the stage and four receivers located in the auditorium (R1 - R4). The positions of these are shown approximately in figure 3.4. Coordinates of the positions used are presented in table 3.3.

Position	x (m)	y (m)	z (m)
S1 ( <i>stage</i> )	-1.00	-1.00	1.70
S2 ( <i>stage</i> )	-6.40	3.75	1.70
R1 ( <i>auditorium</i> )	5.50	-1.50	0.10
R2 ( <i>auditorium</i> )	11.00	-6.83	0.10
R3 ( <i>auditorium</i> )	14.50	-1.50	0.10
R4 ( <i>auditorium</i> )	20.00	-4.00	0.10

Table 3.3 Coordinates of source and receiver positions in enclosure 2

## Enclosure 3

---



---

Figure 3.5 Views and overall dimensions of enclosure 3

Seated Capacity (approx) : 500

Volume (approx) : 2200 m<sup>3</sup>

Reverberation Time at 1 kHz : 1.0 s

Enclosure 3 is commonly used for religious gatherings with music. It was converted from an existing factory space and therefore has a low ceiling height of 3.1 m and asymmetric geometry in the horizontal plane. Absorption is mainly provided from a carpeted floor covered by cloth-covered seats. Diffusion is mainly provided by the seats.

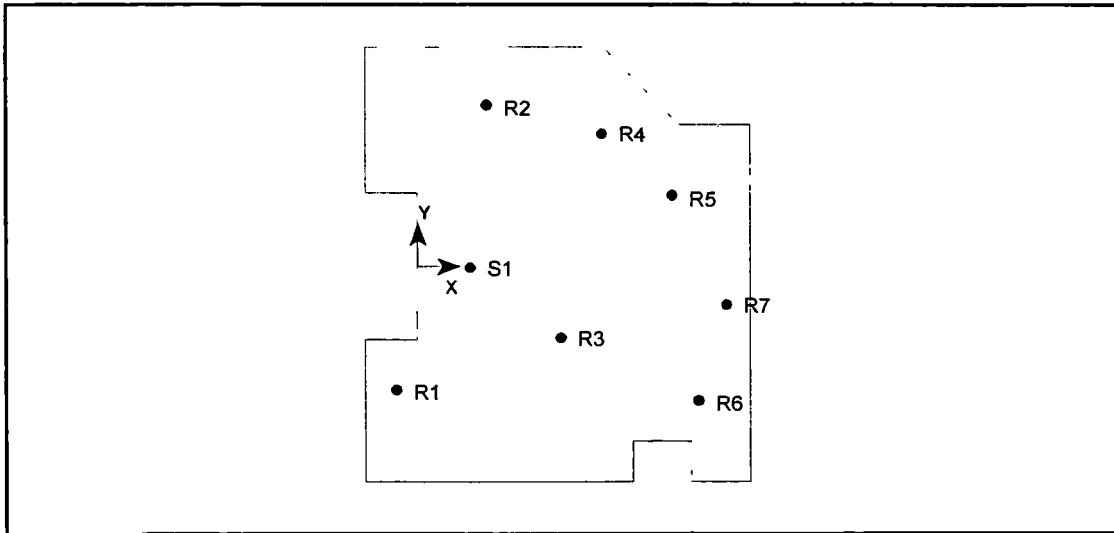


Figure 3.6 Source and receiver positions in enclosure 3

Responses were determined with a source (S1) located on a raised platform with seven receivers located in the auditorium (R1 - R7). The positions of these are shown in figure 3.6. Coordinates of the positions used are presented in table 3.4.

Position	x (m)	y (m)	z (m)
S1 ( <i>floor</i> )	4.40	0.00	2.03
R1 ( <i>seating</i> )	-0.70	-11.50	1.25
R2 ( <i>seating</i> )	5.70	10.50	1.25
R3 ( <i>seating</i> )	9.95	-10.30	1.25
R4 ( <i>seating</i> )	11.40	11.20	1.25
R5 ( <i>seating</i> )	12.90	3.25	1.25
R6 ( <i>seating</i> )	17.30	-9.00	1.25
R7 ( <i>seating</i> )	19.10	-3.20	1.25

Table 3.4 Coordinates of source and receiver positions in enclosure 3

## Enclosure 4

---

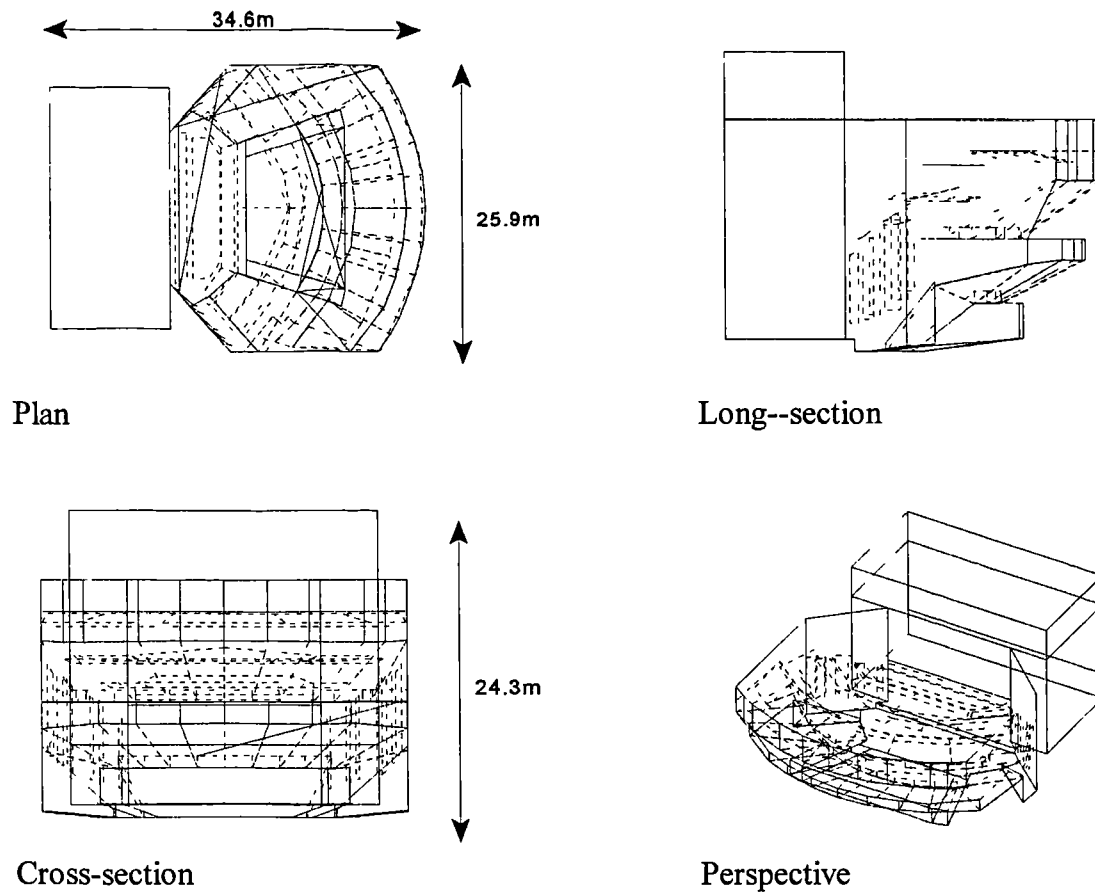


*Figure 3.7* View and overall dimensions of enclosure 4

Seated Capacity (approx) : 1000

Volume (approx) : 12800 m<sup>3</sup>

Reverberation Time at 1 kHz : 0.9 s

Enclosure 4 is commonly used for drama and amplified-music concerts. It has two rear balconies and absorption is mainly provided by cloth-covered seating, carpeted flooring and curtains draped around the stage. The area above the auditorium contains many acoustic reflectors, lighting rigs and walkways for technicians all of which act as diffusing elements along with the seating.

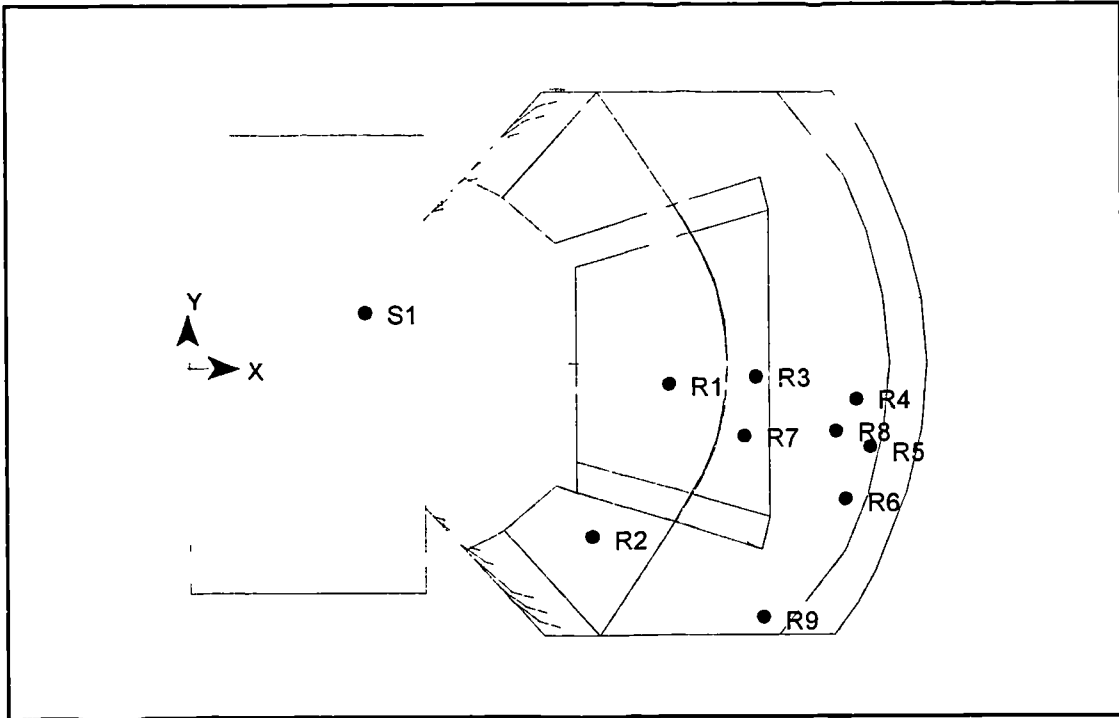


Figure 3.8 Source and receiver positions in enclosure 4

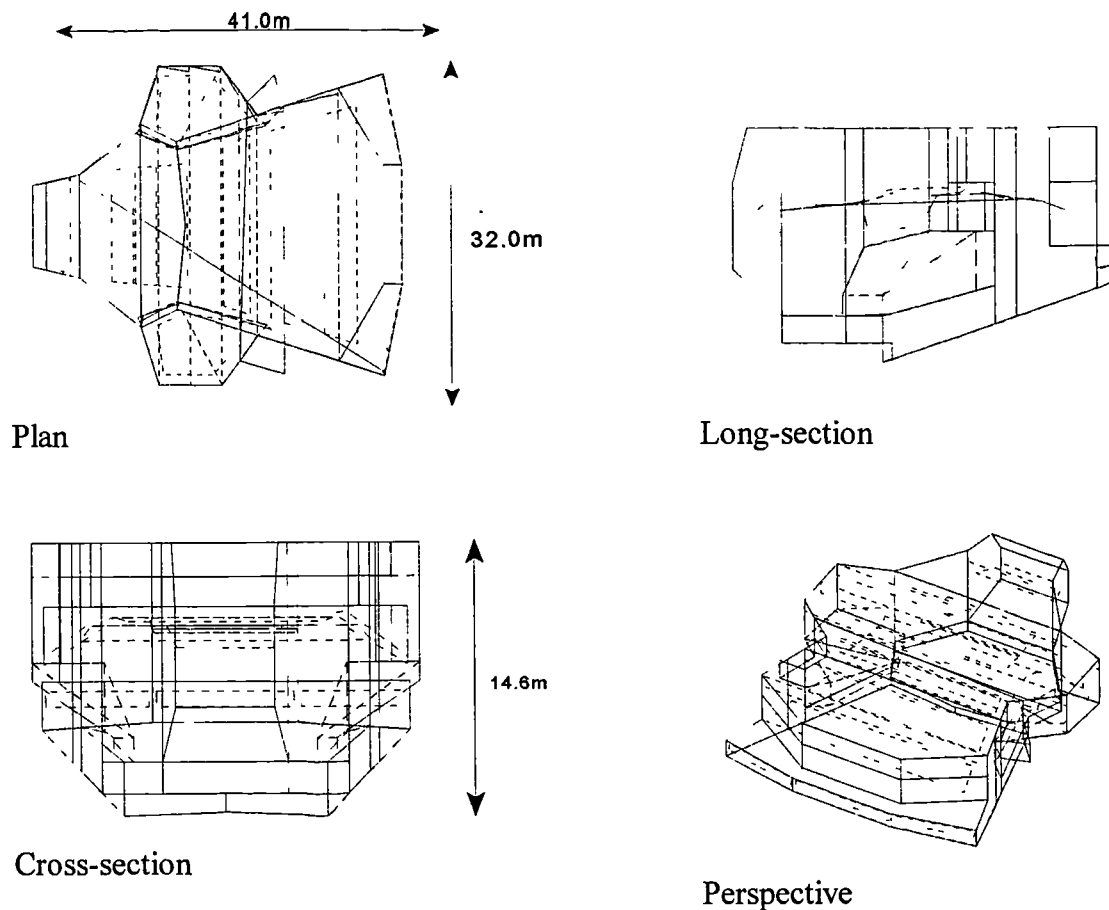
Responses were determined with a source (S1) located on the stage and nine receivers located in the auditorium (R1 - R9). The positions of these are shown in figure 3.8. Coordinates of the positions used are shown in table 3.5.

Position	x (m)	y (m)	z (m)
S1 (stage)	9.50	3.50	1.40
R1 (stalls)	19.40	-1.20	0.25
R2 (stalls)	18.20	-8.20	2.00
R3 (stalls)	26.80	-1.25	4.30
R4 (2 <sup>nd</sup> balcony)	29.00	-2.35	9.50
R5 (2 <sup>nd</sup> balcony)	32.50	-4.50	12.00
R6 (2 <sup>nd</sup> balcony)	31.50	-7.00	12.00
R7 (stalls)	25.90	-4.90	1.00
R8 (1 <sup>st</sup> balcony)	31.00	-3.10	6.20
R9 (1 <sup>st</sup> balcony)	26.50	-10.80	6.20

Table 3.5 Coordinates of source and receiver positions in enclosure 4

## Enclosure 5

---



---

Figure 3.9 Views and overall dimensions of enclosure 5

Seated Capacity (approx) : 1000

Volume (approx) : 9400 m<sup>3</sup>

Reverberation Time at 1 kHz : 1.2 s (lecture mode) to 1.4 s (concert mode)

Enclosure 5 is commonly used for lectures and concerts and changes configuration accordingly. In this study both configurations were investigated. For concerts, absorption is largely provided by cloth-covered seating located in the main auditorium, in the choir area behind the stage and in the side balconies. For the lecture configuration curtains are draped around the stage, including between the choir seating and stage, and

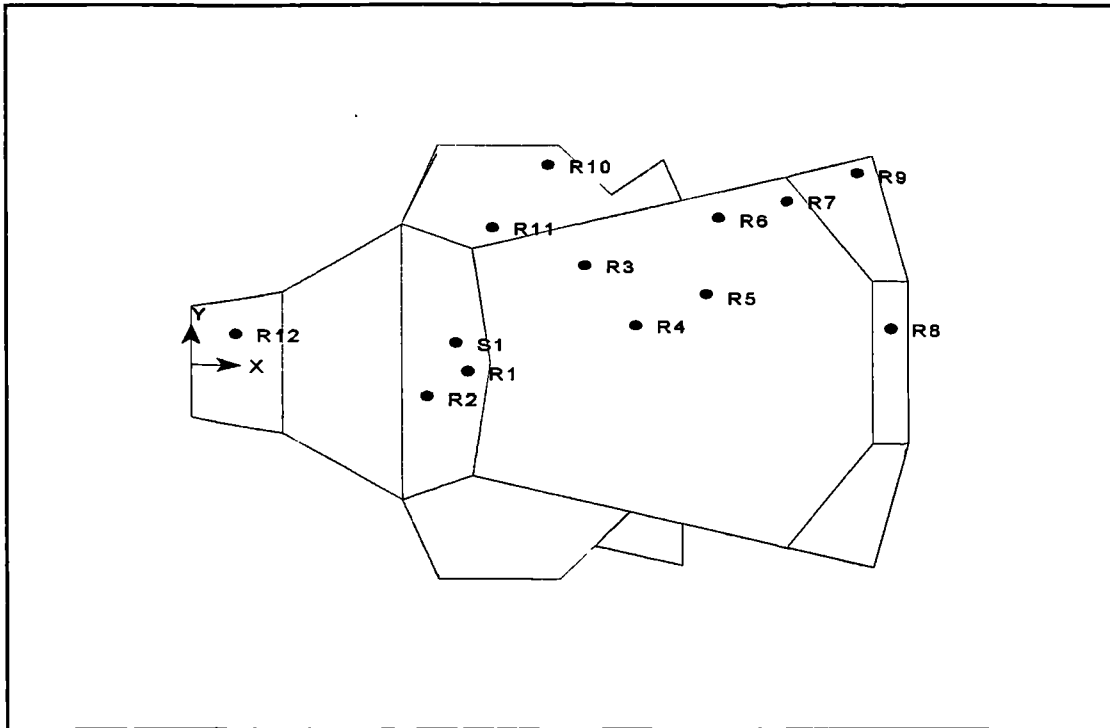


Figure 3.10 Source and receiver positions in enclosure 5

absorbent banners extend across the main auditorium. The walls are of unfinished blockwork providing high-frequency diffusion and reflectors are suspended above the stage and auditorium to diffuse low frequencies while reflecting high frequencies.

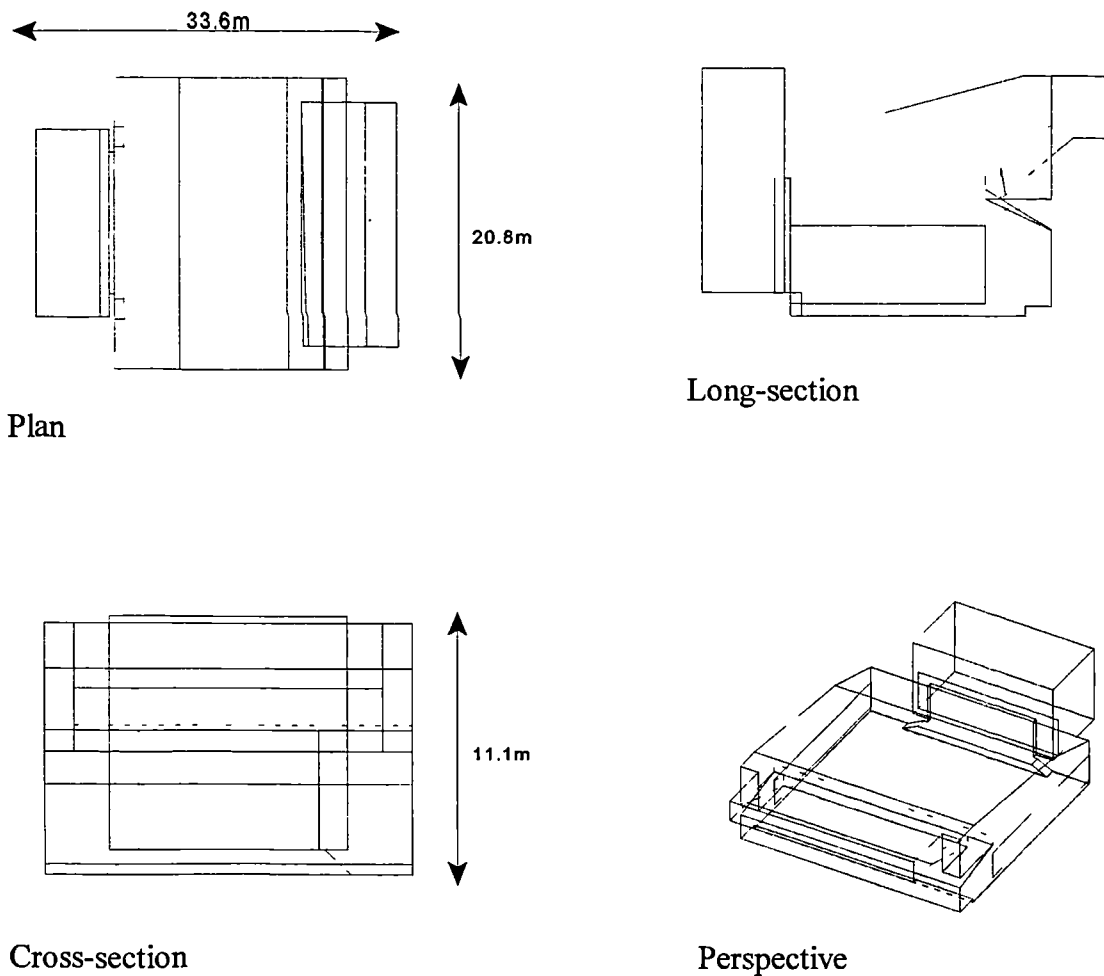
Responses were determined with a source (S1) located on the stage and twelve receivers (R1 - R12) located throughout the enclosure. The positions of these are shown in figure 3.10. Coordinates of the positions used are shown in table 3.6.

Position	x (m)	y (m)	z (m)
S1 ( <i>stage</i> )	13.00	1.84	1.70
R1 ( <i>stage</i> )	15.00	-0.50	1.70
R2 ( <i>stage</i> )	12.60	-0.93	1.30
R3 ( <i>stalls</i> )	18.25	7.40	1.20
R4 ( <i>stalls</i> )	20.90	1.00	1.30
R5 ( <i>stalls</i> )	24.40	3.20	1.90
R6 ( <i>stalls</i> )	23.90	7.80	2.10
R7 ( <i>stalls</i> )	28.00	10.00	2.80
R8 ( <i>stalls</i> )	34.10	2.60	3.40
R9 ( <i>stalls</i> )	37.90	11.90	4.20
R10 ( <i>side balcony</i> )	16.60	14.40	6.40
R11 ( <i>side balcony</i> )	14.35	11.15	5.00
R12 ( <i>choir</i> )	2.00	2.50	5.00

Table 3.6 Coordinates of source and receiver positions in enclosure 5

## Enclosure 6

---



---

Figure 3.11 Views and overall dimensions of enclosure 6

Seated Capacity (approx) : 1000

Volume (approx) : 5600 m<sup>3</sup>

Reverberation Time at 1 kHz : 1.3 s

Enclosure 6 is commonly used for amplified-music concerts, examinations and graduation ceremonies. Absorption is mainly provided by cloth-covered seats, heavy curtains draped round windows and the stage and by perforated acoustic tiling at the rear of the balcony. For some concerts the seats are removed and absorption is provided by the standing audience. For results presented here the hall was unoccupied with the seats

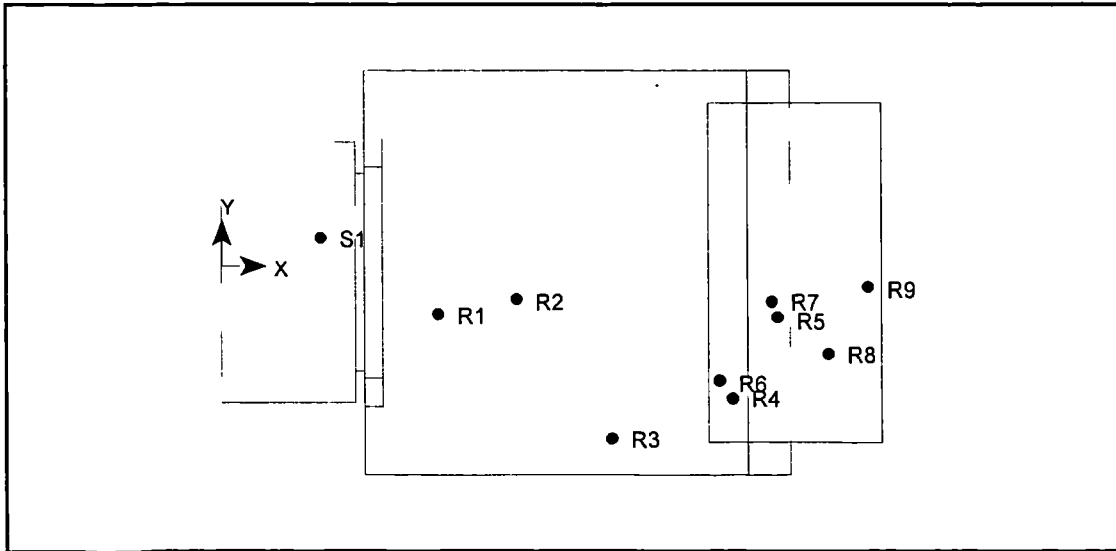


Figure 3.12 Source and receiver positions in enclosure 6

present. The rear wall of the stalls, located under the balcony is formed by sliding wooden doors that separate a storage room from the main auditorium. The walls and ceiling are finished with smooth painted plasterwork and no diffusers are present. The seating areas are therefore the main diffusing surfaces in the enclosure.

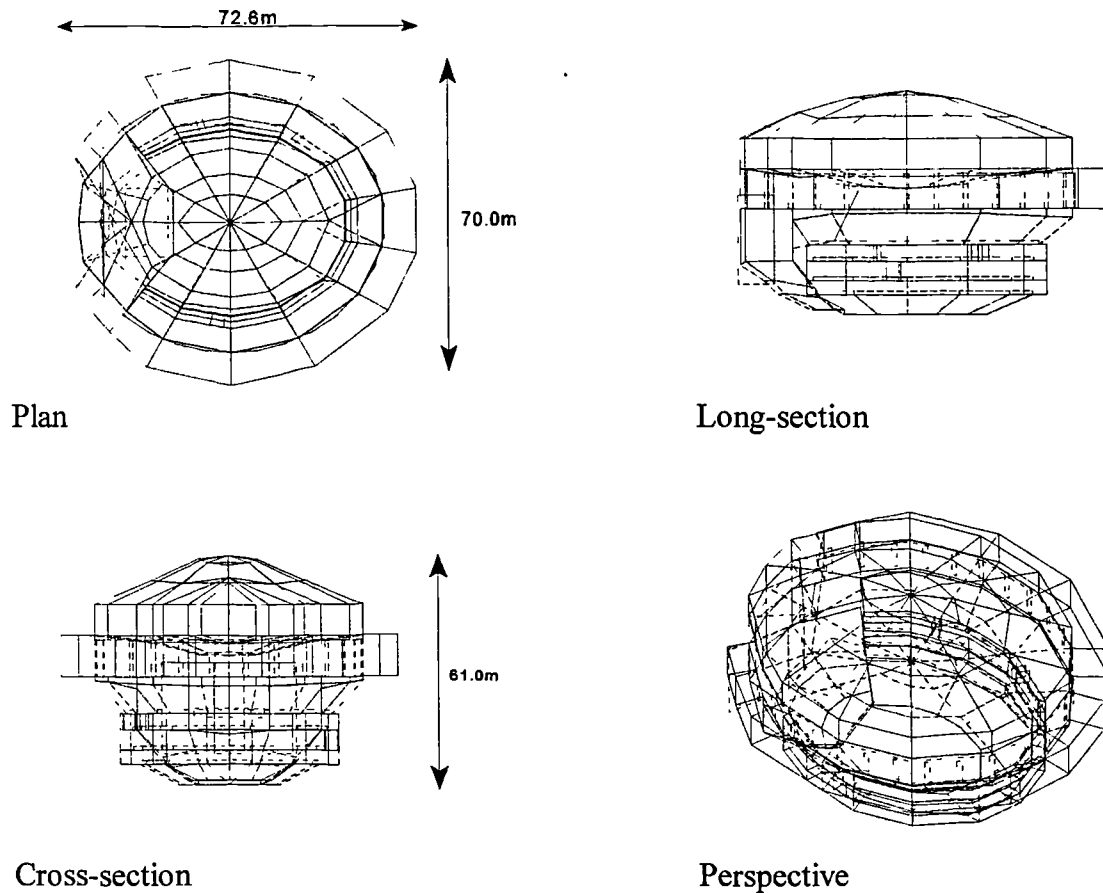
Responses were determined with a source (S1) located on the stage and nine receivers located in the auditorium (R1 - R9). The positions of these are shown in figure 3.12. Coordinates of positions used are presented in table 3.7.

Position	x (m)	y (m)	z (m)
S1 ( <i>stage</i> )	6.30	1.30	1.70
R1 ( <i>stalls</i> )	11.50	-3.60	0.20
R2 ( <i>stalls</i> )	17.50	-3.20	0.20
R3 ( <i>stalls</i> )	19.50	-8.60	0.20
R4 ( <i>stalls</i> )	25.30	-6.80	0.20
R5 ( <i>stalls</i> )	27.40	-3.80	0.64
R6 ( <i>balcony</i> )	25.10	-6.80	5.14
R7 ( <i>balcony</i> )	27.40	-3.40	6.14
R8 ( <i>balcony</i> )	29.50	-5.10	7.00
R9 ( <i>balcony</i> )	31.70	-2.70	7.30

Table 3.7 Coordinates of source and receiver positions used in enclosure 6

## Enclosure 7

---



---

Figure 3.13 Views and overall dimensions of enclosure 7

Seated Capacity (approx) : 5000

Volume (approx) : 110,000 m<sup>3</sup>

Reverberation Time at 1 kHz : 2.9 s

Enclosure 7 is commonly used for concerts, exhibitions and sporting events. For many concerts cloth-covered seating is located on the arena floor of the hall and was present for the measurements made in this study. The enclosure is oval shaped in plan and has a complicated seating arrangement: seating is located around the circumference of the arena and is referred to as stalls seating; a “Grand Tier” of private boxes is located

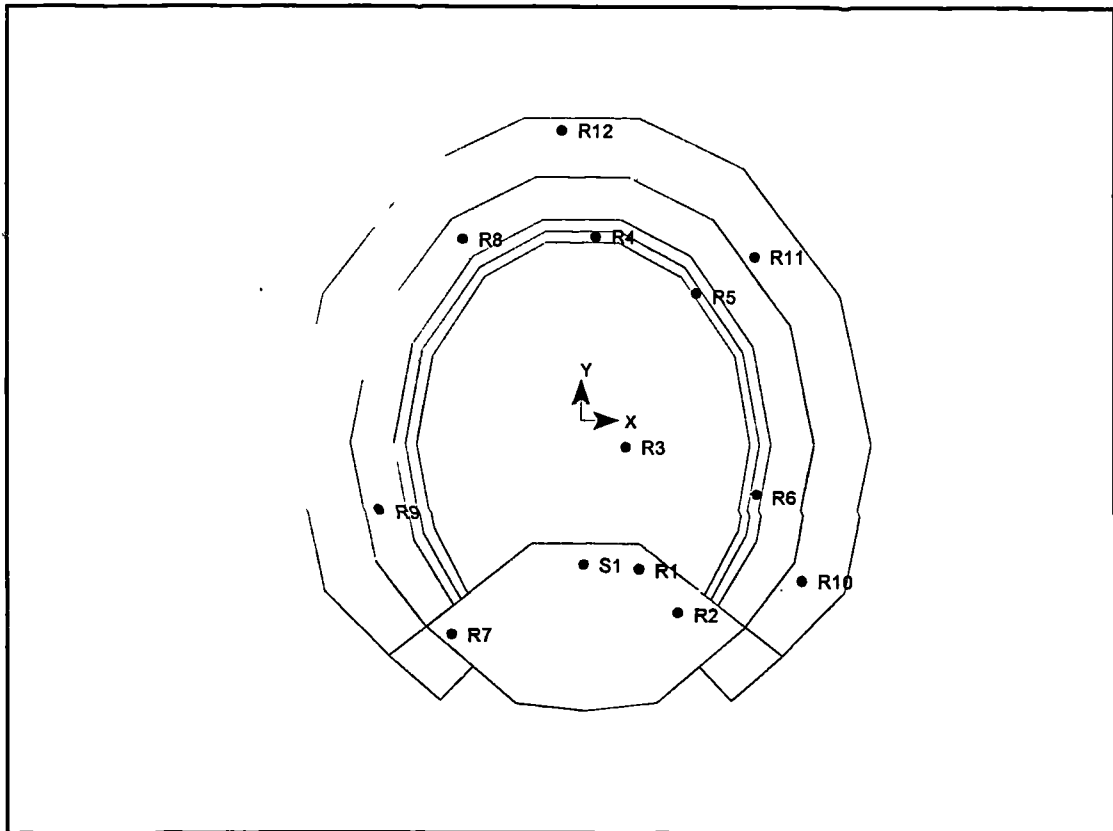


Figure 3.14 Source and receiver positions in enclosure 7

behind the stalls seating and above this is a “First Tier” of private boxes, a “Second Tier” of open boxes and a balcony. Choir seating is also situated behind the stage. In its unoccupied state, absorption is mainly provided by the cloth-covered seats and heavy curtains draped around private boxes.

Diffusion is provided from ornamental plasterwork on the balcony and box fronts and from curved “mushroom” diffusers suspended from the dome ceiling, which occupy approximately 50% of the plan area. Mineral fibre is attached to the top of the diffusers to reduce the strength of reflections from the dome ceiling, which had previously caused flutter echoes<sup>52</sup>. Large organ pipes located behind the stage also provided a diffuse surface.

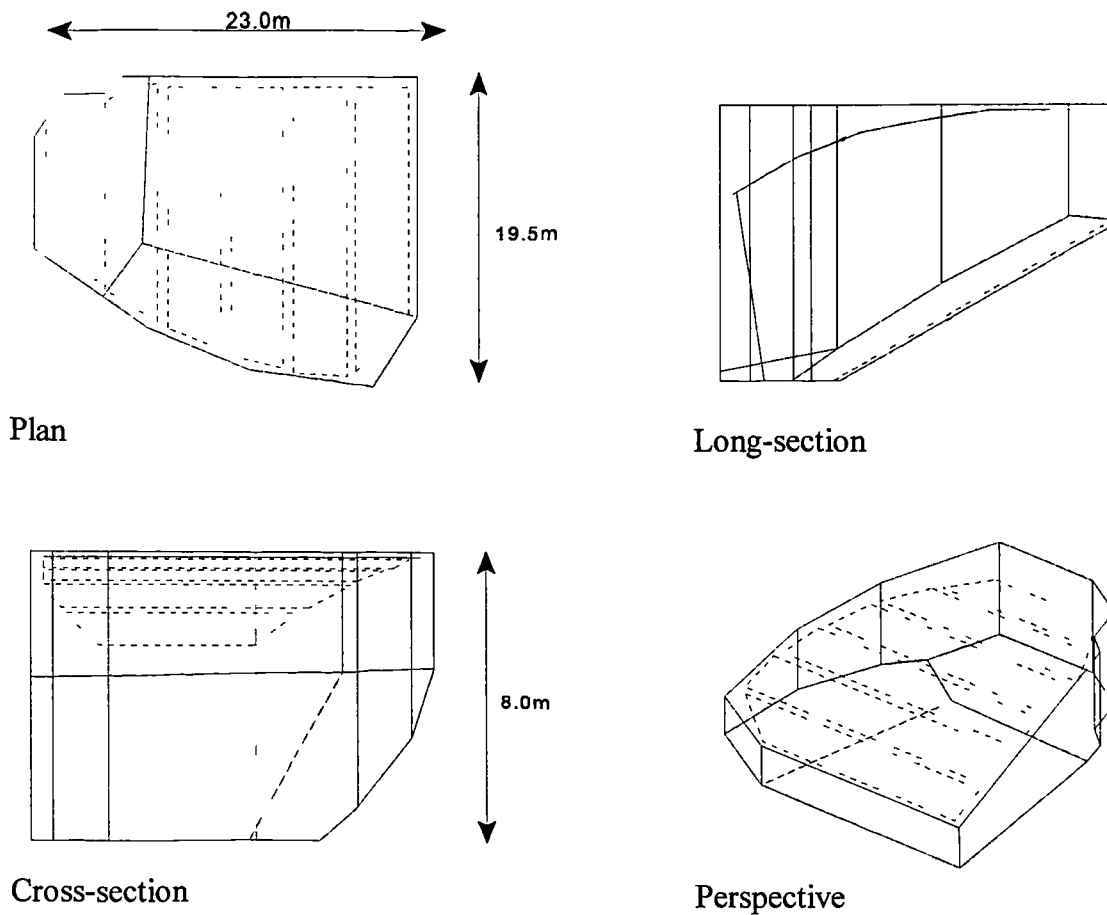
Responses were determined with a source (S1) located on the stage and twelve receivers located in the auditorium (R1 - R12). The positions of these are shown in figure 3.14. Coordinates of the positions used are presented in table 3.8.

Position	x (m)	y (m)	z (m)
S1 ( <i>stage</i> )	0.00	-14.50	2.50
R1 ( <i>stage</i> )	4.70	-14.50	2.05
R2 ( <i>choir</i> )	8.00	-20.00	3.00
R3 ( <i>arena</i> )	4.50	-6.00	1.70
R4 ( <i>stalls</i> )	3.00	14.50	2.50
R5 ( <i>stalls</i> )	14.00	10.00	3.50
R6 ( <i>grand tier</i> )	21.00	-3.00	7.45
R7 ( <i>choir</i> )	-10.50	-20.00	6.00
R8 ( <i>second tier</i> )	-17.00	13.50	11.05
R9 ( <i>second tier</i> )	-20.00	-6.00	11.05
R10 ( <i>balcony</i> )	22.00	-15.00	17.50
R11 ( <i>balcony</i> )	21.00	15.00	17.00
R12 ( <i>balcony</i> )	-5.00	30.00	19.00

Table 3.8 Coordinates of source and receiver positions in enclosure 7

## Enclosure 8

---



---

Figure 3.15 Views and overall dimensions of enclosure 8

Seated Capacity (approx) : 200

Volume (approx) : 2000 m<sup>3</sup>

Reverberation Time at 1 kHz : 0.7 s

Enclosure 8 is commonly used for lectures and classical concerts. It is asymmetric in plan with a concave side wall. When unoccupied absorption is mainly provided by cloth-covered seats, curtains draped over the front wall (behind the 'stage' area) and by acoustic treatment on the rear wall.

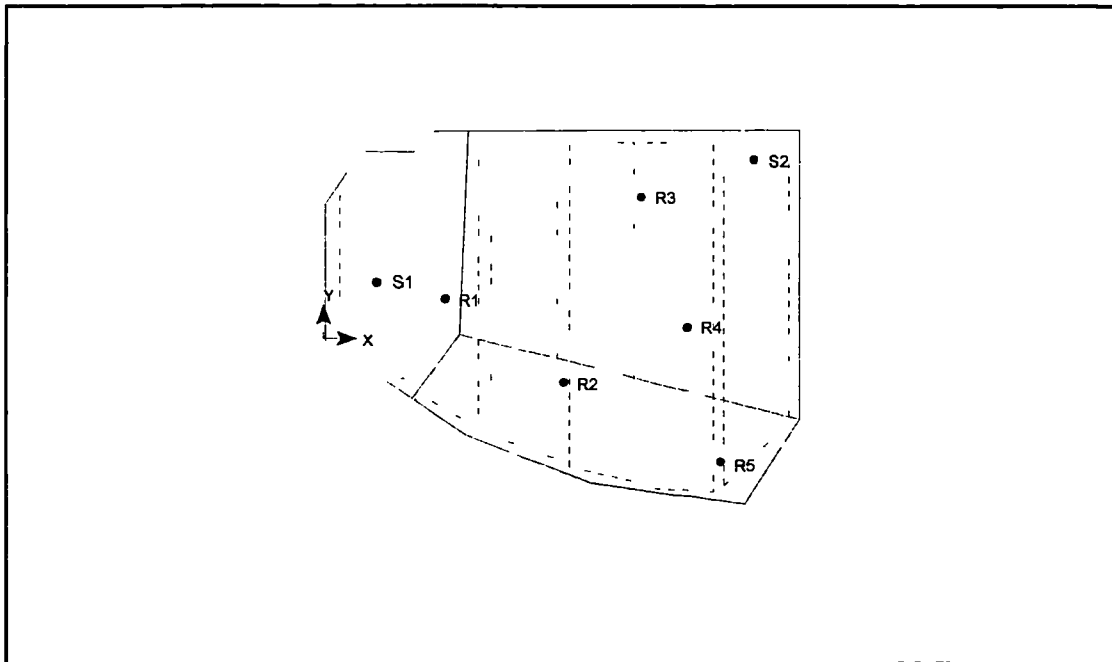


Figure 3.16 Source and receiver positions in enclosure 8

Reflective panels that cover 80% of the plan above the seating are suspended from the ceiling.

Responses were determined from a source (S1) located on the 'stage' (this was an area of flooring at the front of the enclosure that was not raised) and from a source (S2) located to the rear of the seated area. Five receiver positions (R1 - R5) were used throughout the auditorium. The positions used are shown in figure 3.16 with their coordinates presented in table 3.9.

Position	x (m)	y (m)	z (m)
S1 (floor)	3.20	4.50	1.70
S2 (seating)	21.20	7.85	6.70
R1 (floor)	7.70	3.80	2.00
R2 (seating)	11.90	-1.50	3.60
R3 (seating)	13.80	6.00	4.20
R4 (seating)	17.50	-0.10	5.40
R5 (seating)	20.00	-7.40	6.70

Table 3.9 Coordinates of source and receiver positions in enclosure 8

## 3.2 Measurement procedure

### 3.2.1 Instrumentation

The following equipment was used during the measurements

Description	Make	Type	Serial Number
Portable Computer	Compaq	Portable II	1806BE4F0060
Data acquisition card	DRA Labs	AD2-160	582
Microphone	B & K	4165	1547261
Microphone	B & K	4165	1547260
Microphone	AKG	C414 EB/48	25117
Microphone pre-amplifier	B & K	2639	1527966
Microphone pre-amplifier	B & K	2639	1527964
Microphone pre-amplifier	Salford U.	-	SU02
Measurement amplifier	B & K	2610	1501539
Power amplifier	Quad	306	-
Dodecahedron sound source	Salford U.	-	SU01
Temp. and humidity meter	Comark	2020	108614
Calibrator	B & K	4230	431601

Table 3.10 Instrumentation list

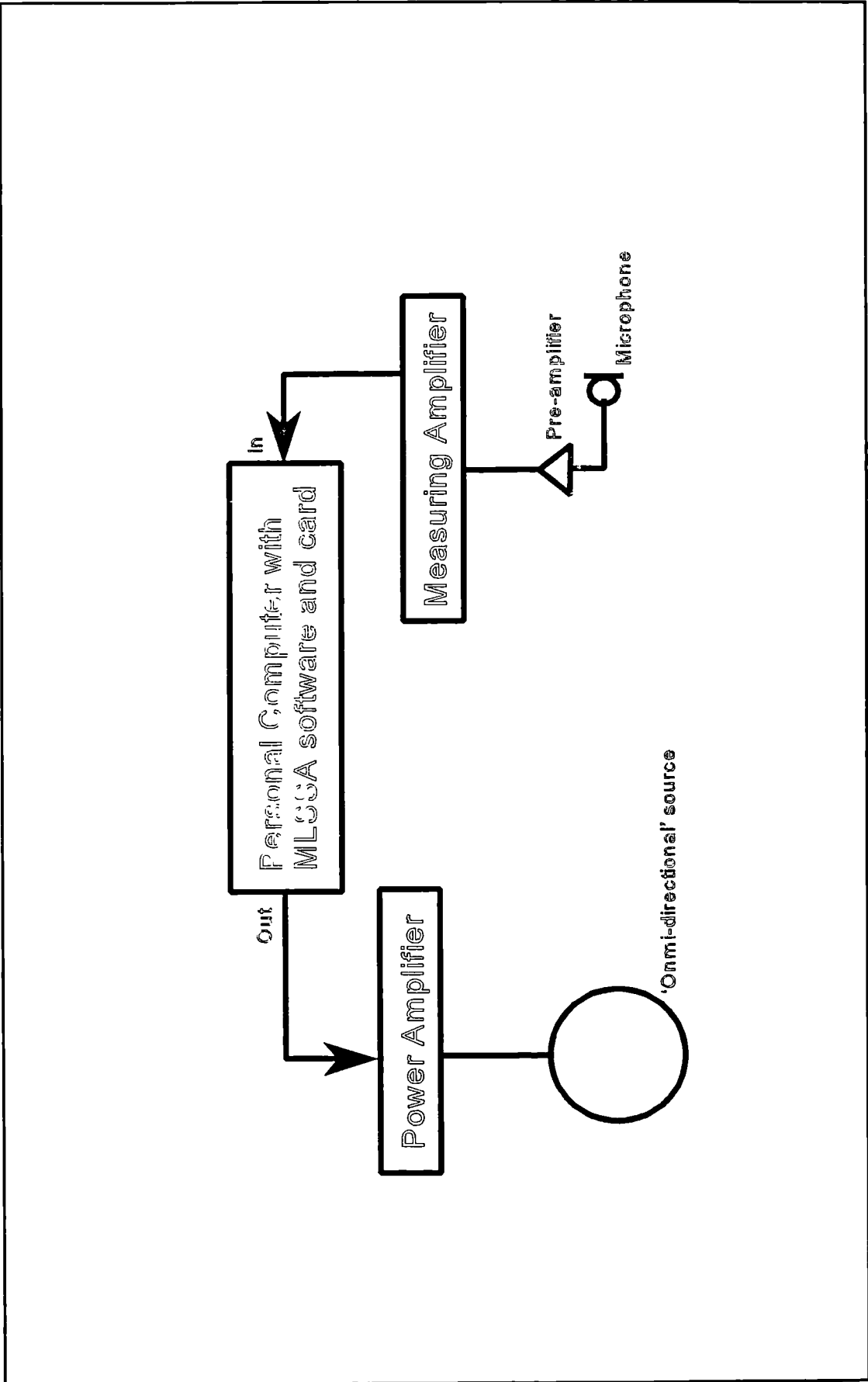


Figure 3.17 Experimental setup for MLS measurements

### **3.2.2 Measurement setup**

The measurement chain was set up as shown in figure 3.17. Measurements of acoustic impulse responses were made at fixed positions in the enclosures in order to determine room acoustic parameters. Source and receiver positions were chosen to represent those normally encountered in each enclosure. For example, in an auditorium the source would be placed on the stage and various receiver positions would be chosen throughout the audience area. In certain halls receiver positions were also chosen to investigate specific acoustic features. Receivers under balcony overhangs were chosen to look at the prediction of acoustic shadowing, while positions close to diffuse surfaces were used to examine the modelling of surface diffusion. In certain enclosures flutter echoes could be heard. Consequently, source-receiver positions were chosen to investigate this feature. During measurements the source centre was located at a height of 1.7 m above the floor corresponding to the average mouth height of a standing speaker. Receiver microphones were positioned at a height of 1.2 m above the floor to correspond to ear height of average listeners in typical chairs.

The MLS source signal was amplified using a Quad 306 power amplifier to drive a dodecahedron sound source. The directivity of the sound source was measured in the horizontal and vertical planes in anechoic conditions and was found to be omnidirectional  $\pm 1$  dB in all octave-bands between 125 Hz and 4000 Hz. Measurements were therefore made over this frequency range except for those using the figure-of-eight microphone, which were made between 250 Hz and 4000 Hz, because of low frequency non-linearity in the microphone pre-amplifier used.

Omni-directional microphone measurements were performed at all receiver positions chosen. Measurements using the figure-of-eight microphone were only made at selected positions because of time constraints. The figure-of-eight microphone was orientated so it 'faced' the source at each receiver position. That is, with its figure-of-eight axis perpendicular to the source-receiver line, as shown in figure 3.18. To minimise measurement uncertainty sixteen impulse responses were averaged at each receiver position.

For the omni-directional microphone measurements, the system was calibrated before each set of measurements using a 1000 Hz tone at 93.8 dB. After each set of measurements the calibration level was again checked. A calibrator was not available for use with the AKG C414 figure-of-eight microphone. However, impulses derived from the figure-of-eight measurements were only used for calculating early lateral energy fractions. Since the AKG C414 microphone has switchable directivity, it was also used for additional omni-directional measurements. Any calibration errors were then cancelled out during the calculation of the parameter (see Appendix A). To reduce any errors due to drift all instrumentation used was allowed a 'warm-up time' of approximately ten minutes. Figure-of-eight and omni-directional measurements using the AKG C414 were made alternately at each receiver position.

Temperature and relative humidity were recorded at the start and end of each set of measurements to determine the speed of sound and for the calculation air absorption in the predictive models.

The software and data acquisition card used employed a *maximum-length sequence* (MLS) system (see subsection 3.2.3). This was used to produce acoustic impulse responses for each source-receiver position.

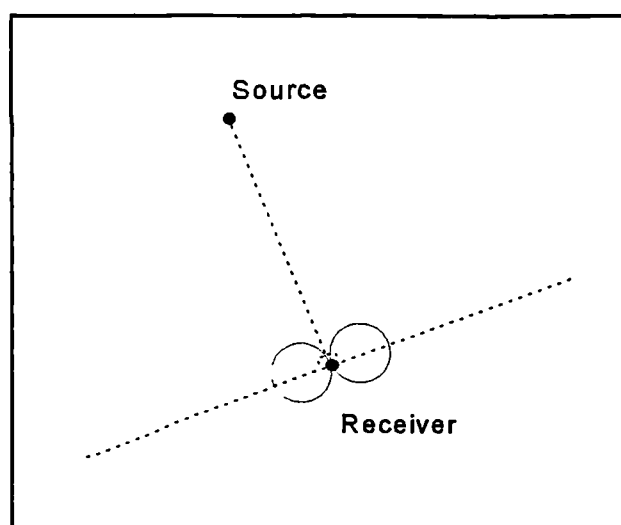


Figure 3.18 Orientation of figure-of-eight receiver

### 3.2.3 The maximum-length sequence measurement method

The MLS method is a way of determining the impulse response of a linear system by cross-correlating a pseudo-random input noise with the measured output of the system. In room acoustics the transfer of sound between a source and receiver in an enclosure can be regarded as a linear system provided there are no significant variations in the characteristics of the system over the measurement period. Use of the method in room acoustics was pioneered by Schroeder<sup>53</sup> in the 1960's because it has important advantages over conventional impulse test methods for the measurement of sound decay. A problem encountered with impulse test methods is the requirement of the sound source to provide a powerful acoustic impulse over a wide frequency range. Traditionally, pistol shots and balloon bursts were used because they provided a powerful acoustic response although the spectra produced were not flat<sup>54</sup>. Impulses input into loudspeakers produced flat spectra but often could not radiate sufficient power to produce required signal-to-noise ratios in concert halls. Pseudo-random noise has a flat spectrum and for the same energy as a single impulse has a peak amplitude that is typically 100 times smaller<sup>55</sup>. This means it can be used to drive a loudspeaker to achieve considerable improvements in the signal-to-noise ratio of measured impulse responses<sup>56</sup>. Since the method cross-correlates the measured output with a known input it is also an effective way of reducing the influence of extraneous noise during measurements<sup>57</sup>. Since the input signal is deterministic and repeatable, impulse responses can be averaged to improve the signal to noise ratio. Any unwanted uncorrelated noise will then be averaged over the number of repeated sequences. The signal to noise ratio improves by 3 dB for every doubling of the number of sequences<sup>58</sup>. In comparisons of different methods for measuring reverberation times by Vorländer and Bietz<sup>59</sup> techniques utilising broad-band pseudo-random sequences, such as MLS, were considered the most powerful available.

From signal theory<sup>60</sup> we know that, for a linear system, the cross-correlation between the input  $x(s)$  and the output  $y(s)$  is equal to the convolution of the system's impulse response with the auto-correlation of the input.

i.e. 
$$R_{xy}(s) = R_{xx}(s) \star h(s)$$

The result of convolving a sequence with a pure impulse, represented by a dirac delta function  $\delta(s)$ , is the sequence itself. Therefore, if the auto-correlation of the input signal is a dirac delta function, the cross-correlation of the input  $x(s)$  and the output  $y(s)$  is equal to the impulse response  $h(s)$ .

i.e. 
$$R_{xy}(s) = \delta(s) \star h(s) = h(s)$$

### 3.2.4 Calculation of acoustic parameters

Seven types of room acoustic parameters were calculated according to definitions in ISO 3382. A summary of these definitions is given in Appendix A. All the acoustic parameters presented, except early lateral energy fraction, were calculated from impulse responses measured using B & K 4165 microphones. For the calculation of early lateral energy fraction, measurements made using a AKG C414 microphone were used. The calculation of early lateral energy fraction involves the ratio of energies measured using figure-of-eight and omni-directional microphones (see Appendix A). Therefore, by using the same microphone and measurement chain for both measurements any calibration errors were eliminated during calculations.

## **Chapter 4**

# **The Conventional Hybrid Model**

### **4.1 Description of the computer model**

Models of enclosures were created using ODEON v.2.5<sup>61</sup> developed at the Technical University of Denmark. In order to assess the performance of existing modelling techniques it would be preferable to compare predictions from a wide variety of algorithms but due to financial constraints this was not possible. However, ODEON was one of the three most accurate programs tested in Vorländer's round-robin survey<sup>62</sup> and can therefore be considered as representative of the best of contemporary modelling techniques.

The model used a modified form of the hybrid ray tracing / image source method, where the calculation is split into two parts by a reflection 'transition order'. Reflections occurring before the transition order are referred to as 'early' reflections and were modelled using specular image sources. Those following it are called 'late' or 'reverberant' reflections and were modelled by secondary diffuse sources located at reflection points.

The image sources used for the modelling of early reflections were generated using a conventional hybrid method. All reflection orders up to and including the transition order were therefore modelled specularly. For the calculation of late reflections ray tracing continued but secondary diffuse sources instead of specular image sources were created at each subsequent surface reflection. These secondary sources were elemental area sources that radiated diffusely into the room from the point of reflection. After the generation of a secondary source the energy was re-grouped back into the primary ray that created it. This ray was then traced forward with a direction determined by Kuttruff's re-direction method. That is, a random number between zero and one was generated, if it was greater than the surface's diffusion coefficient the ray was reflected in a purely specular direction. Otherwise a reflection direction was randomly chosen from a distribution following Lambert's law.

## **4.2 Accuracy of input data**

In any assessment of predictive models the accuracy of the model's input data is of importance. The input data required for the computer models here divides into the following areas

- geometry
- absorption coefficients
- diffusion coefficients.

### **4.2.1 Geometry of enclosures**

Table 4.1 shows sources of geometrical data for each of the enclosures. For enclosures where full architectural drawings were available, detailed plan and sectional views gave accurate geometrical input data for the models.

For enclosures 2 and 6 only plan views were available so sectional geometry had to be measured or estimated. Enclosure 2 had a relatively simple rectangular geometry without a balcony. The height of the stage and its surrounding shell were measured but the height of the vaulted ceiling above the main auditorium had to be estimated. This estimation of

ceiling height is a recognised source of error but was not considered to unduly influence the predictions because the source positions used were located on the stage, which had its own low ceiling. Reflected sound energy from the vaulted ceiling was therefore not prominent in the measured responses because it mainly consisted of reflections greater than the second order that arrived relatively late, that is, mostly after 80 ms. Enclosure 6 had a large balcony at the rear of the hall that contained raked seating. It was therefore possible to measure the height of the balcony and reach the ceiling from the rear of the balcony to determine its height. The main estimated dimension in enclosure 6 was the height of the fly-tower. By viewing the external dimensions of the hall it was possible to see that the fly-tower was only slightly higher than the auditorium ceiling so this was used in the model. However, any errors in the estimated height of the fly-tower were not considered significant because it was lined with sound absorbent material and contained absorbent stage curtains, which reduced the influence of reflections from it.

Enclosure	Source of geometrical data
1	Full architectural drawings
2	Architectural plan, measurements and estimation
3	Measurements
4	Full architectural drawings
5	Full architectural drawings
6	Architectural plan, measurements and estimation
7	Full architectural drawings
8	Full architectural drawings

*Table 4.1 Sources of geometrical data*

No architectural drawings were available for enclosure 3 but the geometry was relatively simple and the dimensions were small and easily measured.

The geometries of enclosures was input into the computer program by creating plane surfaces using corner points: corner points were entered as 3-dimensional coordinates

and then linked together to form plane surfaces.

#### **4.2.2 Absorption coefficients of surfaces**

For enclosures 1, 4 and 5 measured absorption coefficients for seating areas were supplied by acoustic consultancies involved in the original design<sup>63,64</sup>. However, for other enclosures and surfaces measured absorption coefficients were not available. Values used were therefore mainly selected from an absorption coefficient library provided with the program or from literature<sup>65,66,67,68</sup>. This is a recognised source of potential inaccuracies but it is impossible to determine errors in values used without direct measurement of the absorption coefficients of actual materials, which was not possible due to financial constraints. However, since each enclosure contains several different surface treatments and enclosures differ from each other, negative and positive errors in coefficients used should average out when all enclosures are considered. Any analysis of predictive errors encountered in individual enclosures should account for absorption coefficient inaccuracies as a potential cause of problems.

#### **4.2.3 Diffusion coefficients of surfaces**

A standard method for measuring diffusion coefficients of surfaces does not currently exist. However, a current research programme<sup>69</sup> led by Dr T J Cox at the University of Salford is investigating this problem. For the purposes of this study model surfaces were therefore classified as either 'rough' or 'smooth'. This simplification has been used with some success in previous studies comparing predictions with scale model measurements<sup>70</sup>. A surface representing audience seating was considered highly diffusing or 'rough' and was assigned a high diffusion coefficient. A painted plaster surface or similar was considered 'smooth'.

Hodgson<sup>25</sup> noted that diffusion coefficients of surfaces should be frequency dependent but direct definition of coefficients in the frequency domain was not possible with the program used. However, by repeating calculations with different assigned diffusion coefficients the effect of changes at different frequencies could be assessed. To maximise the effect of this variation a transition order of zero was used (see section 4.3) so that

diffusion coefficients were used in the calculation of all reflection orders. For simplification, only 'smooth' surface diffusion coefficients were varied because in most of the enclosures studied the majority of surfaces were considered 'smooth'.

Research by Lam<sup>71</sup> indicated that diffusion coefficients of 0.1 and 0.7 were best suited for smooth and rough surfaces respectively and noted that a diffusion coefficient of 0.0 was not suitable for accurate predictions. These results were used as guide for the coefficients used in this study. A diffusion coefficient of 0.7 was therefore used for rough surfaces such as areas of seating. To study the influence of changes in diffusion coefficients those on smooth surfaces were varied between values of 0.05, 0.1, 0.2 and 0.4. Smooth rather than rough surface coefficients were varied because the majority of surfaces were considered smooth and many of the rough surfaces were highly absorptive so a stronger more discernible effect on predictions was expected.

### **4.3 Modelling of early reflections**

The importance of early reflections on the subjective impression of listeners has been noted by many acousticians<sup>72</sup> and has engendered the development of various objective acoustic parameters<sup>73,74,75</sup>. It was therefore considered important to investigate the effect of modelling early reflections using different techniques. This was possible with the program used because it had the capability to model early reflections using a specular method or by using diffuse secondary sources. This choice was determined by the program's transition order parameter. Therefore, predictions in each enclosure were made with transition order values of zero, one, three and five, with diffusion coefficients held at 0.1 and 0.7. With a transition order of zero, all reflections were modelled diffusely; with a transition order of five, the first five reflections were modelled specularly.

Table 4.2 summarises the combination of diffusion coefficients and transition orders employed for each enclosure model.

Ds, Dr	TO 0	TO 1	TO 3	TO 5
0.05, 0.7	✓	-	-	-
0.1, 0.7	✓	✓	✓	✓
0.2, 0.7	✓	-	-	-
0.4, 0.7	✓	-	-	-

*Table 4.2* Combination of diffusion coefficients and transition orders employed, Ds = Smooth surface diffusion coefficient, Dr = Rough surface diffusion coefficient, TO = transition order

## **Chapter 5**

# **Performance of the Hybrid Model**

### **5.1 Assessment of model performance**

The performance of the hybrid model was assessed by comparing its predictions of room acoustic parameters with measured values. These comparisons were analysed in two stages both of which are presented in this chapter.

In the first stage, presented in section 5.2, an overall indication of accuracy is given by comparing errors averaged over all receiver positions measured. For most of the parameters, this is eighty-five receiver positions over ten enclosures (including different enclosure configurations). For lateral energy fraction a separate measurement set-up was required so only forty-four receiver positions were compared. This overall view of comparisons gives an indication of the performance of the model for the prediction of various parameters at different frequencies and illustrates how changes in the way reflections are modelled influence average predictive accuracy.

However, the overall performance of the model does not illustrate what happens in individual enclosures. Therefore to understand the model's behaviour in detail, its

performance for each enclosure was examined at individual receiver positions. This second analysis stage is presented in section 5.3.

## 5.2 Overall prediction of room acoustic parameters

### 5.2.1 Prediction of reverberation time

The effect of transition order variation on the prediction of reverberation time is shown in table 5.1. Values shown are averaged over all receiver positions in all enclosures.

Frequency (Hz)	TO 0		TO 1		TO 3		TO 5	
	Mean Error (%)	Standard Deviation in Error (%)						
125	31.0	48.5	31.3	47.7	30.8	47.8	36.5	48.0
250	28.0	55.7	27.3	54.8	27.9	55.1	31.9	55.1
500	9.2	32.2	10.7	31.8	12.4	31.1	16.1	34.3
1000	0.6	25.4	2.9	25.7	5.9	24.9	9.0	26.8
2000	-0.9	22.2	1.2	22.2	4.3	22.5	7.0	23.6
4000	-0.4	20.5	1.7	21.1	3.8	22.3	8.1	22.2

Table 5.1 Effect of varying transition order on prediction of reverberation time ( $D_s = 0.1$ ,  $D_r = 0.7$ )

At low frequencies transition orders of zero, one and three produced similar average errors while at higher frequencies variation in transition order had a greater influence on results. Overall, a transition order of zero produced the smallest average errors. This is clearer at mid- to high frequencies while at lower frequencies transition orders of one and three resulted in similarly low errors. All transition orders produced similar standard deviations in errors. This indicates that, for the most reliable predictions of reverberation time, diffuse effects should be included for all reflections and not introduced at higher reflection orders.

Average errors were mostly positive, indicating over-prediction, and were only within a difference limit of 5% at 1000 Hz and above. For all transition orders investigated, errors at low frequencies were significantly higher than those at mid- and high frequencies. This decrease in accuracy at low frequencies is possibly attributable to other factors, which are considered in more detail in subsection 5.3.1.

The effect of smooth surface diffusion coefficient ( $D_s$ ) variation on the prediction of reverberation time is shown in table 5.2. Values shown are averaged over all receiver positions in all enclosures.

Frequency (Hz)	Ds 0.05		Ds 0.1		Ds 0.2		Ds 0.4	
	Mean Error (%)	Standard Deviation in Error (%)						
125	63.7	109.3	31.0	48.5	34.5	48.8	25.2	47.7
250	72.4	142.3	28.0	55.7	30.9	57.9	23.8	56.4
500	56.8	170.3	9.2	32.2	13.0	44.4	5.9	34.5
1000	32.0	110.3	0.6	25.4	1.6	28.7	-3.0	26.5
2000	20.4	69.6	-0.9	22.2	-0.4	19.6	-3.7	21.6
4000	12.3	39.4	-0.4	20.5	0.6	17.4	-1.6	20.3

Table 5.2 Effect of varying diffusion coefficient on prediction of reverberation time ( $T_0 = 0$ ,  $D_r = 0.7$ )

At low to mid-frequencies a diffusion coefficient of 0.4 on average produced the most reliable predictions with the smallest errors and the lowest standard deviations in errors. A diffusion coefficient of 0.05 resulted in high average errors and standard deviations. However, at higher frequencies lower diffusion coefficients of 0.1 and 0.2 produced the most reliable predictions. As with predictions shown with variation of transition order, only average errors at 1000 Hz and above were within a difference limen of 5%. However, a notable decrease in low frequency errors did occur when smooth surface diffusion coefficients were increased. This indicates that, for prediction of reverberation time, smooth surface diffusion coefficients should be defined in the frequency domain with higher values at low frequencies and lower values at high frequencies. One of the reasons for needing higher smooth surface diffusion coefficients at low frequencies is that the wavelengths of sound at these frequencies are comparable to many of the reflecting surface dimensions. This means scattering of sound occurs from surface edge diffraction and the assumptions of geometrical sound reflection become invalid. Factors affecting the prediction of room acoustic parameters at low frequencies are discussed further in subsection 5.3.1

At mid- to high frequencies a smooth surface diffusion coefficient of 0.1 or 0.2 produced the smallest average errors, which agrees with similar previous findings by Lam<sup>38</sup>. A

lower coefficient of 0.05 produced over-predictions while a higher diffusion coefficient of 0.4 produced under-predictions. A possible explanation for this is that as diffusion coefficients are increased the randomization of ray directions is increased. On average this results in more energy being more evenly distributed around an enclosure which means more energy is incident upon absorptive areas, such as seating. This causes a more rapid decay of energy in the modelled enclosure and consequently shorter reverberation time predictions. This agrees with research by Hodgson that concluded that in rooms with only specularly reflecting surfaces the rate of sound decay is less than that predicted by Eyring theory.

### 5.2.2 Prediction of sound strength

Frequency (Hz)	TO 0		TO 1		TO 3		TO 5	
	Mean Error (dB)	Standard Deviation in Error (dB)						
125	6.5	5.8	6.6	5.8	6.8	5.8	6.6	5.7
250	2.6	4.2	2.7	4.1	2.9	4.1	2.8	4.1
500	1.4	3.2	1.6	3.2	1.8	3.2	1.7	3.2
1000	0.6	2.7	0.8	2.7	1.1	2.6	1.0	2.6
2000	-0.0	2.4	0.2	2.4	0.4	2.3	0.4	2.3
4000	0.5	2.5	0.8	2.6	1.0	2.6	1.0	2.6

Table 5.3 Effect of varying transition order on prediction of sound strength ( $D_s = 0.1$ ,  $D_r = 0.7$ )

Table 5.3 and table 5.4 show average errors in the prediction of sound strength with variation in transition order and diffusion coefficient respectively. Values shown are averaged over all receiver positions in all enclosures.

As with reverberation time the introduction of diffusion from the first reflection by use of a transition order of zero produced the smallest errors. However, variation of transition order did not have a large influence on the errors produced: a transition order of five resulted in mean errors only a fraction of a decibel above those produced using a transition order of zero. This is probably because the sound strength is determined from the energy received in the whole decay so variation in the way the first few reflection orders are calculated has little influence. This also explains the marginal influence of diffusion coefficient variation on the prediction of sound strength shown in

table 5.4.

Frequency (Hz)	Ds 0.05		Ds 0.1		Ds 0.2		Ds 0.4	
	Mean Error (dB)	Standard Deviation in Error (dB)						
125	6.4	5.9	6.5	5.8	6.4	5.9	6.3	5.9
250	2.6	4.2	2.6	4.2	2.5	4.2	2.4	4.3
500	1.4	3.2	1.4	3.2	1.4	3.2	1.2	3.3
1000	0.6	2.7	0.6	2.7	0.6	2.7	0.4	2.8
2000	-0.1	2.4	-0.0	2.4	0.0	2.4	-0.2	2.5
4000	0.5	2.6	0.5	2.5	0.6	2.6	0.4	2.7

Table 5.4 Effect of varying diffusion coefficient on prediction of sound strength (TO = 0, Dr = 0.7)

### 5.2.3 Prediction of early decay time

The effect of transition order variation on the prediction of early decay time is shown in table 5.5. Values shown are averaged over all receiver positions in all enclosures.

As early decay time is calculated in a similar manner to reverberation time it is useful to compare the resulting errors from their respective predictions. Reverberation time is determined from the slope of the decay between the -5 dB point and the -35 dB point; early decay time is determined from the slope of the decay from the 0 dB point to the -10 dB point. The accuracy of early decay time predictions is therefore affected more by the modelling of early reflections. This is apparent from the values shown in table 5.5, which vary more with transition order than equivalent values for reverberation time (see table 5.1).

Frequency (Hz)	TO 0		TO 1		TO 3		TO 5	
	Mean Error (%)	Standard Deviation in Error (%)						
125	26.9	60.8	23.3	60.5	20.1	56.5	24.7	59.4
250	21.1	60.7	17.1	60.0	15.2	58.9	15.9	60.6
500	-1.1	40.0	-3.0	39.2	-5.2	39.1	-5.5	46.4
1000	-3.5	34.1	-4.4	36.0	-9.2	33.6	-9.6	41.4
2000	-5.2	31.1	-6.6	33.6	-12.4	27.4	-15.0	30.6
4000	-4.6	31.2	-6.1	34.0	-14.1	27.1	-18.1	28.8

Table 5.5 Effect of varying transition order on prediction of early decay time (Ds = 0.1, Dr = 0.7)

The standard deviations in errors for early decay time predictions were also notably higher than for reverberation time predictions. This is possibly because any variations in determination of the slope of the 10 dB decay are multiplied by six to calculate early decay time, whereas for reverberation time the slope is determined over a 30 dB range and any variations are only doubled.

As with reverberation time, the smallest average errors at mid- to high frequencies occurred with a transition order of zero indicating that the modelling of diffusion should be included in all reflection orders. At low frequencies a transition order of three produced the smallest errors. This is probably because the introduction of specular reflections decreases the gradient of the energy decay, which at low frequencies is steeper than it should be due to other factors (see subsection 5.3.1). If these other factors were removed, the predicted decay at low frequencies would possibly also require the introduction of diffuse modelling from the first order reflection.

At low frequencies average errors in the prediction of early decay time were smaller in magnitude than for reverberation time. Average errors at mid- to high frequencies were generally larger in magnitude and were all negative, showing under-predictions. This differs from reverberation time, where average errors mainly showed over-predictions. This indicates possible problems with the prediction of early energy and suggests that the early part of the modelled energy decay slope is too steep. The modelling of this early energy is investigated in more detail in subsection 5.3.2.

The effect of changing the diffusion coefficient of smooth surfaces ( $D_s$ ) on the prediction of early decay time is shown in table 5.6. Values shown are averaged over all receiver positions in all enclosures.

As with reverberation time, a diffusion coefficient of 0.4 produced the lowest average errors at low to mid-frequencies and lower coefficients were more suited to higher frequency predictions. This again highlights the need for diffusion coefficients to be defined in the frequency domain.

Frequency (Hz)	Ds 0.05		Ds 0.1		Ds 0.2		Ds 0.4	
	Mean Error (%)	Standard Deviation in Error (%)						
125	34.6	61.4	26.9	60.8	26.5	56.9	23.6	57.6
250	37.0	79.2	21.1	60.7	21.8	58.3	19.8	58.2
500	17.2	87.2	-1.1	40.0	1.0	41.4	-0.4	38.0
1000	11.7	71.1	-3.5	34.1	-1.5	35.0	-2.1	31.9
2000	0.4	35.9	-5.2	31.1	-3.6	28.9	-3.3	29.2
4000	-4.0	29.2	-4.6	31.2	-1.5	29.3	-2.0	29.5

Table 5.6 Effect of varying diffusion coefficient on prediction of early decay time (TO = 0, Dr = 0.7)

#### 5.2.4 Prediction of clarity index

Predictions of clarity index using various transition orders are shown in table 5.7. Values shown are averaged over all receiver positions in all enclosures. As with reverberation time the choice of transition order used for low frequency predictions was not so critical with transition orders of zero, one and three producing similar average errors. This is possibly because factors other than transition order cause much of the errors encountered at low frequencies.

Frequency (Hz)	TO 0		TO 1		TO 3		TO 5	
	Mean Error (dB)	Standard Deviation in Error (dB)						
125	-0.3	2.8	0.1	2.9	0.7	2.9	1.0	3.2
250	-0.7	2.9	-0.3	2.8	0.3	2.9	0.6	3.2
500	-0.1	2.4	0.2	2.4	0.9	2.6	1.3	3.0
1000	-0.1	2.2	0.2	2.2	0.9	2.5	1.4	2.9
2000	-0.0	2.0	0.3	2.1	1.1	2.2	1.6	2.7
4000	-0.1	1.9	0.2	2.1	1.1	2.4	1.6	2.9

Table 5.7 Effect of varying transition order on prediction of clarity index (Ds = 0.1, Dr = 0.7)

At mid- to high frequencies average errors using transition orders of zero and one were within a difference limen of 0.5 dB. As with reverberation time and early decay time, this indicates that diffusion should be accounted for in the modelling of early reflection orders.

Frequency (Hz)	Ds 0.05		Ds 0.1		Ds 0.2		Ds 0.4	
	Mean Error (dB)	Standard Deviation in Error (dB)						
125	-0.4	2.9	-0.3	2.8	-0.4	2.9	-0.4	2.9
250	-0.9	2.8	-0.7	2.9	-0.8	2.8	-0.9	2.6
500	-0.3	2.5	-0.1	2.4	-0.3	2.2	-0.3	2.1
1000	-0.2	2.4	-0.1	2.2	-0.2	2.0	-0.2	1.9
2000	-0.1	2.1	-0.0	2.0	-0.2	1.9	-0.2	2.0
4000	-0.2	1.9	-0.1	1.9	-0.4	2.0	-0.4	2.0

Table 5.8 Effect of varying diffusion coefficient on prediction of clarity index (TO = 0, Dr = 0.7)

The influence of smooth surface diffusion coefficient changes on the prediction of clarity index is shown in table 5.8. Unlike with variation of transition order only slight changes occurred in the average errors for different diffusion coefficients. A diffusion coefficient of 0.1 produced the smallest average errors but for all the coefficients studied all mid- and high frequency average errors were within the difference limen of 0.5 dB. This is possibly because the calculation of clarity index considers the balance between energy arriving in the first 80 ms and energy arriving after 80 ms. Any differences in the way reflections are modelled will therefore be balanced as long as they affect all reflection orders, which with a transition order of zero is the case.

### 5.2.5 Prediction of *deutlichkeit*

Average errors in the prediction of *deutlichkeit* using various transition orders are shown in table 5.9. Values shown are averaged over all receiver positions in all enclosures. As with other parameters studied, introducing diffusion from the first reflection on average produced the smallest errors. However, these average errors were still greater than the difference limen of 5%. The average errors produced were all positive indicating over-prediction of *deutlichkeit*. As with the under-prediction of early decay time, this is probably because of errors in the modelling of early energy. This is discussed further in subsection 5.3.2.

Frequency (Hz)	TO 0		TO 1		TO 3		TO 5	
	Mean Error (%)	Standard Deviation in Error (%)						
125	35.0	89.3	47.5	94.5	58.3	103.7	59.8	101.2
250	5.3	58.2	13.3	57.9	20.0	62.5	23.3	67.2
500	9.1	83.4	16.8	76.0	23.3	82.9	26.0	87.1
1000	9.1	84.1	17.6	77.3	23.3	83.0	25.4	86.4
2000	8.9	79.4	17.3	71.8	22.3	76.7	24.2	79.5
4000	5.4	60.7	14.2	55.4	18.5	58.7	20.1	61.3

Table 5.9 Effect of varying transition order on prediction of deutlichkeit (Ds = 0.1, Dr = 0.7)

As with the prediction of clarity index, average errors in the prediction of deutlichkeit varied only slightly with variation in smooth surface diffusion coefficients. This is shown in table 5.10. The calculation of deutlichkeit balances early and late energies, in a similar manner to clarity index, . Therefore, if errors occur consistently throughout the energy decay they will often cancel out in the final calculation.

Frequency (Hz)	Ds 0.05		Ds 0.1		Ds 0.2		Ds 0.4	
	Mean Error (%)	Standard Deviation in Error (%)						
125	36.4	92.5	35.0	89.3	32.8	88.6	30.4	87.5
250	4.4	57.8	5.3	58.2	3.7	56.2	0.8	52.7
500	9.4	84.8	9.1	83.4	8.3	81.4	6.5	76.9
1000	9.7	86.3	9.1	84.1	8.7	82.5	8.2	78.3
2000	9.7	79.7	8.9	79.4	8.3	77.1	7.9	73.8
4000	6.4	60.2	5.4	60.7	4.1	59.5	4.3	57.1

Table 5.10 Effect of varying diffusion coefficient on prediction of deutlichkeit (TO = 0, Dr = 0.7)

### 5.2.6 Prediction of centre time

As with clarity index and deutlichkeit, centre time is used to describe the balance between early and late energy at a receiver. However, its calculation does not rely on a 'temporal-divider' and its value is not as strongly affected by the prediction of early reflections. This is considered in more detail in subsection 5.3.3.

Frequency (Hz)	TO 0		TO 1		TO 3		TO 5	
	Mean Error (ms)	Standard Deviation in Error (ms)						
125	21.7	84.3	13.3	82.9	8.7	82.3	10.0	83.7
250	34.8	110.8	27.6	108.8	23.5	109.2	23.5	110.0
500	9.8	66.2	3.3	63.0	-0.7	62.4	-2.3	64.5
1000	3.8	53.2	-2.3	50.5	-6.6	49.9	-8.0	51.9
2000	1.0	44.6	-5.2	42.6	-9.3	42.3	-10.6	43.9
4000	-3.8	32.0	-8.9	31.1	-12.4	31.0	-13.6	32.2

Table 5.11 Effect of varying transition order on prediction of centre time ( $D_s = 0.1$ ,  $D_r = 0.7$ )

Average errors in the prediction of centre time with different transition orders are shown in table 5.11. Values shown are averaged over all receiver positions in all enclosures. The variation in these was small when compared to a difference limen of 10 ms. As with prediction of sound strength this is probably because the whole energy decay is used to determine centre time so changes in the way the first few reflection orders are modelled has a marginal affect on the predictive errors.

Frequency (Hz)	Ds 0.05		Ds 0.1		Ds 0.2		Ds 0.4	
	Mean Error (ms)	Standard Deviation in Error (ms)						
125	26.9	82.8	21.7	84.3	19.8	79.6	17.9	80.4
250	41.5	108.8	34.8	110.8	31.8	106.7	31.6	106.7
500	15.4	72.3	9.8	66.2	6.9	62.0	7.1	62.1
1000	9.6	61.5	3.8	53.2	1.0	48.7	0.8	49.4
2000	4.6	47.6	1.0	44.6	-0.8	41.7	-1.2	42.5
4000	-2.9	32.0	-3.8	32.0	-2.9	32.4	-3.8	31.9

Table 5.12 Effect of varying diffusion coefficient on prediction of centre time ( $TO = 0$ ,  $Dr = 0.7$ )

As with other energy-balance parameters, changes in the diffusion coefficients of smooth surfaces were found to only marginally affect the average errors in the prediction of centre time. This is shown in table 5.12. At mid- to high frequencies all diffusion coefficients investigated produced average errors within a difference limen of 10 ms.

### 5.2.7 Prediction of lateral energy fraction

Lateral energy fraction is more complicated to predict than standard energy decay parameters because the direction as well as the time of sound arriving at a receiver must

be known. Its determination involves the use of a temporal-divider, similar to those in the calculation of clarity index and *deutlichkeit*, and as with early decay time it is only used to describe the early part of an energy decay.

Average errors and standard deviations of errors in the prediction of lateral energy fraction are shown in table 5.13. Values shown are averaged over all receiver positions in all enclosures. Only average errors from some of the predictions using a transition order of three were within the difference limen of 5%. This is notably different from average errors in other parameter predictions where transition orders of zero and one have often produced the smallest errors. This suggests the use of diffuse secondary sources for the modelling of reflections causes problems with the determination of reflection directivities.

Frequency (Hz)	TO 0		TO 1		TO 3		TO 5	
	Mean Error (%)	Standard Deviation in Error (%)						
250	37.9	61.5	26.9	54.5	11.3	54.0	89.1	232.0
500	24.8	52.3	16.2	42.5	2.8	47.2	114.9	253.0
1000	16.6	43.6	7.7	35.3	-4.9	38.1	48.6	176.7
2000	41.5	57.7	32.0	53.1	14.1	52.5	120.2	266.1
4000	21.6	48.6	12.8	44.8	-4.5	40.6	103.2	223.4

Table 5.13 Effect of varying transition order on prediction of lateral energy fraction ( $D_s = 0.1$ ,  $D_r = 0.7$ )

With a transition order of zero all reflections are modelled using diffuse secondary sources, which scatter reflected energy according to Lambert's cosine law. This causes additional lateral energy to arrive at receivers from reflections that would not be received in reality. With a transition order of one, the first order reflections are modelled specularly and the average errors reduce. A further improvement in average predictive accuracy occurs when the first three reflections are modelled geometrically. However, using a transition order of five produces large errors and considerable standard deviations in errors. This is possibly because modelling the first five reflection orders specularly ensures that very little, if any, diffuse energy is received before 80 ms (the temporal cut-off used in the calculation of lateral energy fraction). The modelled early sound field therefore largely consists of specular rays, which may not produce a

sufficient spatial density of energy for reliable prediction of lateral energy fraction.

Specific predictions of lateral energy fraction using various transition orders are considered in more detail in subsection 5.3.4.

Frequency (Hz)	Ds 0.05		Ds 0.1		Ds 0.2		Ds 0.4	
	Mean Error (%)	Standard Deviation in Error (%)						
250	40.4	61.8	37.9	61.5	38.7	60.5	36.3	58.8
500	25.4	45.6	24.8	52.3	24.1	44.1	22.0	43.8
1000	17.7	40.1	16.6	43.6	16.9	41.6	14.3	40.6
2000	43.3	56.8	41.5	57.7	41.9	57.5	39.0	55.7
4000	23.5	47.3	21.6	48.6	22.3	47.8	20.1	46.4

Table 5.14 Effect of varying diffusion coefficient on prediction of lateral energy fraction (TO = 0, Dr = 0.7)

Changes in smooth surface diffusion coefficients only slightly alter the average errors of lateral energy fraction predictions as shown in table 5.14. This is because lateral energy fraction is a measure of the balance between early lateral energy and early omnidirectional energy. These are affected similarly by changes in the way reflections are modelled meaning the balance between them changes only slightly.

## **5.3 A more detailed view of predictive accuracy**

### **5.3.1 Factors affecting low frequency accuracy**

Many of the average errors presented in section 5.2 were larger at low frequencies than at mid- and high frequencies. This indicates that additional factors may affect accuracy at low frequencies that are not present at higher frequencies. When individual enclosures were investigated it was found that five of the ten configurations used had notably larger errors at low frequencies. These were enclosures 2, 3, 4, 6 and 7, which all had over-predicted low frequency reverberation times. However, these enclosures were not similar, so this pattern cannot be attributed to similarities in their design. Failure to account for the following features may be responsible for error increases encountered in these enclosures at low frequencies

- Additional low frequency absorption
- Dimensions of reflecting surfaces
- Interference

The first of these is an input data problem that could occur with any model and was probably the cause of over-predicted reverberation times in enclosure 6 and partly responsible for errors in enclosure 2. In enclosure 6 there were two areas that may have provided more sound absorption at low frequencies than initially expected. Firstly the side walls contained windows that were difficult to estimate an absorption coefficient for; the sound insulation and consequent 'absorption' provided by windows is often dependent on their dimensions<sup>76</sup> and since absorption coefficients were chosen from standard coefficient libraries these were not accounted for. Secondly the rear stalls 'wall', which consisted of a series of sliding wooden doors separating an empty storage area, was considered to have poor sound insulation, particularly at low frequencies, which caused sound energy to escape from the enclosure and provide additional low frequency absorption.

In enclosure 2 reverberation times at 125 Hz were over-predicted on average by 130%. This was possibly caused by a combination of absorption coefficient errors and a failure

to account for the dimensions of reflecting surfaces. Unlike other enclosures investigated, there was no absorptive seating present in enclosure 2 so the absorption coefficients assigned to walls and other 'reflective' surfaces were more influential. For example, in a room with reflective walls and a floor covered with absorptive seating changes in the absorption coefficients of the walls would have little influence because the energy decay would be controlled by the absorptive seating. In a room with only reflective surfaces, a change in assigned absorption coefficients from 0.04 to 0.08 would result in an approximate halving of the reverberation time. In enclosure 2 the walls were finished with plaster on laths, the auditorium floor was wooden and the side walls contained windows. As with enclosure 6, the absorption provided by windows is thought to be dimensionally dependent so additional low frequency absorption could have been present in the real enclosure that was not accounted for in the computer model. The backing behind the plaster-on-laths wall finishing was also unknown. If the laths were attached to studwork, an air-gap would have been present between the plaster on laths and the solid wall, which would act as a panel absorber and provide additional low frequency absorption that was not included in the model<sup>66</sup>. Similarly, the structure under the floor was not known, this may also have contained an air space, which could have affected the low frequency absorption provided by the floor. The curved geometry of the barrel-vaulted ceiling may also have caused errors in predictions at low frequencies; this is discussed below.

A second cause of low frequency errors is possibly the modelling of reflections from surfaces that have dimensions comparable to the wavelengths of low frequency sound. This possibly contributed to low frequency errors in enclosure 2 and probably caused much of the low frequency errors observed in enclosures 4 and 7. These enclosures contained curved surfaces that had to be modelled using combinations of small plane surfaces. In geometrical acoustics, the size of the reflecting surface is not considered (see section 2.1), meaning reflections from small surfaces are modelled as those from large surfaces, that is, they have exaggerated strength. At low frequencies this is particularly inaccurate since in reality small surfaces act as diffusers rather than reflectors. This suggests that low frequency reflections were not attenuated to the same extent as in real

enclosures, which contributed to the over-prediction of reverberation times.

Interference effects cannot be predicted directly by an energy-based model such as the one used in this study and this probably caused low frequency errors observed in predictions from enclosure 3. This enclosure was geometrically unique among those studied: having fewer surfaces, a smaller volume, a horizontal floor and a low ceiling. This caused the sound propagation to be predominantly close to grazing incidence across the seating. Predictions of reverberation time using a transition order of zero with diffusion coefficients of 0.1 and 0.7 are compared with measured values for this enclosure in Figure 5.1. This shows that the measured reverberation times in the 250 Hz

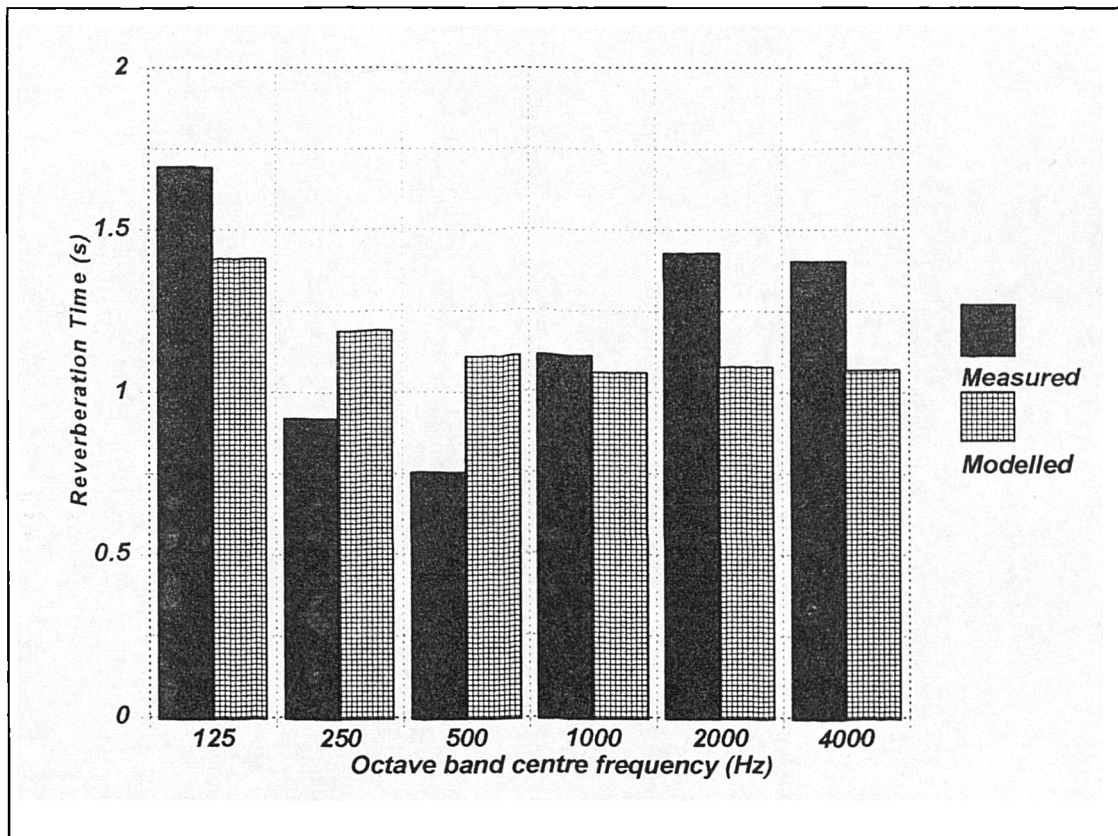


Figure 5.1 Measured and modelled results at receiver 7 in enclosure 3 (TO = 0, D<sub>s</sub> = 0.1, D<sub>r</sub> = 0.7)

and 500 Hz octave bands were notably lower than at other frequencies. This is possibly caused by an interference phenomena known as the 'seat-dip effect'. This effect was first quantified by researchers in the 1960's<sup>77,78</sup> and is caused when grazing incidence sound is reflected from rows of seats with a phase shift of 180°. This reflected sound

destructively interferes with the direct sound propagating above the seating<sup>4</sup>. More recent research<sup>79</sup> has shown that the effect varies over time and is influenced by many small reflections from seats and floors in addition to the width of seating blocks. This suggests that the modelling of seating surfaces by use of plane surfaces may also be inappropriate.

### 5.3.2 Modelling of the early energy decay

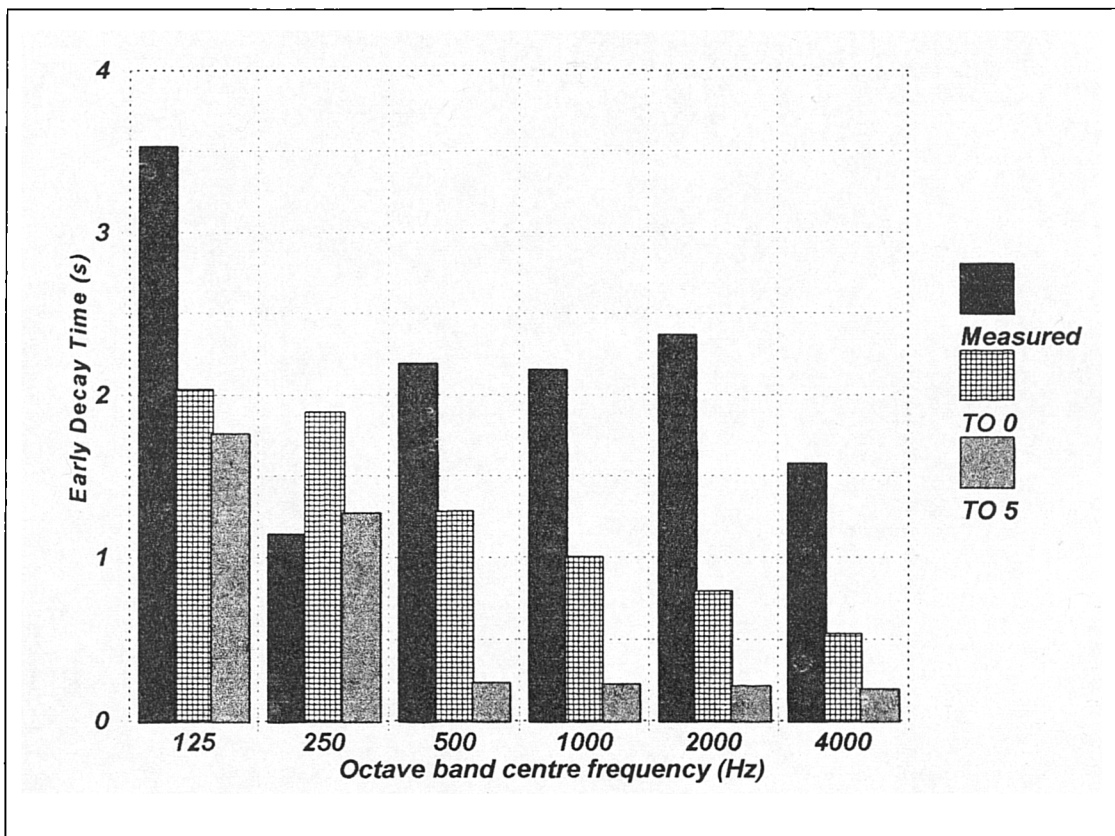


Figure 5.2 Measured and modelled early decay times at receiver 7 in enclosure 7 ( $D_s = 0.1$ ,  $D_r = 0.7$ )

Average errors in the prediction of early decay time, shown in subsection 5.2.3, indicated that the modelling of early energy decays was too steep. This particularly occurred when initial reflections were modelled specularly, which led to significant under-predictions of early decay times. A specific example of this is illustrated in Figure 5.2, which shows measured and predicted early decay times at receiver 7 in enclosure 7. The predicted results are from a model using diffuse secondary sources for all reflections (TO 0) and from a model using specular reflections up to the fifth order (TO 5). This receiver was

located in the upper choir seating behind the stage. The seat-dip effect occurred in the 250 Hz band, which, as discussed in section 5.3.1, was not accounted for in the models so that early decay time was over-predicted. However, at other frequencies, both diffuse and specular models under-predicted early decay time. This was probably caused by early energy being too strong in both cases. With reflections modelled by diffuse secondary sources additional early energy is thought to have arrived from surfaces which did not contribute to the measured response; with reflections modelled specularly the lack of scattering caused individual reflections to be too strong. Receiver 7 was located in the upper choir seating behind the stage and as such was relatively close to the source. After the initial strong reflections there was a considerable delay before other reflections arrived due the large size of enclosure 7. The early decay was therefore largely determined by the direct sound and the initial reflections, if either of these were too strong the early decay would have had a steeper gradient and therefore a shorter early decay time.

### **5.3.3 Prediction of 'energy-balance' parameters**

Predictions of clarity index in enclosure 7, using various transition orders, are shown with measured values in figure 5.3. At receiver 1 a difference of approximately 7 dB occurred between the predictions made using transition orders of zero and five. This receiver was situated on the stage at a distance of 4.5 m from the source and its measured impulse response was dominated by the direct sound with reinforcement from a first order reflection from the stage floor. With diffuse secondary source reflections the predicted clarity index was 1 dB lower than that measured. When the first order reflections were modelled specularly the predicted value increased by 1.5 dB. This illustrates that the real reflection was partially scattered since the diffuse secondary source reflection was not strong enough and the specular reflection directed too much energy towards the receiver. The transition order five model significantly over-predicted at this position because the first secondary source reflection did not arrive until 113 ms. Before this only the direct sound and stage reflection arrived, since this also occurred for the other transition order models, the modelled energy after 80 ms must have decreased. It is therefore thought that the lack of secondary source energy between 80 ms and

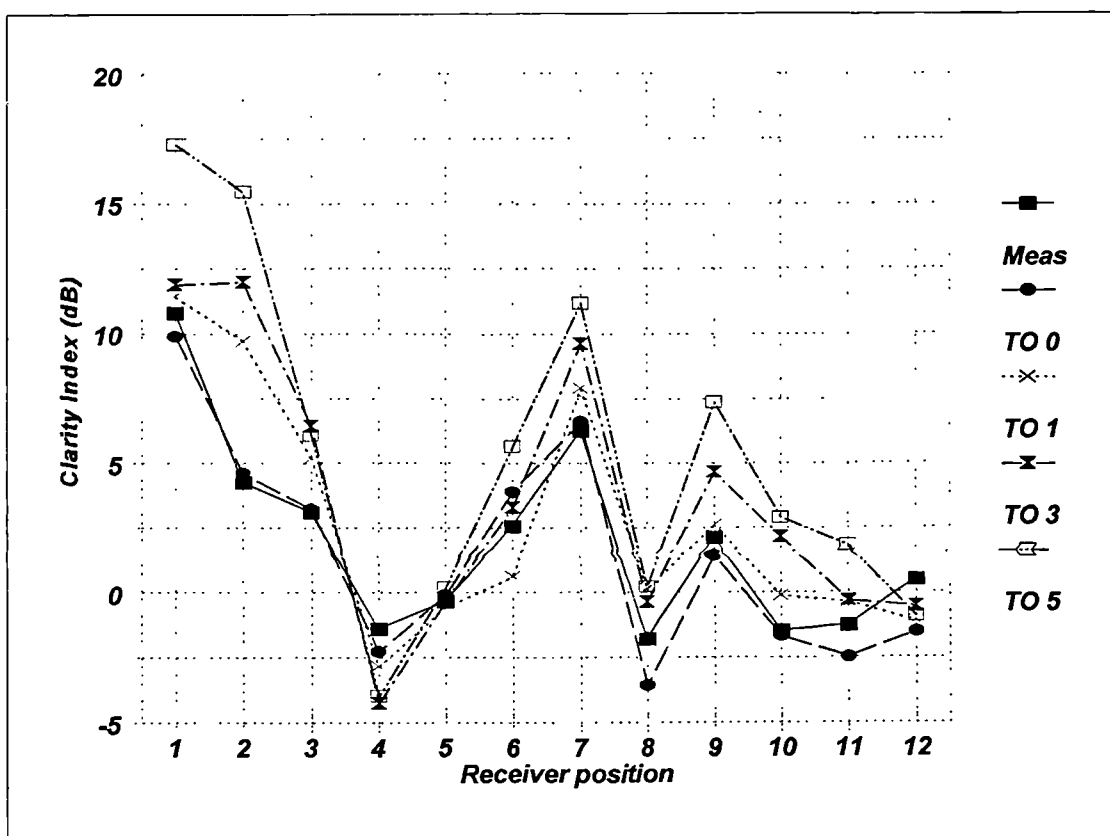


Figure 5.3 Measured and predicted clarity index at 1000 Hz in enclosure 7 ( $D_s = 0.1$ ,  $D_r = 0.7$ )

113 ms was not compensated for by additional specular reflections (with reflection orders of 3, 4 and 5) arriving after 80 ms. Increasing the ray density in the model may have reduced this error but this was not possible because of computer memory limitations.

At most receivers, clarity index predictions increased as the transition order was increased. However, at receiver 4 the opposite effect occurred and at receivers 5 and 12 the transition order had little effect on the predictions. Receiver 4 was located in the rear stalls, approximately 30 m from the source. Transition orders of zero and one produced predictions approximately 1 dB and 1.5 dB lower than measured respectively. Since only one first order reflection was received in the transition order one model, early energy received from secondary sources in the transition order zero model was not compensated for by the extra strength of the specular reflection. As with early decay time predictions at receiver 7 in enclosure 7, this suggests that, in the transition order zero model, energy arrives from reflections modelled by diffuse secondary sources that would not contribute

in reality and that this additional energy compensates for the weakness of the energy from individual diffuse secondary sources. Models using transition orders of three and five under-predicted the clarity index by 3 dB. This is thought to be because of the high ceiling in this enclosure - most of the early order reflections arrive 70 to 90 ms after the direct sound. This means that very little reflected energy arrives before 70 ms. With the lower transition orders this was partially compensated for by energy from secondary sources. At receivers 5 and 12, variation of transition order had little effect on the predicted clarity index. This is possibly because the high transition order models produce many specular reflections that are evenly spread throughout the early energy decays. These are therefore thought to compensate for loss of secondary source energy that arrives in the lower transition order models.

Figure 5.4 shows both measured and predicted *deutlichkeit* values in enclosure 5a.

At receivers 1, 2 and 3, which were close to the source, the direct sound dominated the energy in the first 50 ms. The predicted *deutlichkeit* values were therefore close to those measured and varied only slightly with transition order. At most positions, modelling all reflections using diffuse secondary sources produced the most accurate *deutlichkeit* predictions. However, the predicted values were still generally higher than those measured. This is thought to have been caused by additional energy arriving in the first 50 ms from reflections modelled by diffuse secondary sources located on surfaces that in reality would not contribute significant energy. However, specular modelling of early reflections, with higher transition orders, also over-predicted *deutlichkeit*. Therefore, since no scattering occurs reflections modelled specularly must be stronger than in reality.

At receiver 8 there was a wider difference between values predicted using diffuse secondary sources and those predicted using specular reflections than at other receiver positions. This was because receiver 8 was located in the stalls such that it was close to being equidistant from the two side walls. It therefore received a greater number of first order reflections than other receivers before the 50 ms threshold. For a transition order

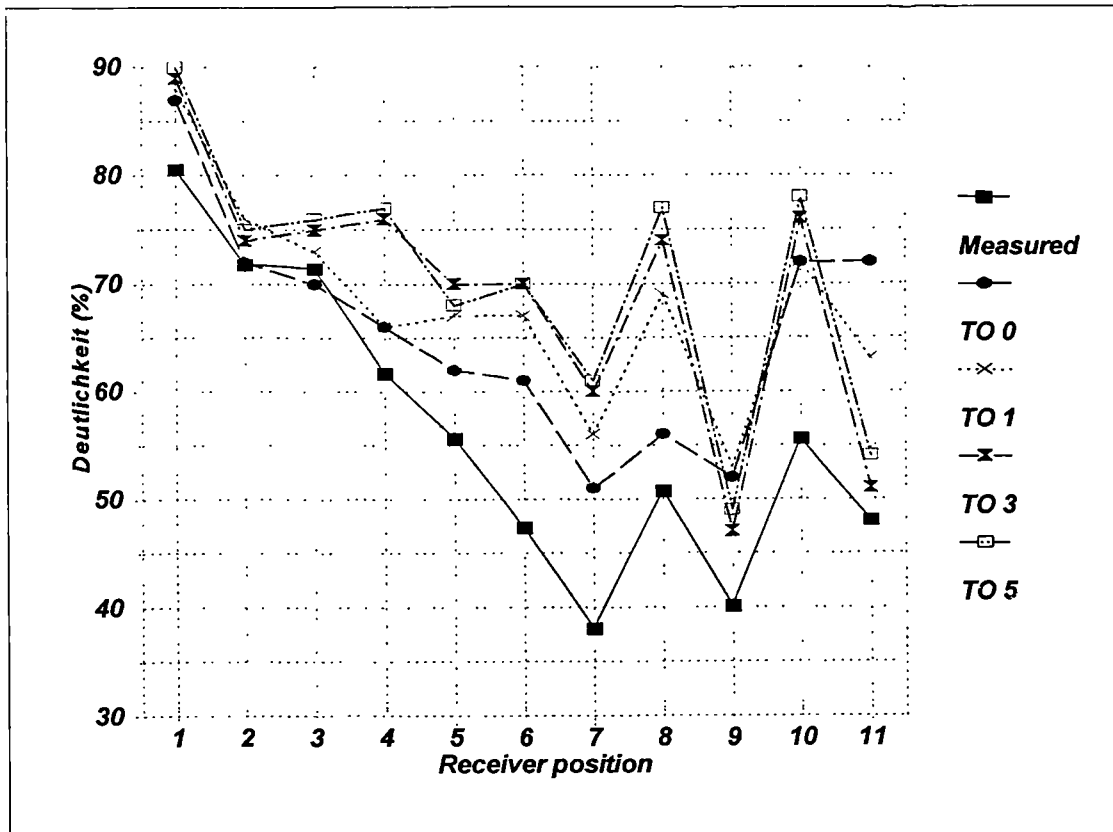


Figure 5.4 Measured and predicted Deutlichkeit at 1000 Hz in enclosure 5a ( $D_s = 0.1$ ,  $D_r = 0.7$ )

of zero these first order reflections were modelled using diffuse secondary sources, which contributed to the received energy along with other visible diffuse secondary sources around the enclosure. For a transition order of one, first order reflections were modelled geometrically and were stronger than in reality. As more first order reflections arrived at receiver 8 than at other receivers the effect of increasing the transition order from zero to one was more pronounced.

Deutlichkeit predictions at receivers 10 and 11 are interesting to compare since increasing the transition order had a different effect on each even though both were located close to each other, on the same side balcony. Receiver 10 was partially shielded from the source position used by a balcony front but a higher deutlichkeit was still measured at receiver 10 than at receiver 11. This was possibly because receiver 10 received reflections from orchestra reflectors (above the stage) before 50 ms. Whereas, for the source position used, receiver 11 was not in the reflection coverage area of the orchestra reflectors. With a transition order of zero deutlichkeit values for both receivers

were over-predicted and almost identical. This is because at receiver 10 the modelled direct sound was received without any shielding, which made it stronger than in reality. For receiver 11 modelled energy was received from diffuse secondary sources formed on the orchestra reflectors that were not received in reality. The modelled early energy at both receivers was therefore formed from the direct sound and diffuse secondary sources on the orchestra reflectors. However, with specular first order reflections the predicted *deutlichkeit* at receiver 11 decreased, while that at receiver 10 did not change. This decrease possibly occurred because with a transition order of zero, receiver 11 was irradiated by all visible diffuse secondary sources, which caused more energy to arrive before 50 ms. With a transition order of one these reflections were modelled specularly and were not directed towards receiver 11. An explanation for the predicted *deutlichkeit* values not changing at receiver 10 is that any first order reflections received with a transition order of zero were possibly weak and therefore not missed when not modelled by the transition order one model.

With a transition order of three the predicted value at receiver 10 increased; at receiver 11 it decreased to a value close to that measured. At receiver 10, only the direct sound was received before the first secondary source reflection arrived at approximately 45 ms. The *deutlichkeit* was therefore over-predicted because the measured effect from the balcony shielding was not modelled. For receiver 11, only the direct sound arrived before the first secondary source reflection occurred at 32 ms and the first specular reflection did not arrive until after 50 ms. Although the *deutlichkeit* prediction was relatively accurate, the energy prediction before 32 ms was possibly too low since only the direct sound was received, whereas in reality some sound scattered from surfaces and edges would inevitably have been received. From 32 ms to 50 ms the predicted energy is thought to have been too high because energy arrived from diffuse secondary sources that would not have arrived in reality. This combination of low and high predicted energy is thought to have balanced out over the first 50 ms leading to a relatively accurate prediction of *deutlichkeit*.

With a transition order of five, no specular or secondary source reflections arrived at

receivers 10 or 11 before 50 ms and the predicted *deutlichkeit* values were higher than those calculated by the transition order three model. This was therefore attributable to a decrease in the received energy after 50 ms, which was caused by fourth and fifth order reflections being modelled specularly in the transition order five model. With a transition order of three these reflections were modelled using diffuse secondary sources that, as discussed above, radiated to all visible receivers. However, as specular modelling produces over-strength reflections the reduction in energy after 50 ms was possibly caused by reflections not arriving at receiver 11. This suggests the modelled sound field was less diffuse when modelled by specular reflections.

In summary, comparisons so far have indicated that energy from individual secondary sources is too weak. This can be compensated for by additional energy arriving from other reflections modelled by secondary sources but these would not contribute in reality. Specular modelling has been found to produce over-strength individual reflections and a low resolution of energy density. This could be improved by increasing the number of rays but this would increase calculation times and was not possible in the program used because of computer memory limitations.

### 5.3.4 Directivity of reflected energy

Comparisons of average errors in the prediction of lateral energy fraction, shown in subsection 5.2.7, indicated that modelling the first three reflection orders on average produced the most accurate predictions and suggested that the scattering of sound from diffuse secondary sources may cause additional lateral energy to arrive at receivers that would not be received in reality.

Specific predictions of lateral energy fraction in enclosure 3 using various transition orders are shown in figure 5.5. In these a transition order of zero over-predicted lateral energy fraction at all receivers. This is probably because all reflections were modelled using secondary sources, which scatter energy more widely than in reality, thus producing more lateral energy at receivers. A schematic representation of two partially diffused first order reflections is shown in figure 5.6 where sound rays are scattered into solid angles of less than  $2\pi$  sr. This represents how sound energy was probably reflected from surfaces in the real enclosure 3. The receiver is shown with a figure-of-eight

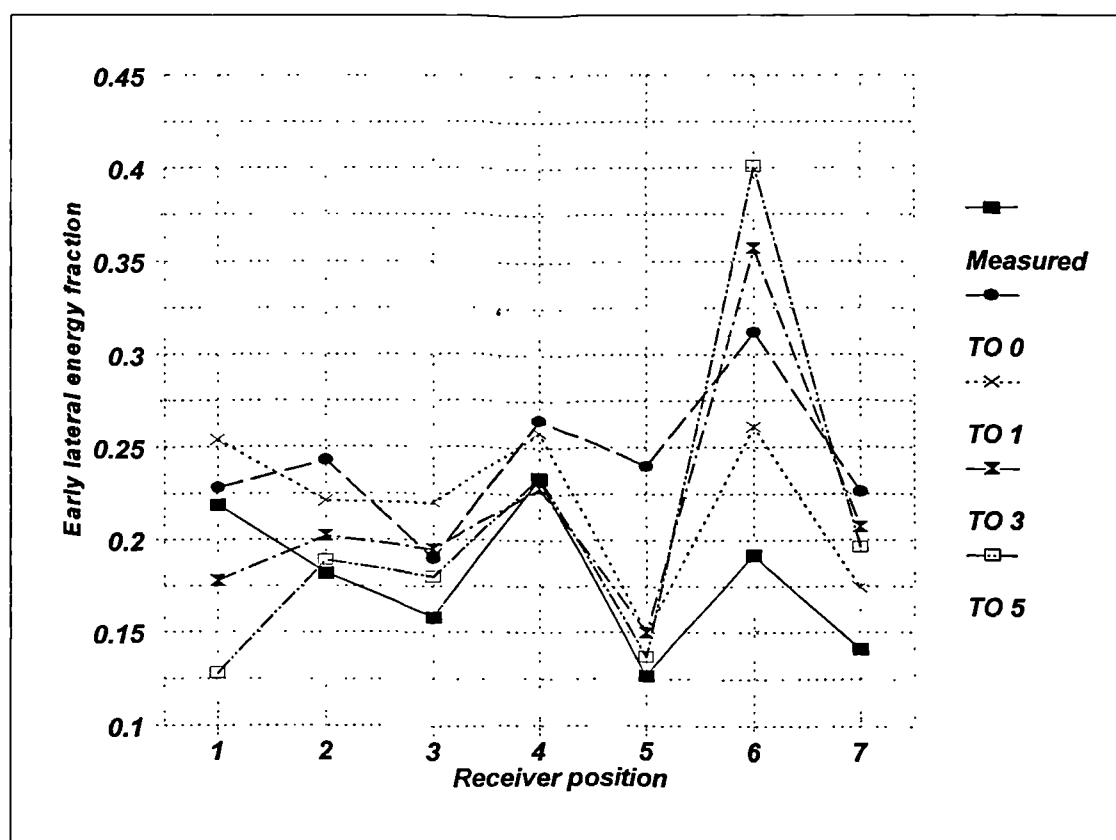


Figure 5.5 Lateral energy fraction at 1000 Hz in enclosure 3 ( $D_s = 0.1$ ,  $D_r = 0.7$ )

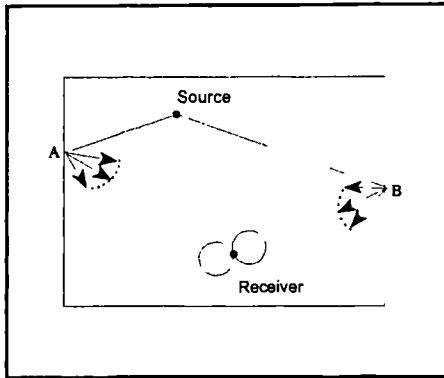


Figure 5.6 Scattered first order reflections into solid angles  $< 2\pi$  sr

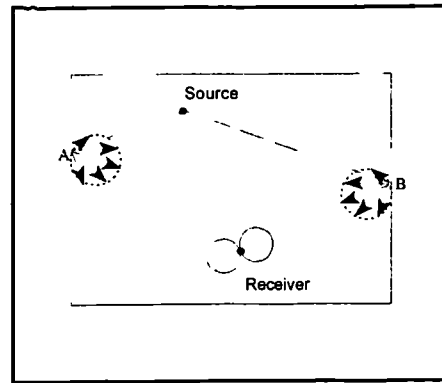


Figure 5.7 First order reflections modelled by diffuse secondary sources

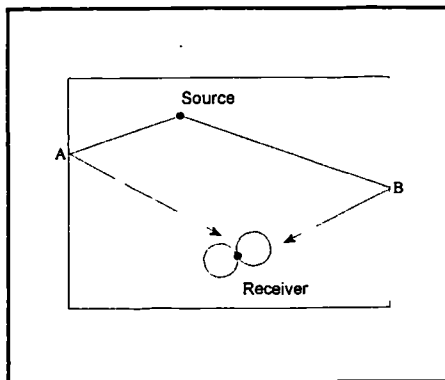


Figure 5.8 First order reflections modelled specularly

directivity for measurement of lateral energy fraction. Energy reflected from point A is directed in a solid angle towards the 'face' of the receiver with spatial spreading ensuring part of the energy is received laterally. Energy from point B is received laterally but spatial spreading directs part of the energy away from the receiver and weakens the specular reflection component.

Figure 5.7 shows equivalent reflections modelled using diffuse secondary sources where energy reflected from points A and B is directed into solid angles of  $2\pi$  sr with intensities proportional to  $\cos\theta$  in accordance with Lambert's law. This reduces the directivity of reflections and results in less spatially dependent lateral energy fractions, indicating increased diffusivity of the modelled sound field. This is illustrated by the transition order zero predictions shown in figure 5.5, which vary less with position than the measured values or those from other predictions: the measured values have a standard deviation of 0.036; the modelled values have standard deviations ranging from 0.035 for a transition order of zero to 0.085 for a transition order of five.

With a transition order of one first order reflections were modelled specularly. In enclosure 3 this resulted in similar predictions to those obtained using a transition order of zero for receivers 1 to 4. For receivers 5, 6 and 7, the predicted values were less than

those of the transition order zero model and were therefore more dependent upon first order reflections. Figure 5.8 shows a schematic representation of two first order reflections modelled specularly. Energy from point A is directed towards the 'face' of the receiver, while energy from point B is received laterally. This increases the directivity of reflections and the consequent spatial dependency of the resulting lateral energy fractions, indicating decreased diffusivity of the modelled sound field. Since diffuse secondary source modelling of first order reflections predicted higher lateral energy fractions at receivers 5, 6 and 7 than specular modelling, these positions probably received lateral energy from over-scattered reflections that were directed away from the receiver (or towards its face) when modelled specularly.

With models using transition orders of three and five, lateral energy fraction predictions at receivers close to the source were lower, and consequently more accurate, than predictions from models with lower transition orders. However, at receiver 6 the higher transition order models over-predicted lateral energy fraction significantly. This position must have therefore received strong specular reflections, of second order and above, from lateral directions in the model. With a transition order of one the energy received from these reflections was not so strong because it was modelled by diffuse secondary sources, which do not direct energy in a single direction.

Figure 5.9 shows predicted and measured lateral energy fraction values in octave bands for receiver 4 in enclosure 1a. For the predictions shown, diffusion coefficients of 0.1 and 0.7 were used.

Measured lateral energy fractions varied much more with frequency than other room acoustic parameters indicating directivity of reflections is frequency dependent. This was emphasised by the predicted results: modelling using diffuse secondary sources resulted in lateral energy fractions that varied only slightly with frequency as did those that used specular modelling up to the first three reflection orders. This was as expected since the directivities of both diffuse secondary sources and specular image sources are not frequency dependent. However, a transition order of five produced erroneous predicted

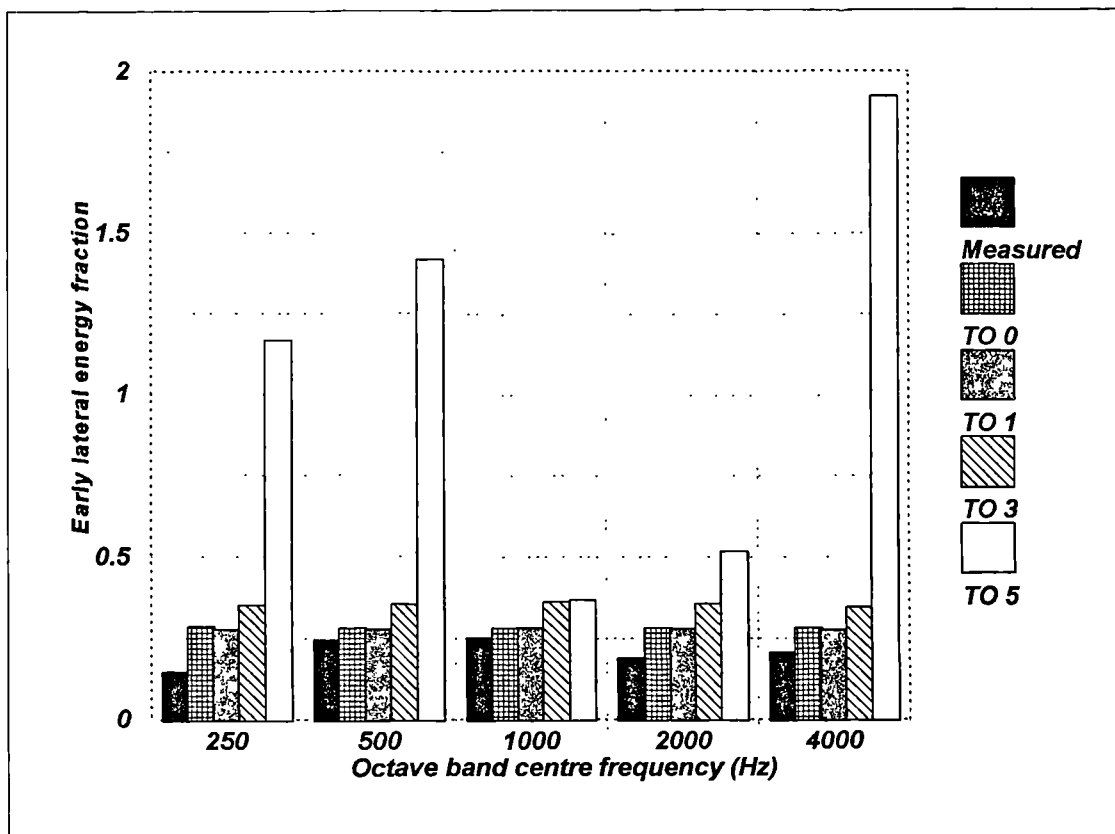


Figure 5.9 Measurement and predictions of LF at receiver 4 in enclosure 1a ( $D_s = 0.1$ ,  $D_r = 0.7$ )

values that were highly frequency dependent. The reason for these results is not clear, the same image sources and diffuse secondary sources were used for predictions in each band and none of the absorption coefficients varied with a similar frequency profile. Without full knowledge of the program's algorithms the cause of these errors is difficult to determine.

Analysis of average errors in lateral energy fraction predictions indicated that modelling the first three reflection orders specularly resulted in the most accurate predictions. However, by looking at specific predictions it is apparent that neither diffuse secondary sources nor specular reflections can be used to reliably determine the directional component of reflections. Diffuse secondary sources produce over-scattered weak reflections; specular modelling produces excessively directional over-strength reflections. Directivities of reflections therefore need to be accounted for in computer modelling and predicted results in octave bands indicate that these need to be defined in the frequency domain.

### 5.3.5 Modelling of barriers

A fall in predicted levels occurred on the balcony of enclosure 6, which did not occur in the measured levels. This is illustrated in figure 5.10 where predictions using a transition order of zero and diffusion coefficients of 0.1 and 0.7 are shown.

In particular, prediction accuracy fell for receiver positions 6 to 9 (at position 6 it reduced to almost -6 dB). While for receivers 1 to 5 the accuracy remained approximately within  $\pm 1$  dB. Receivers 6 to 9 were all situated on the rear balcony of the hall and were shielded, or at least partially shielded, from the source by the balcony front. In the measurements diffraction is thought to have occurred over the top of the balcony front, which subsequently scattered sound energy onto the balcony seats. In the computer model this was not accounted for; the direct sound was a ray that was simply reflected when it met the balcony front. This difference between the real and modelled shielding was further magnified because the source used in the measurements was a dodecahedron with a diameter of 0.5 m, that is, not a dimensionless point source. This means that sound from the top of the real source could have radiated to receivers

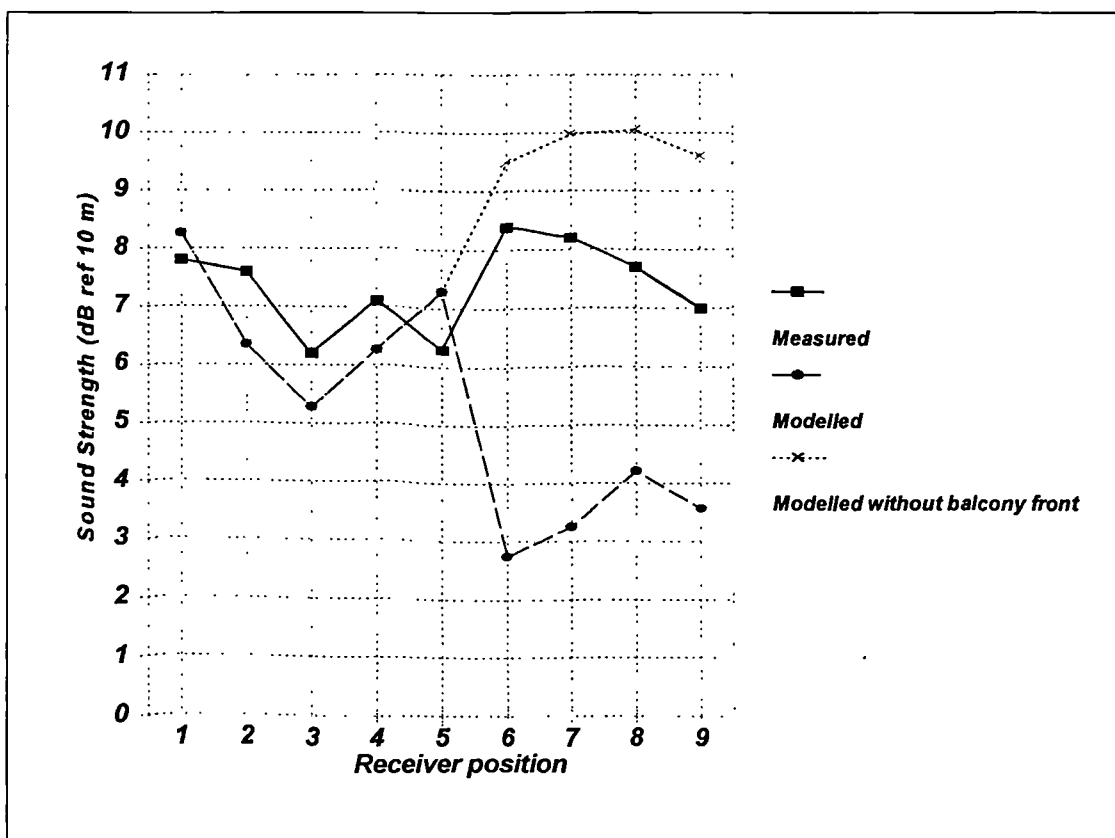


Figure 5.10 Sound strength at 1000 Hz in enclosure 6 (TO = 0, Ds = 0.1, Dr = 0.7)

directly, whereas sound from the source 'centre' (the position of the modelled source) was shielded by the balcony front. To verify this hypothesis, enclosure 6 models were re-run without a balcony front. As shown in figure 5.10, this resulted in increased predicted levels that were above those measured. This indicates that modelling of barrier edge diffraction should be accounted for in computer models to avoid over-emphasising the barrier effects.

### 5.3.6 The influence of ray re-direction

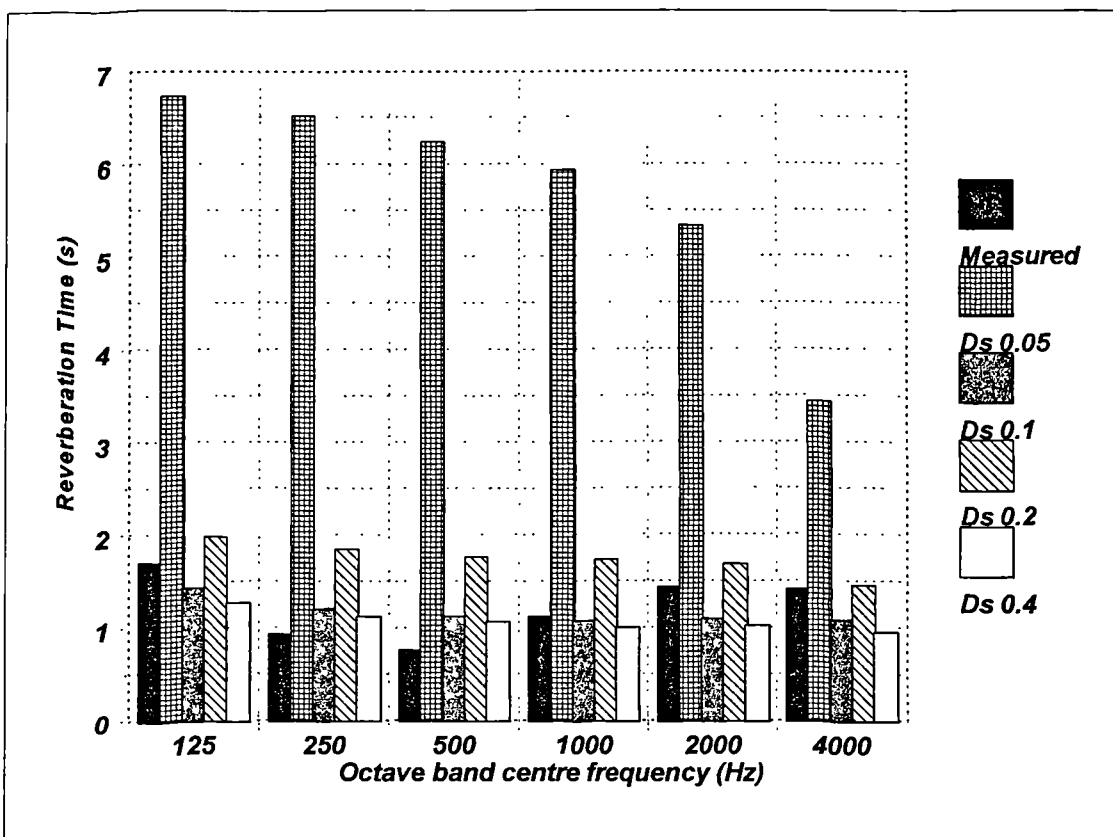


Figure 5.11 Effect of varying diffusion coefficients at receiver 7 in enclosure 3 (TO 0)

Figure 5.11 shows the effect of diffusion coefficient variation on predicted reverberation times at receiver 7 in enclosure 3 with all reflections modelled by diffuse secondary sources. A diffusion coefficient of 0.05 produced predicted values much higher than those measured and significantly above those predicted with higher diffusion coefficients. This possibly occurred because many of the rays traced were not reflected onto the absorptive seating and therefore formed more diffuse secondary sources on the reflective

walls and ceiling. With higher diffusion coefficients the probability of rays being re-directed onto the seating increased, which accelerated their attenuation. However, the reduction in predicted reverberation times was not linearly related to an increase in smooth surface diffusion coefficients. In the example shown, for instance, a diffusion coefficient of 0.2 predicted reverberation times higher than those that used a diffusion coefficient of 0.1. The random nature of the ray re-direction procedure used was a possible cause of this. In enclosure 3 diffusion coefficients of 0.1 and 0.4 possibly produced more diffuse secondary sources on the absorbent seating surface than diffusion coefficients of 0.2 and 0.05. The inclusion of a random element in the calculation of reflection angle may therefore limit the potential for optimization of diffusion coefficients since 'ideal' values will be partially dependent on the random number generation process, which differs for each model. However, although the re-direction method used by ODEON is based on that used by Kuttruff it is different because the ray tracing with re-direction is used in isolation to generate diffuse secondary sources whereas in Kuttruff's original method the ray tracing with re-direction is used in combination with a conventional specular ray tracing procedure. Consequently, the problems discussed here may not be transferable to other programs that use Kuttruff's re-direction technique.

### 5.3.7 Prediction of echoes

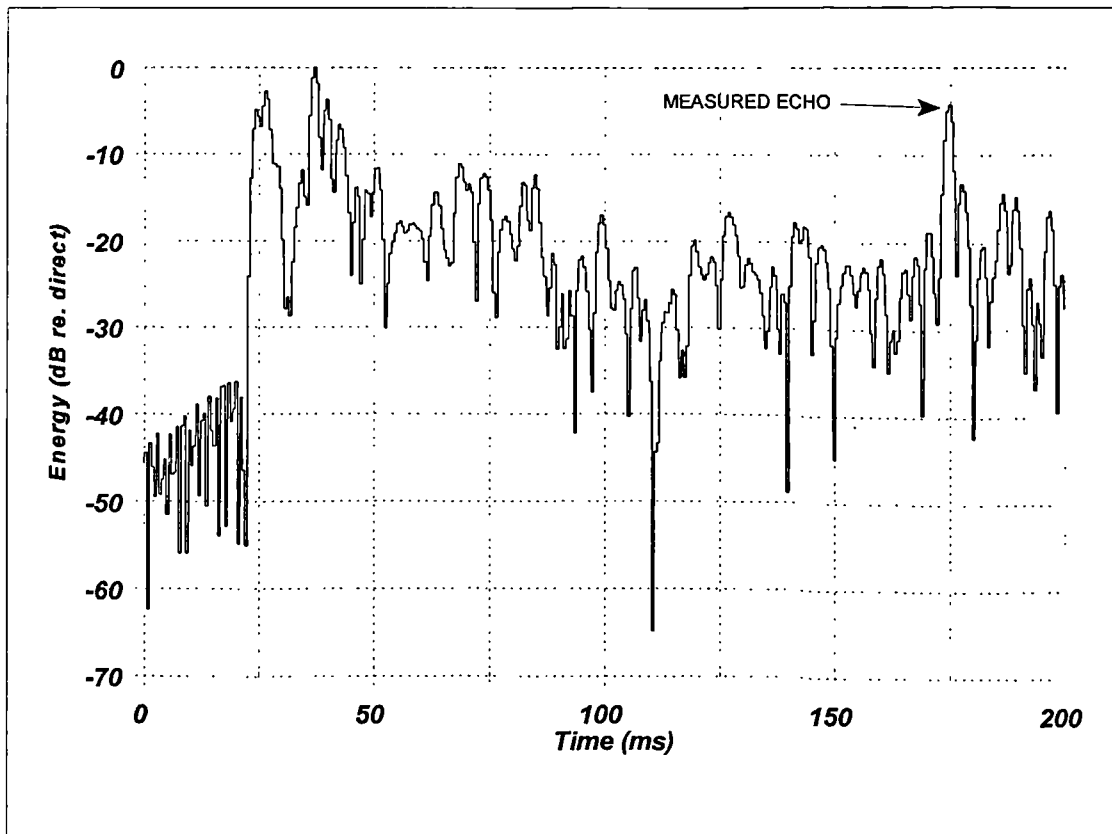


Figure 5.12 Measured energy decay at receiver 4 (source 2) in enclosure 8 at 1000 Hz

In enclosures 3 and 8 echoes were measured at specific source-receiver locations. These are distinct acoustic features that can cause speech intelligibility problems. The

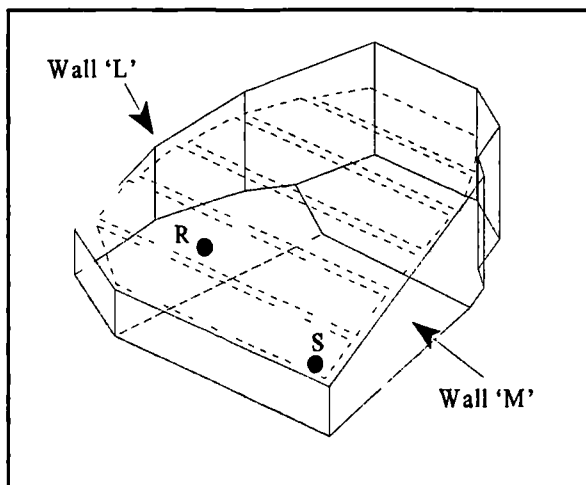


Figure 5.13 Enclosure 8 source and receiver positions for echo measurement

prediction of echoes requires a more detailed energy decay than for many of the room acoustic parameters previously discussed because details of late individual reflections are required.

In enclosure 8 the measured response presented in figure 5.12 shows an echo at approximately 175 ms. Although shown in the 1000 Hz octave band, the measured echo occurred in all octave-

bands centred on 250 Hz and above.

The echo is thought to have been caused by focusing from a concave surface, shown as wall 'L' in figure 5.13. This occurred when energy from source, S, reflected from wall 'L' onto wall 'M' and back to wall 'L' where the curvature of the wall was such that the energy was focussed back towards receiver, R. Since walls 'L' and 'M' have a low absorption coefficient (0.03 at 1000 Hz was used in the model) only a small amount of energy was lost which formed the strong late reflection measured.

Use of diffuse secondary sources for energy decay prediction was found to produce smooth decays that could not be used for the prediction of strong late reflections. This was probably because they did not account for the directivity of reflections and consequently produced diffuse modelled sound fields (as discussed in subsection 5.3.4). For the modelling of strong late reflections the energy decay was therefore modelled using purely specular reflections. To obtain a suitable reflection density at late decay times 6000 rays were modelled up to the tenth reflection order. This was close to the

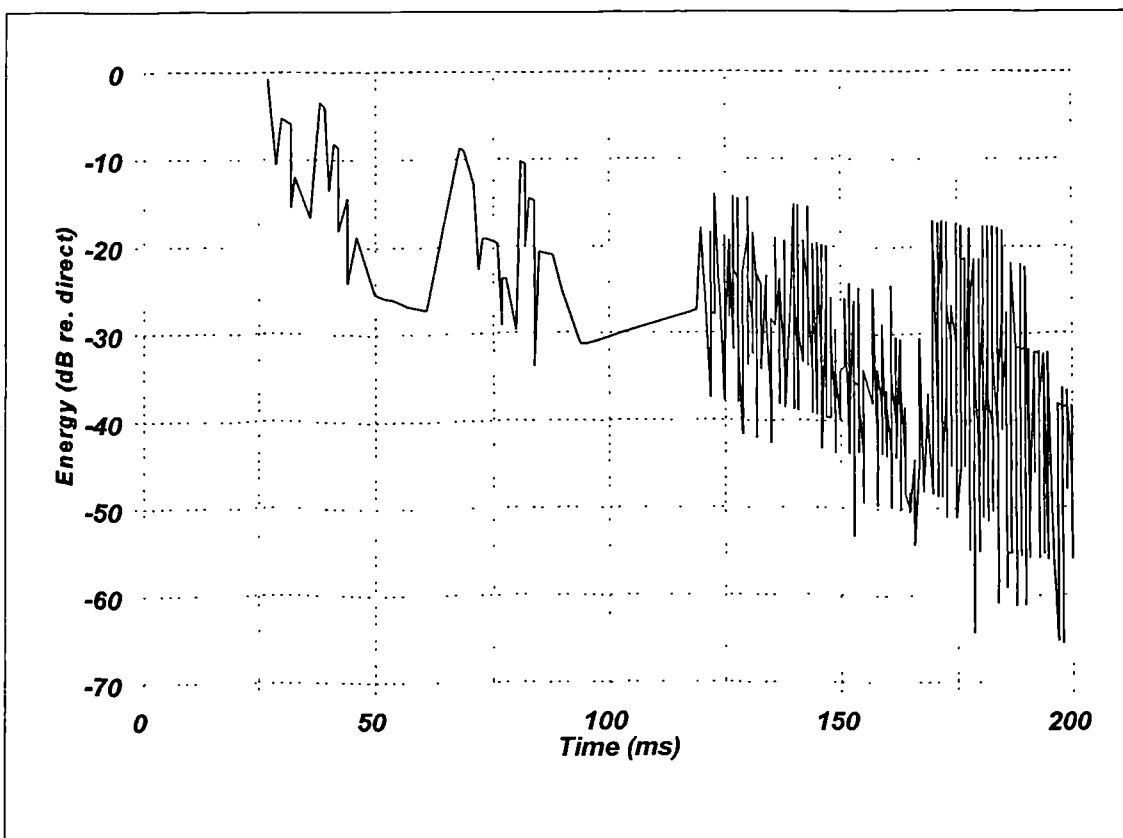


Figure 5.14 Modelled (bucketed) energy decay at receiver 4 (source 2) in enclosure 8 at 1000 Hz

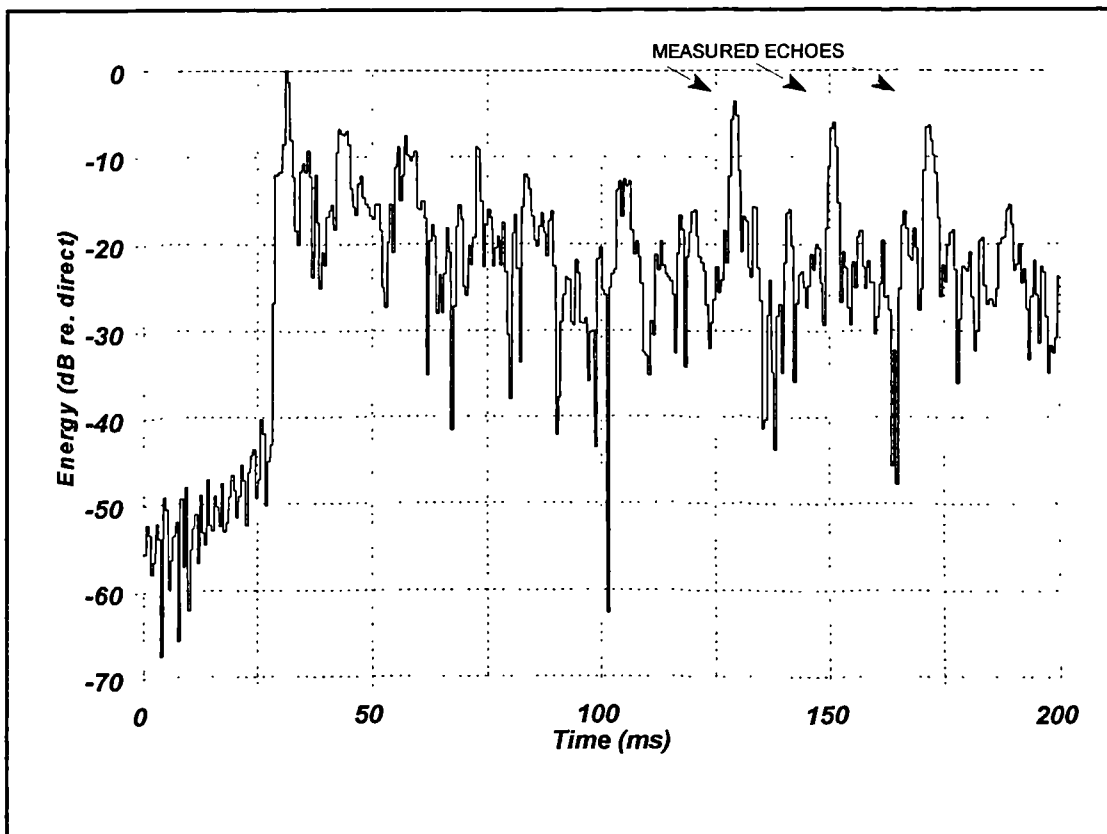


Figure 5.15 Measured energy decay at receiver 2 in enclosure 3 at 2000 Hz

maximum number of reflections achievable under the memory limitations of the software used.

Figure 5.14 shows the modelled version of the energy decay shown in figure 5.12. Strong late reflections were predicted at approximately 175 ms but they were smeared in the time domain and consequently not as strong as those measured. This was possibly due to the modelling of concave wall 'L' as three plane surfaces. As discussed previously (see subsection 5.3.1), curved surfaces were approximated by splitting surfaces into a number of smaller plane surfaces. However, for focusing effects to be predicted correctly each specular reflection's direction should have been determined according to the tangent at the point of reflection. With curved surfaces modelled as a combination of plane surfaces this requirement was not satisfied. For the correct prediction of echoes the geometry of curved surfaces would therefore have to be included in models.

In enclosure 3 echoes were heard at receiver position 2. This can be seen in the measured energy decay shown in figure 5.15. The decay shown is for the 2000 Hz octave band because the measured echo was strongest in that band. Unlike the echo measured in enclosure 8, the echoes in enclosure 3 were only clear at frequencies above 500 Hz.

Three particularly strong peaks in the energy decay were measured at approximately 129 ms, 151 ms and 172 ms. These peaks were initially thought to be components of a flutter echo because the time periods between them were similar. However, according to Kuttruff<sup>23</sup>, flutter echoes occur when “*sound is reflected repeatedly to and fro between parallel walls*” and on closer inspection of the dimensions of enclosure 3 no distances between reflecting surfaces could have produced the repetitive reflections required. The average time period between the peaks shown was 21.5 ms, which equates to a distance of approximately 7.3 m, receiver 2 would therefore have to have been located at a point 3.65 m from two such parallel surfaces, which was not the case. Figure 5.16 shows a perspective view of enclosure 3 with the source and receiver positions used. The echoes were therefore probably formed by different combinations of unattenuated reflections. Details of the reflection directions during the measurements are not known, however, comparison of the figure-of-eight measured response with the omni-directional response showed that the 172 ms peak had a lower amplitude in the figure-of-eight response indicating that it arrived non-laterally. This reflection was therefore possibly formed by sound energy from source, S reflecting from wall ‘A’ then from wall ‘D’ before being received at R. The 129 ms peak was present in the measured figure-of-eight response and therefore arrived laterally, this could have occurred by

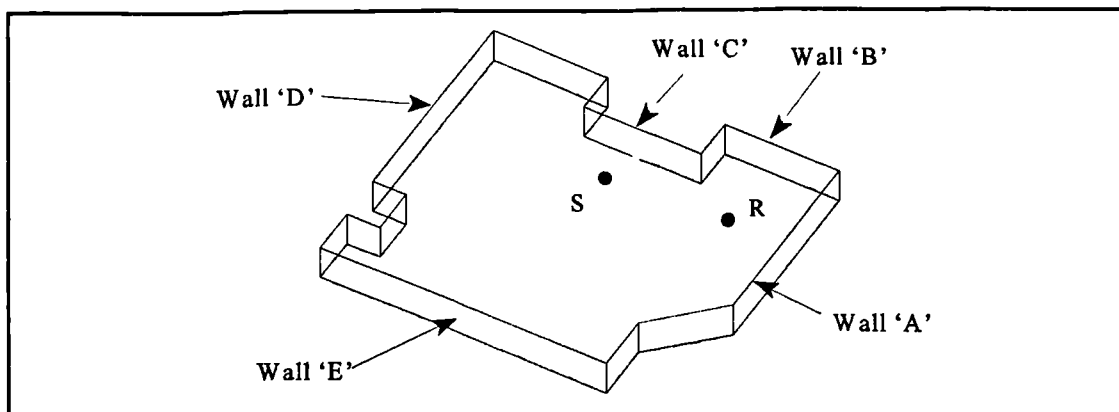


Figure 5.16 Enclosure 3 source and receiver positions for measurement of echoes

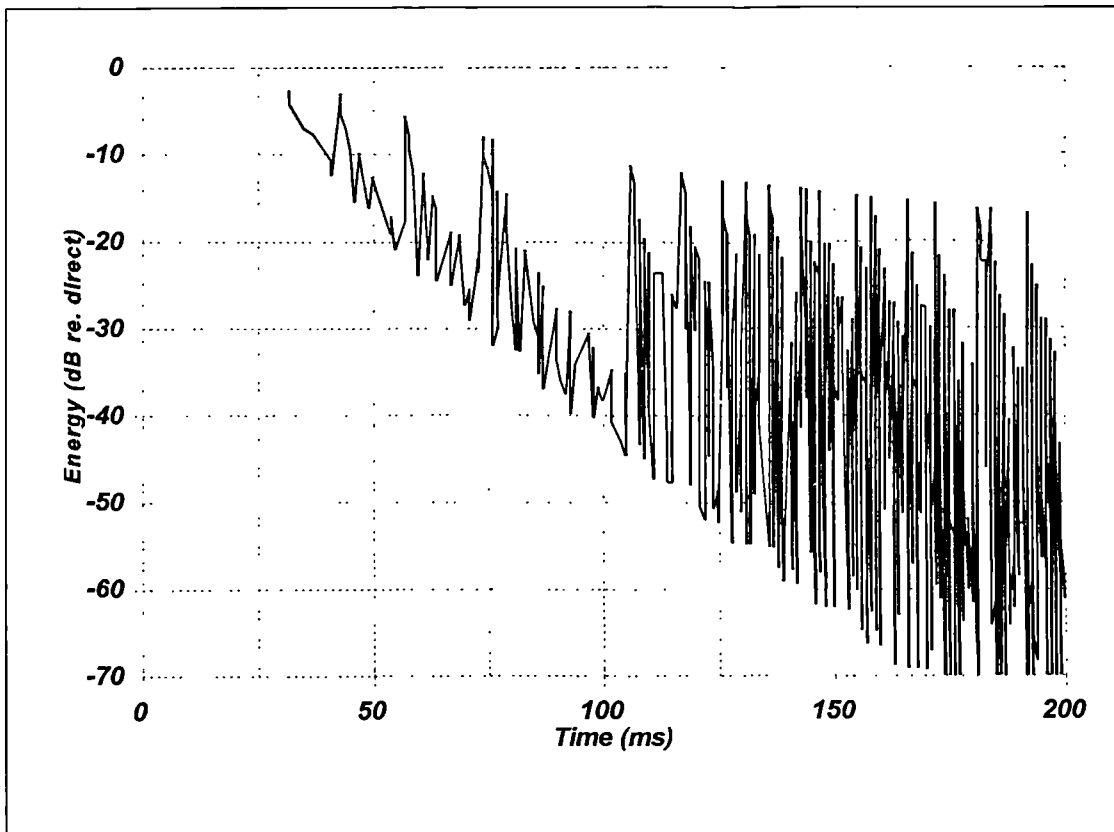


Figure 5.17 Modelled (bucketed) energy decay at receiver 2 in enclosure 3 at 2000 Hz

sound from the source reflecting from walls 'E' and 'B' before arriving at the receiver. Both of these peaks therefore probably formed from second order reflections, the 151 ms peak, however, also arrived laterally and was therefore possibly caused by a third order reflection that reflected from walls 'C', 'E' and 'B' before arriving at the receiver. The echoes were possibly stronger at higher frequencies because the dimensions of the reflecting walls were too small to reflect efficiently at low frequencies and the low floor-ceiling distance probably contributed to a more rapid attenuation of low frequency energy.

The modelled decay shown in figure 5.17 was generated using 6000 rays and specular reflections up to the tenth order. This was considered necessary to obtain a high enough reflection density at times greater than 100 ms. Reflections were predicted at times where echoes were measured but were lower in amplitude and were amongst other strong late reflections that were not present in the measured decay. The lower

amplitudes of the reflections were probably attributable to errors in absorption coefficients assigned to the walls. Reducing these absorption coefficients did increase the reflection amplitudes but also increased the amplitudes of other received reflections. Consequently, the measured echoes were not correctly predicted because they were indistinguishable from other late reflections. Attenuation of these other reflections probably occurred in the real enclosure from the seating because its height of 0.7 m (the distance from the floor to the top of the seat back) was a significant proportion of the floor-ceiling height of 3.1 m. This seat height was not accounted for in the computer model where the seating was considered as a homogeneous absorbing surface at floor level. In addition, some scattering of sound probably occurred from the enclosure walls that was not accounted for by the specular model used. In reality much of the energy reflected from the walls would have been partially scattered onto the absorbent floor and consequently attenuated more rapidly.

## **5.4 Summary of comparisons**

### **5.4.1 Overview of errors found**

The comparisons presented in sections 5.2 and 5.3 give clear indications of how changes in the way early reflections are modelled affect the prediction of room acoustic parameters. The following points were drawn from the comparisons made

- For sound strength and centre time changes in the way early reflections were modelled on average had little influence on the predicted values. This is probably because they are calculated from complete energy decays.
- For prediction of reverberation time, early decay time, clarity index and deutlichkeit introduction of diffuse reflections from the first reflection order produced the smallest average errors.
- Lateral energy fractions were on average predicted best with a transition order of three. Specific comparisons indicated that neither diffuse secondary sources nor specular image sources predicted the directivities of reflections accurately.
- For clarity index, deutlichkeit and lateral energy fraction, which are all energy-balance parameters concerned with the early part of the energy decay, changes

in diffusion coefficients had little influence on the average accuracy because changes were on average cancelled out in the parameter calculation.

- For reverberation time and early decay time, which are both calculated from slopes of energy decays, the choice of diffusion coefficients is important and should be frequency dependent. Diffusion coefficients of 0.1 and 0.2 on smooth surfaces produced the best average predictions at mid- and high frequencies; at low frequencies predictions were on average best with a higher coefficient of 0.4.

#### 5.4.2 Specific causes of errors

The comparison of various predictions and measurements discussed in this chapter highlights problems that can occur with the modelling techniques studied. Apart from problems attributable to errors in input absorption coefficients, interference effects and to practical limitations of comparing point source predictions with measurements made using a sound source of finite dimensions, the remaining problems discovered were associated with the modelling of sound reflecting from surfaces. The summary below attempts to demarcate the problems encountered into eight key points.

i) *Directivity of diffuse secondary sources*

Secondary sources that radiate energy according to Lambert's cosine law from surfaces 'illuminate' areas of enclosures that would not be reached by real reflections from 'semi-diffuse' surfaces. This caused errors in the prediction of clarity index at receiver 4 in enclosure 7 and lateral energy fraction at all receivers in enclosure 3.

ii) *Directivity of specular reflections*

Specular modelling of reflections directs energy in single rays and does not scatter sound into a wider solid angle. Reflections can therefore 'miss' receivers and avoid surfaces that they would otherwise illuminate. This caused errors in the prediction of *deutlichkeit* at receiver 11 in enclosure 5a, lateral energy fraction at receivers 5, 6 and 7 in enclosure 3 and of echoes in enclosure 3.

iii) *Strength of specular reflections*

Specular reflections can be too strong. This is related to the lack of scattering from specular reflections as energy that should be scattered is concentrated into a single ray. This caused errors in predictions of early decay time at receiver 7 in enclosure 7, clarity index at receiver 1 in enclosure 7, deutlichkeit at receiver 8 in enclosure 5a and of lateral energy fraction at receiver 6 in enclosure 3.

iv) *Reflections from finite surfaces*

Reflection strength does not take account of the dimensions of a reflecting surface. This is implicit in the assumptions of geometrical acoustics and particularly causes errors at low frequencies where wavelengths of sound are comparable to surface dimensions. This was credited as the cause of over-predicted reverberation times in enclosures 4 and 7.

v) *Modelling of curved surfaces*

Modelling curved surfaces using small plane surfaces exacerbates problems caused by the omission of reflecting surface dimensions in the calculation of reflection strength and presents difficulties with the modelling of focussing effects. This caused over-predictions of reverberation time in enclosure 4 and a failure of echo prediction in enclosure 8.

vi) *Definition of diffusion coefficients*

Diffusion coefficients are not defined in the frequency domain. Average errors in predictions of reverberation time and early decay time indicated higher diffusion coefficients were more appropriate at low frequencies. Errors in the prediction of reverberation time at receiver 7 in enclosure 3 indicated the existence of non-linearity between diffusion coefficient value and predicted results for the program used.

vii) *Modelling of barriers*

Shielding effects of barriers such as balcony fronts are not predicted correctly. This resulted in under-prediction of sound strength at receivers 6 to 9 in enclosure 6.

viii) *Modelling of surface diffusion in the time domain*

The categorisation of reflections as specular or diffuse according to reflection order is groundless and means that surface diffusion is not defined correctly in the time-domain. This caused inconsistent variations in predictions of lateral energy fraction in enclosure 3 and larger average errors in predictions of reverberation time, early decay time, clarity index and deutlichkeit.

## **Chapter 6**

# **Development of a New Calculation Procedure**

### **6.1 Specification for a suitable algorithm**

Any new modelling method needs to eliminate or reduce the effects of the problems summarised in subsection 5.4.2. It also needs to be flexible and robust enough for a wide variety of enclosure types and provide a framework for future development. To be a practical tool for the design of enclosures the calculation method should also produce predictions relatively quickly.

The modelling of the reflection of sound from various types of surfaces has emerged as a major weakness in the modelling techniques investigated. The new method should therefore be able to model specular reflections, diffuse reflections and any semi-diffuse combination of the two. Edge-diffraction, particularly from internal barriers, should also be modelled. Prediction of interference effects, particularly the seat-dip effect would also be useful to improve accuracy at low frequencies.

Previous modelling of diffuse reflections included a 'diffusion coefficient' that controlled the probability of a ray reflecting specularly or reflecting in a non-specular direction. The

new method needs to include a similar parameter that can be assigned to surfaces to control the fraction of reflected energy directed in specular and non-specular directions. A further parameter to control the degree of scattering is also required.

## **6.2 The new ‘Hybrid-Markov’ model**

The development of a completely new program was outside the scope and timescale of this project and an existing hybrid model was available for modification. This was therefore used for the modelling of enclosure geometry and for the generation of specular reflections. This section gives an overview of the procedure adopted for the modified program. A flowchart summarising the new calculation procedure is shown in figure 6.1. A listing of the main program code (in Turbo Pascal) is given in Appendix B.

The new procedure uses a conventional hybrid method to calculate specular reflections up to a high reflection order (typically over fifty). However, at each reflection energy is subtracted twice: once using the factor  $(1-\alpha)$  to account for energy absorbed; and once using the factor  $(1-\delta)$  to account for energy diffused. A similar technique was used by Heinz<sup>36</sup> to extract diffuse energy from a ray tracing procedure. Since both  $\alpha$  and  $\delta$  are defined for octave bands between 125 Hz and 4000 Hz, this is used to form a ‘specular energy decay’ in each frequency band. As with previous models, the parameter ‘ $\delta$ ’ is referred to as the diffusion coefficient. However, it is important to note that it is used in the calculation to directly control the fraction of energy entering the diffuse process at each reflection. This differs from Heinz’s method and the models assessed in chapter 5 where diffusion coefficients were used to influence reflecting angles of rays.

Prediction of the seat-dip effect would require the modelling of sound pressure or an empirical method based on detailed measurements. Both of these were considered beyond the scope of this project and were therefore not attempted.

Energy subtracted for diffusion at each reflection is then input into an active radiant-exchange procedure, similar to the Markov-chain method used by Gerlach<sup>39</sup>. This is used to generate a ‘diffuse energy decay’ in each frequency band.

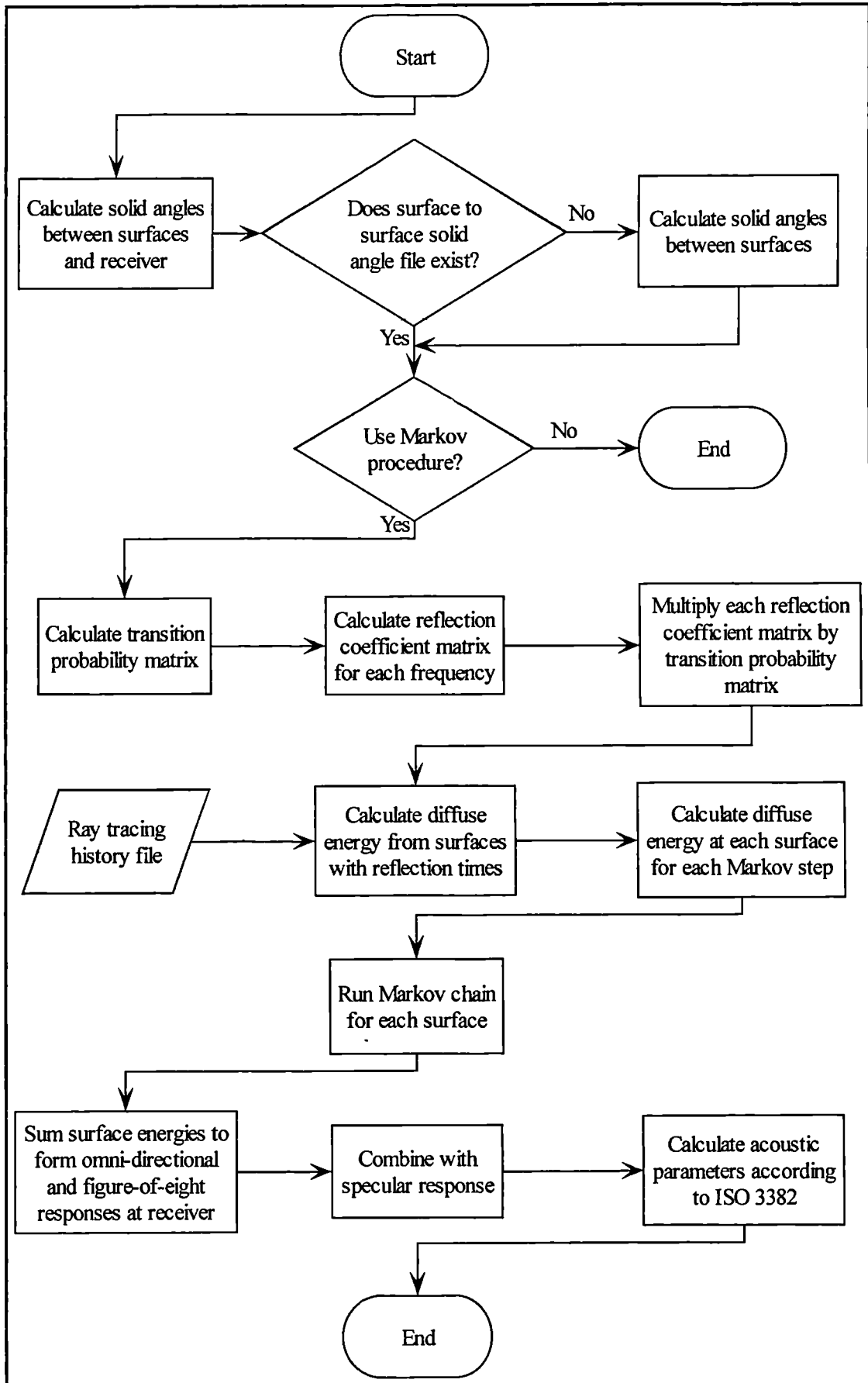


Figure 6.1 Flowchart of program operation

In the radiant-exchange method an enclosure bounded by  $n$  surfaces is excited by a sound source switched off at time  $t = 0$ . The probability of energy travelling from surface  $i$  to surface  $k$  is referred to as the 'transition probability',  $p_{ik}$  (Note: this should not be confused with the 'transition order' discussed in previous chapters). The Markov-chain process then proceeds at discrete time intervals of length  $\bar{t}$

If the surfaces energies at Markov-chain step  $N$  are described by the vector

$$e^{(N)} = (e_1^{(N)}, \dots, e_n^{(N)})$$

the initial energy is given by

$$e^{(0)} = (e_1^{(0)}, \dots, e_n^{(0)})$$

where  $e_i^{(0)}$  is the 'diffuse' energy at surface  $i$  at  $t = 0$ .

At time  $t = N\bar{t}$  the diffuse energy at surface  $i$ , is determined from diffuse energy stored from the hybrid process at that surface for step  $N$ , which is given by

$$D_i^{(N)} = \int_{N\bar{t}-\bar{t}}^{N\bar{t}} \delta_i(1-\alpha_i).E_i dt$$

plus energy radiantly-exchanged from other surfaces. Therefore at time  $t = \bar{t}$  when the first transition occurs,

$$e_i^{(1)} = D_i^{(1)} + \sum_{j=1}^n e_j^{(0)} (1-\alpha_j) p_{ji}$$

which can be written in matrix form

$$e^{(1)} = D^{(1)} + e^{(0)} A P$$

where,

$$D^{(N)} = (D_1^{(N)}, \dots, D_n^{(N)})$$

and  $A$  is the diagonal matrix of the reflection coefficients and  $P$  is the matrix of the transition probabilities.

Similarly, after  $N$  steps,

$$e^{(N)} = D^{(N)} + e^{(N-1)} A P$$

The total energy at step  $N$  is therefore

$$\epsilon_N = \sum_{k=1}^n e_k^{(N)}$$

With the procedure developed here the initial energy at the surfaces is zero. As the ray tracing is performed energy is then placed into the appropriate Markov step according to diffusion coefficients assigned to surfaces. The Markov step length is chosen to be equal to the mean free path length divided by the speed of sound (the mean free path length is estimated using a low resolution ray trace prior to the main calculations).

Transition probabilities are determined by the geometry of the model and are calculated according to solid angles between surfaces. The solid angles are calculated prior to the Hybrid-Markov procedure and are stored in files that are accessed during subsequent calculations. The transition probability from a surface  $i$  to surface  $k$  is determined by dividing the solid angle,  $\Omega_{ik}$ , subtended from the centre of surface  $i$  to the visible part of surface  $k$  by the total solid angle visible from the centre of surface  $i$ . This solid angle is estimated for each surface by a ray-tracing procedure: rays are traced from the centre of each surface into  $4\pi$  space at a resolution of approximately one ray per degree. This resolution gives a ray separation of 0.7 m at a distance of 40 m and is therefore considered fine enough to illuminate all influential surfaces.

The required solid angle is then given by

$$\Omega_{ik} = \frac{4\pi N_k}{N_i}$$

Where,

$\Omega_{ik}$  is the solid angle subtended by the visible part of surface  $k$  to surface  $i$ .

$N_i$  is the number of rays emitted from the centre of surface  $i$

$N_k$  is the number of rays that hit surface  $k$

The transition probability from surface  $i$  to surface  $k$ ,  $p_{ik}$ , is then given by

$$p_{ik} = \frac{\Omega_{ik}}{\sum_{j=1}^n \Omega_{ij}}$$

For a boundary surface, approximately half of the rays emitted hit other surfaces the remainder are traced outside the enclosure and are therefore discarded.

Therefore,

$$\sum_{j=1}^n \Omega_{ij} \approx 2\pi$$

For an internal partition, such as a balcony front, emitted rays radiate into  $4\pi$  space.

That is,

$$\sum_{j=1}^n \Omega_{ij} = 4\pi$$

This ensures that the sum of transition probabilities from one surface is equal to one. Consequently, internal partitions are effectively ‘translucent’ to diffuse sound. Since the concept of ‘diffuse reflection’ includes scattering due edge diffraction, this ‘translucency’ is an attempt to model its effects. It would be possible in any future refinements to include diffraction effects and the directivity of scattering in the calculation of the transition probabilities.

Once the diffuse energies at the surfaces have been determined for each time step, the energy at the receiver is calculated. Consider a surface  $i$  at time  $t$  with energy  $E_{it}$ . If this surface is divided into  $m$  diffusely radiating elements, each of area  $A_{im}$ , then each element will radiate according to Lambert's law. If  $r_{im}$  and  $\theta_{im}$  represent the element-receiver distance and angle respectively, the energy received from one element is given by

$$\frac{E_{it}}{m} \cdot \frac{1}{4\pi r_{im}^2} \cdot \cos\theta_{im}$$

The energy received from the whole surface is therefore

$$\frac{E_{it}}{m} \cdot \sum \frac{1}{4\pi r_{im}^2} \cdot \cos\theta_{im}$$

Since  $m = A_i/A_{im}$

$$\frac{E_{it}}{A_i} \cdot \sum \frac{1}{4\pi r_{im}^2} \cdot \cos\theta_{im} \cdot A_{im}$$

With infinitely small elements this becomes

$$\frac{E_{it}}{A_i} \cdot \frac{1}{4\pi} \int \frac{\cos\theta_i}{r_i^2} dA_i$$

Since,

$$\Omega_i = \int \frac{\cos\theta_i}{r_i^2} dA_i$$

Where  $\Omega_i$  is the solid angle from surface  $i$  to the receiver, the energy received from

surface  $i$  is given by

$$E_r = \frac{E_{it}}{A_i} \cdot \frac{\Omega_i}{4\pi}$$

Where  $A_i$  is the area of surface  $i$

The 'specular decay' and the 'diffuse decay' are then combined to give the complete energy decay. Standard acoustic parameters are then calculated according to ISO 3382.

## **Chapter 7**

# **Performance of the Hybrid-Markov Model**

### **7.1 Program operation**

It was not possible to run the new Hybrid-Markov method for enclosures 1a, 1b and 7 because of memory limitations of the computer operating system used. Available memory was limited to approximately 610 kbytes since the original program used as a base for the new calculation method was written in "Turbo Pascal v.6" for "MS-DOS" based systems. The program relied on conventional memory; extended and expanded memory were not available.

This memory limitation restricted the maximum number of surfaces available for use with the hybrid-markov model to 161. Enclosures 1a, 1b and 7 had 205, 207 and 375 surfaces respectively. With a more modern operating system this memory limitation would not occur and many of the program's routines could utilise RAM for data storage rather than having to rely on relatively slow hard-disk data storage. This would reduce calculation times considerably.

Models were run using 'IBM-compatible' personal computers with Intel processors ranging from 486-66 MHz to Pentium-200 MHz. Calculation times were between 5 minutes and 30 minutes for a single source-receiver response. However, this calculation time was found to be more dependent on disk writing speed than processor speed. This was because calculation arrays used within the program were restricted to a maximum of 64 Kbytes by the Turbo Pascal compiler so the large data arrays required had to be stored on disk.

With more memory available and with less stringent restrictions on the size of arrays calculations would run significantly faster and larger models could be run. Calculation arrays were at most 21 Mbytes in size, which could be accommodated by RAM in relatively inexpensive modern personal computers.

## **7.2 Overview of predictive accuracy**

### **7.2.1 Remarks regarding comparisons with hybrid model predictions**

The following comparisons between results from the Hybrid-Markov model and results from the hybrid (with diffuse secondary sources) model are a useful qualitative guide to the scale of accuracies achieved but should be regarded with caution. The Hybrid-Markov predictions presented here are preliminary results as further work is required to optimize the diffusion coefficients and transition probabilities used. In particular, it is important to note that the diffusion coefficient used in the Hybrid-Markov model operates differently from the diffusion coefficient used in the hybrid model.

The Hybrid-Markov method of modelling diffuse surface reflections has the following advantages over the hybrid / diffuse secondary source technique

- Diffusion coefficients directly control the amount of energy diffused from a surface
- Directivity of diffuse energy radiating from surfaces can be controlled
- Diffusion coefficients can be defined in the frequency domain
- Edge-diffraction over barriers can be modelled

- There is no dividing transition order between early and late reflections
- Dependence on random number generation is eliminated

The new method is therefore more flexible than its predecessor and constructs a framework that allows further research to continue to improve the accurate modelling of diffuse reflections.

For comparisons of average predictive errors with the models discussed in chapter 5, diffusion coefficients of 0.1 and 0.7 were used for smooth and rough surfaces respectively. Transition probabilities were calculated as described in chapter 6, that is, surfaces were assumed to radiate diffusely from their centre point. This allowed transition probabilities to be calculated in reasonable times with the limited computing capability available.

### 7.2.2 Prediction of 'decay slope' parameters

Reverberation time and early decay time are both measures of the slope of an energy decay. Average errors in their Hybrid-Markov predictions are shown with those from the hybrid model with diffuse secondary sources (transition order zero) in tables 7.1 and 7.2. These show on average both parameters were over-predicted by the Hybrid-Markov model, indicating the gradient of the modelled energy decay was too low.

Frequency (Hz)	TO 0		Hybrid-Markov	
	Mean Error (%)	Standard Deviation in Error (%)	Mean Error (%)	Standard Deviation in Error (%)
125	31.7	55.8	14.5	30.8
250	31.2	64.6	20.5	23.9
500	12.1	36.8	20.2	21.9
1000	3.5	28.7	13.1	21.0
2000	1.2	25.7	9.7	24.2
4000	3.3	22.5	19.1	35.6

Table 7.1 Errors in prediction of  $T_{30}$  from Hybrid-Markov and TO 0 models ( $D_s = 0.1$ ,  $D_r = 0.7$ )

Predictions of early decay time resulted in higher average errors than those of reverberation time, which suggests changes in the gradient of the modelled energy decay occurred. Early decay time is determined by the slope of a decay between the 0 dB and

-10 dB points; reverberation time is determined by the slope between the -5 dB and -35 dB points. Higher average errors in the prediction of early decay time therefore signify that the early part of the modelled energy decay had a lower gradient than the latter part. The difference between this and the lower errors that occurred with the transition order zero model was possibly caused by the modelling of diffusion in the Hybrid-Markov model.

Frequency (Hz)	TO 0		Hybrid-Markov	
	Mean Error (%)	Standard Deviation in Error (%)	Mean Error (%)	Standard Deviation in Error (%)
125	34.0	65.7	44.6	67.4
250	27.0	67.8	53.8	71.2
500	5.4	43.2	31.3	37.4
1000	4.4	35.0	28.7	47.1
2000	0.6	31.3	21.2	47.1
4000	1.3	31.1	32.7	61.0

Table 7.2 Errors in prediction of EDT from Hybrid-Markov and TO 0 models ( $D_s = 0.1$ ,  $D_r = 0.7$ )

With the transition order zero model all reflected energy was modelled diffusely; with changes in diffusion coefficients only determining the location of diffuse secondary sources. However, in the Hybrid-Markov model, diffusion coefficients directly determine the amount of energy diffused. Therefore with a diffusion coefficient of 0.1, 90 % of energy reflected from a surface is directed specularly while 10 % is diffused. The resulting differences in average errors may therefore indicate that higher diffusion coefficients are required with the Hybrid-Markov method. Optimization of diffusion coefficients is beyond the scope of this project but would be useful for future research.

### 7.2.3 Prediction of sound strength

Average errors in predictions of sound strength for the Hybrid-Markov and transition order zero models are shown in table 7.3. The Hybrid-Markov model resulted in slightly higher errors than the transition order zero model, which concurred with resulting errors in the prediction of reverberation time and early decay time. These results indicate that the overall modelled energy was too high because it decayed too slowly. This possibly occurred because too much energy was modelled specularly and was therefore not scattered onto absorbent surfaces. This also occurred, to a lesser degree, when the first

five reflections of the earlier model were modelled specularly. As with predictions of reverberation time and early decay time this indicates that diffusion coefficients may have to be increased for use with the Hybrid-Markov method.

Frequency (Hz)	TO 0		Hybrid-Markov	
	Mean Error (dB)	Standard Deviation in Error (dB)	Mean Error (dB)	Standard Deviation in Error (dB)
125	6.6	6.7	5.8	8.4
250	2.6	4.8	3.0	5.7
500	1.3	3.6	1.9	4.3
1000	0.4	3.0	1.4	3.5
2000	-0.3	2.5	0.8	3.1
4000	-0.1	2.2	1.1	2.9

Table 7.3 Errors in prediction of sound strength from Hybrid-Markov and TO 0 models ( $D_s = 0.1$ ,  $D_r = 0.7$ )

Hybrid-Markov errors, as with errors from other models, also showed an increase at low frequencies. This was as expected because none of the three possible causes of low frequency errors detailed in subsection 5.3.1 were addressed by the new model. These problems should therefore be the subject of further research.

#### 7.2.4 Prediction of ‘energy balance’ parameters

Comparisons of predicted results with measurements presented in chapter 5 indicated that modelling of diffusion should be accounted for all reflection orders for the prediction

Frequency (Hz)	TO 0		Hybrid-Markov	
	Mean Error (dB)	Standard Deviation in Error (dB)	Mean Error (dB)	Standard Deviation in Error (dB)
125	-0.5	3.1	-1.0	2.7
250	-0.5	3.2	-1.6	2.8
500	-0.1	2.6	-1.4	2.5
1000	-0.3	2.4	-1.4	2.7
2000	-0.0	2.1	-0.9	2.9
4000	-0.2	1.9	-1.3	3.4

Table 7.4 Errors in prediction of clarity index from Hybrid-Markov and TO 0 models ( $D_s = 0.1$ ,  $D_r = 0.7$ )

of clarity index and deutlichkeit, which occurs with the Hybrid-Markov model. Average errors in predictions of clarity index, deutlichkeit and centre time from the transition order zero and Hybrid-Markov models are presented in tables 7.4, 7.5 and 7.6

respectively. Hybrid-Markov predictions of these parameters were more accurate than of reverberation time and early decay time, which indicates that errors in the modelled decay were partially balanced-out in ratios of early to late energy. This signifies errors were present throughout the decays. These errors could therefore be caused by incorrect diffusion coefficients or transition probabilities because they would affect both early and late reflections.

Frequency (Hz)	TO 0		Hybrid-Markov	
	Mean Error (%)	Standard Deviation in Error (%)	Mean Error (%)	Standard Deviation in Error (%)
125	14.3	58.8	4.3	44.6
250	4.1	45.1	-8.9	31.0
500	-1.5	28.2	-5.7	28.1
1000	-4.9	21.7	-4.4	30.3
2000	-1.7	32.2	-0.1	29.4
4000	-2.0	21.4	-3.7	30.0

Table 7.5 Errors in prediction of *deutlichkeit* from Hybrid-Markov and TO 0 models ( $D_s = 0.1, D_r = 0.7$ )

When compared with average errors from transition order zero predictions, the Hybrid-Markov method performed similarly. For prediction of clarity index average errors were slightly higher, while for prediction of *deutlichkeit* and centre time the Hybrid-Markov model produced slightly smaller errors at mid-frequencies. This suggests the balance between early and late energies is predicted relatively accurately by the Hybrid-Markov method.

Frequency (Hz)	TO 0		Hybrid-Markov	
	Mean Error (ms)	Standard Deviation in Error (ms)	Mean Error (ms)	Standard Deviation in Error (ms)
125	25.3	89.6	41.6	87.6
250	43.3	121.7	59.4	109.9
500	20.0	62.5	18.2	27.3
1000	17.2	42.9	9.8	33.6
2000	11.0	33.2	4.0	30.1
4000	3.5	16.6	9.0	31.6

Table 7.6 Errors in prediction of centre time from Hybrid-Markov and TO 0 models ( $D_s = 0.1, D_r = 0.7$ )

### 7.2.5 Prediction of lateral energy fraction

Analysis of predictions in chapter 5 suggested that the introduction of diffuse reflections after the first three reflection orders were modelled specularly produced the most accurate results on average. However, when specific predictions were investigated it was found that neither specular nor diffuse secondary source modelling produced satisfactory results. Since predictions of other room acoustic parameters require that diffusion should be introduced from the first reflection order it would be impractical to design a method that could predict one group of parameters accurately but not another. Average errors resulting from Hybrid-Markov predictions along with those from transition order zero models and transition order three models are shown in table 7.7.

Frequency (Hz)	TO 0		TO 3		Hybrid-Markov	
	Mean Error (%)	Standard Deviation in Error (%)	Mean Error (%)	Standard Deviation in Error (%)	Mean Error (%)	Standard Deviation in Error (%)
250	38.1	63.2	4.6	49.9	42.6	77.3
500	25.8	53.6	-3.3	40.8	31.1	54.6
1000	19.8	44.0	-7.6	38.0	25.7	44.7
2000	44.2	59.4	9.4	52.0	48.0	63.6
4000	24.8	49.0	-7.2	40.0	31.2	55.3

Table 7.7 Errors in prediction of LF from Hybrid-Markov, TO 0 and TO 3 models ( $D_s = 0.1$ ,  $D_r = 0.7$ )

Average errors in the Hybrid-Markov predictions were considerably larger than those from the transition order three model and slightly above those from the transition order zero model. As predictions of other parameters indicated, the diffusion coefficients used were probably too low, which meant that much of the reflected energy was reflected specularly because smooth surfaces were assigned diffusion coefficients of 0.1, while those classified as rough were usually absorbent. This would have produced problems in the spatial distribution of the modelled sound field as detailed in subsection 5.3.4. Specific predictions of lateral energy fraction are discussed in section 7.3.

### 7.3 Were problems encountered with the hybrid method solved?

Specific causes of errors encountered in the models investigated were summarised in subsection 5.4.2. This section therefore examines specific results from the Hybrid-Markov model to determine whether these problems were solved.

#### 7.3.1 Directivity of diffuse secondary sources

The Hybrid-Markov model allows the directivities of diffuse reflections to be controlled through its transition probability parameter, which determines the proportion of diffuse energy that transfers from one surface to another. However, the Hybrid-Markov method models reflections by combining a radiant-exchange procedure with a specular hybrid procedure. As a consequence, reflections are unlikely to be modelled only diffusely. This would only occur if all surfaces were assigned diffusion coefficients of 1.0 at all frequencies.

Figure 7.1 shows Hybrid-Markov and transition order zero model predictions of lateral

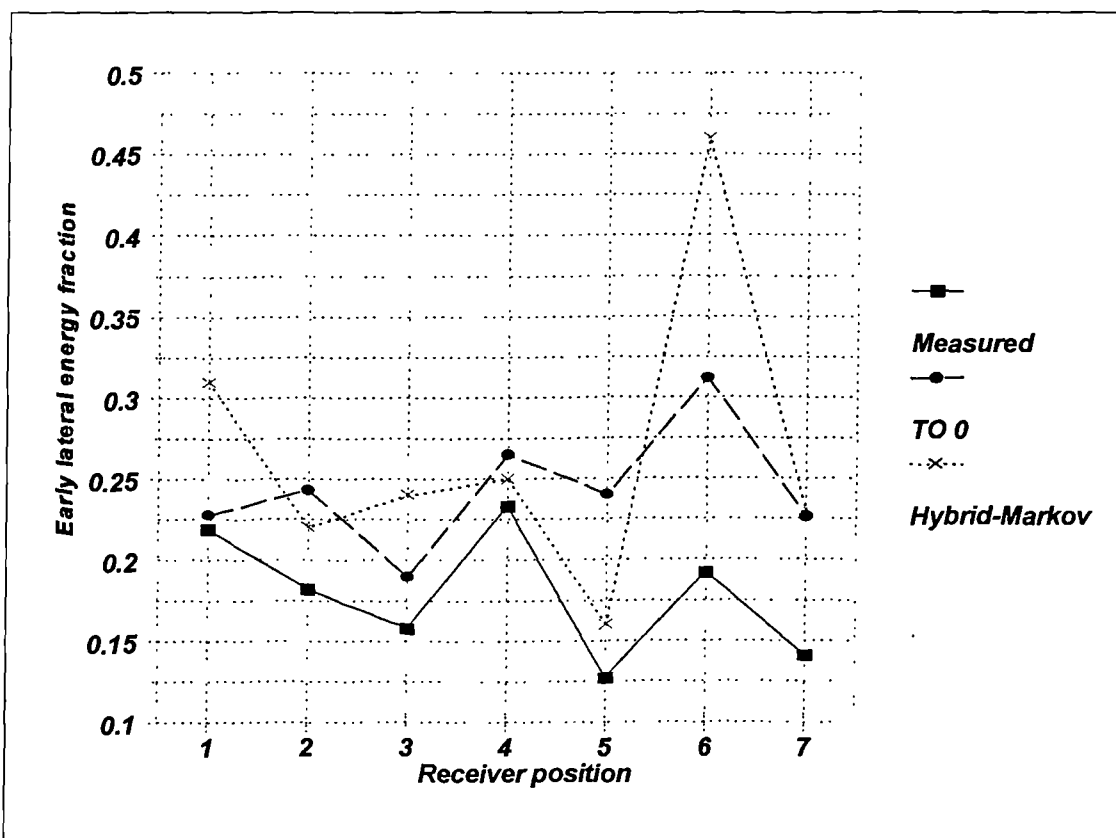


Figure 7.1 Early lateral energy fraction predictions at 1 kHz in enclosure 3

energy fraction at 1 kHz in enclosure 3. The over-prediction of results with the transition order zero model was attributed to the over-scattering of energy from diffuse secondary sources (see subsection 5.3.4). Predictions from the Hybrid-Markov model showed more spatial variation than the transition order zero predictions, which is probably attributable to the high proportion of energy modelled specularly by the Hybrid-Markov model. Predicted lateral energy fractions from higher transition order models shown in subsection 5.3.4 had a similar spatial variation. The proportion of energy modelled specularly is controlled by the surface diffusion coefficients. These operate differently from diffusion coefficients in other models so further work is required to find optimum values necessary for accurate predictions, since this requires comparisons with measurements made in controlled conditions it is considered beyond the scope of this project.

Predictions of lateral energy fraction at receiver 6 are discussed further in subsection 7.3.3.

### **7.3.2 Directivity of specular reflections**

When specular reflections were used to model reflections up to the fifth order in enclosure 5a deutlichkeit was over-predicted at receiver 11 (see subsection 5.3.3). This was attributed to specular reflections not directing energy towards this position causing insufficient energy to arrive after 50 ms. Figure 7.2 shows those predictions along with measured values and predictions from the Hybrid-Markov model. The over-predictions that occurred with the specular reflections did not occur with the Hybrid-Markov model. This is due to the way energy arriving after 50 ms was modelled: in the Hybrid-Markov model specular reflections were modelled as before but a fraction of their energy was transferred to the radiant-exchange process which, in this case, scattered energy diffusely towards the receiver. This increased the energy received at this position after 50 ms and effectively modelled the partial scattering that probable occurred in the real reflections thus reducing the predictive errors.

The lack of scattering in specular modelling was also considered partly responsible for

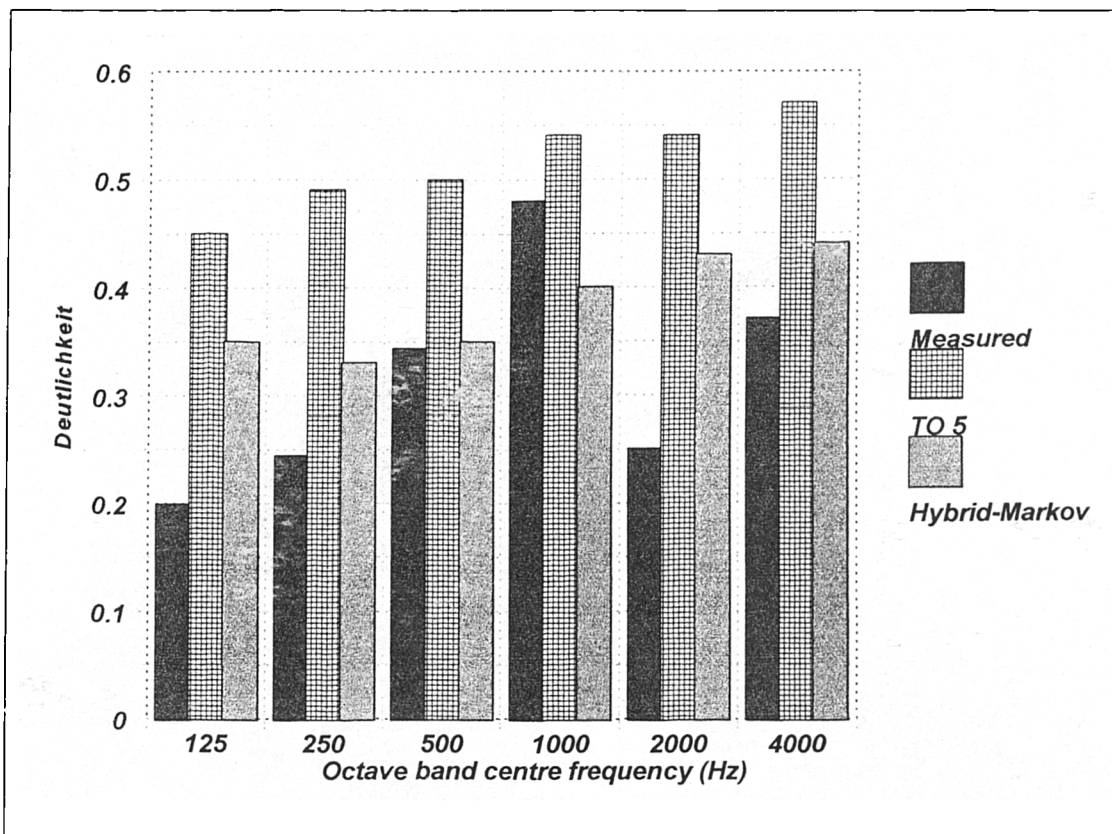


Figure 7.2 Prediction of deutlichkeit at receiver 11 in enclosure 5a ( $D_s = 0.1$ ,  $D_r = 0.7$ )

a failure to predict echoes in enclosure 3. However, initial results from the Hybrid-Markov model have not been able to predict these either. This suggests that more detailed modelling of the seating in enclosure 3 may be required.

### 7.3.3 Strength of specular reflections

The concentration of energy in single rays with specular modelling of reflections means that the strength of individual reflections can be too high. This caused problems with the prediction of deutlichkeit at receiver 8 in enclosure 5a (see subsection 5.3.3). Predictions from the Hybrid-Markov model at this receiver are shown in figure 7.3, along with the measured values and those predicted by a hybrid model. In the first 50 ms at this position many first order reflections were received from the side walls. The hybrid model therefore over-predicted deutlichkeit when these early order reflections were modelled specularly, that is, using a transition order of five. In the models the side walls were assigned diffusion coefficients of 0.1 so in the Hybrid-Markov model 10 % of the energy incident on the walls was transferred to the radiant-exchange calculation. This reduced

the strength of the received specular reflections and scattered energy away from the receiver.

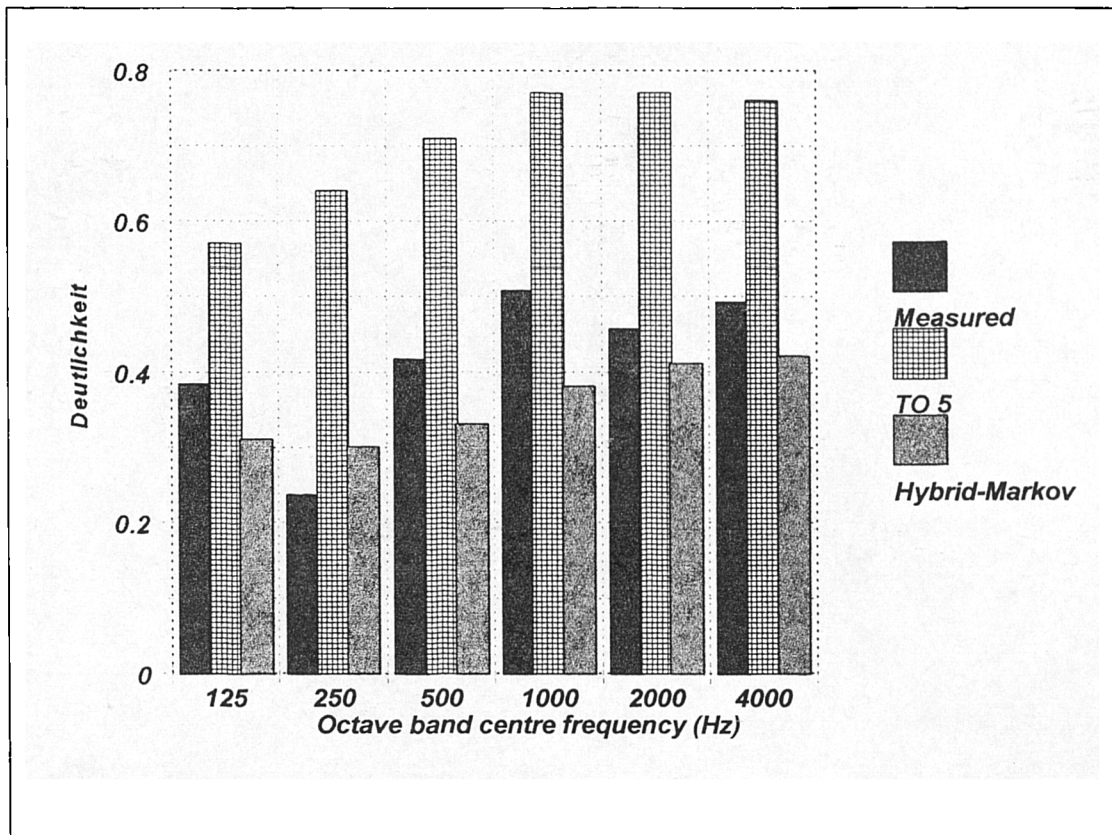


Figure 7.3 Measured and predicted deutlichkeit at receiver 8 in enclosure 5a ( $D_s = 0.1$ ,  $D_r = 0.7$ )

Figure 7.1, in subsection 7.3.1, shows that the Hybrid-Markov prediction of lateral energy fraction at receiver 6 in enclosure 3 was significantly higher than the measured value. This over-prediction also occurred with the hybrid model when early reflections were modelled specularly. In subsection 5.3.4 this was attributed to energy arriving from specular rays that were too strong because the energy they contained was not dissipated through surface scattering.

When diffusion coefficients of 0.1 and 0.7 were used on 'smooth' and 'rough' surfaces respectively the Hybrid-Markov model also over-predicted at this receiver. This was probably because 90 % of energy reflected from the side walls was modelled specularly. Consequently, when the diffusion coefficient of the side walls was increased there was a corresponding decrease in the predicted lateral energy fraction. This is illustrated in

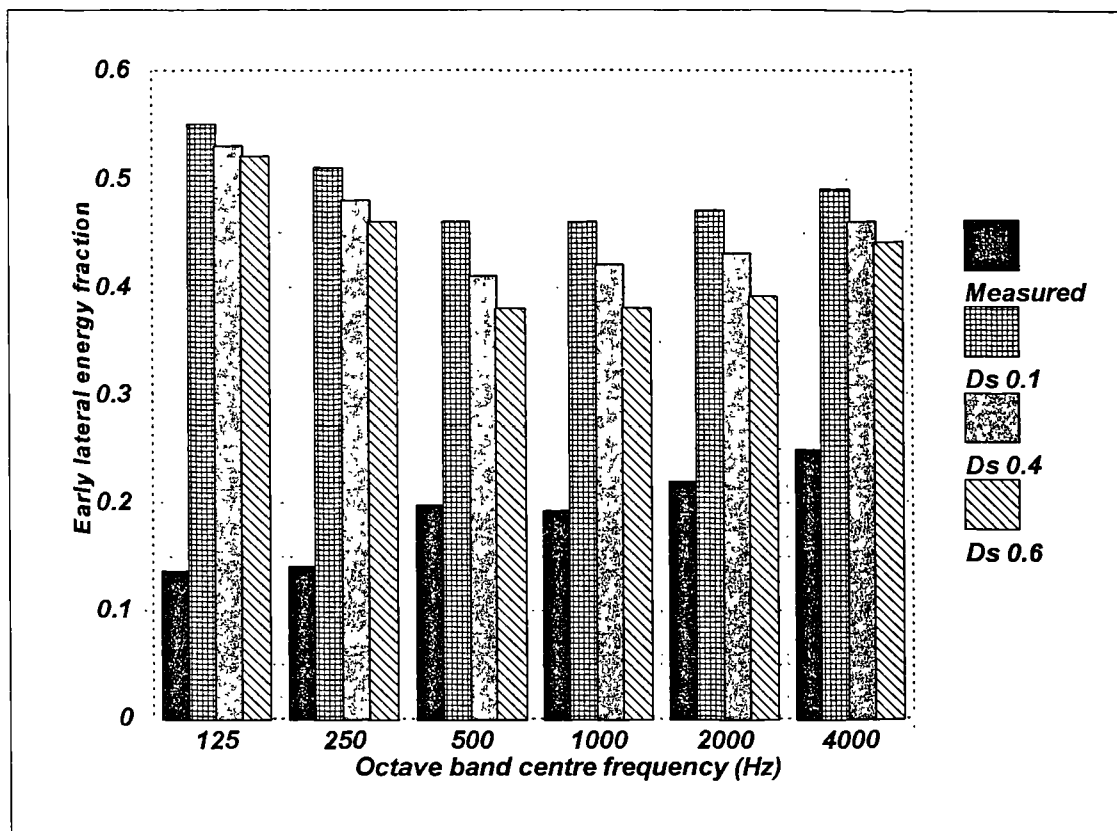


Figure 7.4 Hybrid-Markov predictions of lateral energy fraction at receiver 6 in enclosure 3 ( $D_r = 0.7$ )

figure 7.4. However, even with a relatively high diffusion coefficient of 0.6 assigned to the ‘smooth’ walls, the lateral energy fraction was still over-predicted. This was probably due to the transition probabilities, which controlled the directivity of surface radiation in the radiant-exchange process. These probabilities can be calculated in numerous ways but those used here assume that diffuse energy radiates hemi-spherically from point sources located at the centre of each surface. This is similar to the over-prediction of lateral energy fraction by diffuse secondary sources as discussed in subsection 5.3.4. To avoid this problem the calculation of transition probabilities needs refining.

### 7.3.4 Reflections from finite surfaces

In the Hybrid-Markov models used in this study, the dimensions of reflecting surfaces have not been considered in the determination of reflection strength. However, this is related to the defining of diffusion coefficients in the frequency domain, which is possible in the Hybrid-Markov model (see subsection 7.3.6). The scattering caused by dimensions of surfaces being comparable to sound wavelengths could therefore be simulated by

'manually' increasing the diffusion coefficients of these surfaces at appropriate frequencies.

Frequency dependent directivities of diffuse reflections could also be accounted for by calculating transition probabilities separately for each frequency band. This was considered impractical with the limited availability of computer memory in this study but is a possible direction for further improvement.

### **7.3.5 Modelling of curved surfaces**

As an existing program was used for the modelling of geometrical data, the modelling of curved surfaces was not improved. This caused inaccuracies in the prediction of reverberation times in enclosure 4 and prevented the prediction of a measured echo, caused by concave surface focussing, in enclosure 8. This is an area where further work is required.

### 7.3.6 Definition of diffusion coefficients

In subsection 5.2.2 variation of diffusion coefficients in the hybrid model was found to have little influence on the prediction of sound strength. Figure 7.5 shows that variation of diffusion coefficients in the Hybrid-Markov model has a more significant effect. This is as expected since the diffusion coefficient controls the amount of energy entering the radiant-exchange process rather than just the location of diffuse secondary sources. The results also demonstrate that diffusion coefficients should be defined in the frequency domain. For this particular receiver it appears that higher diffusion coefficients may be required at lower frequencies. However, these results are only indicative since the diffusion coefficient for 'rough' surfaces remained at 0.7 during these calculations.

A non-linear relationship between diffusion coefficients and predicted results was found in comparisons of results from diffuse secondary source models. This was considered to have been caused by a random element in the modelling of diffusion and was expected to limit the potential for optimizing diffusion coefficients (see subsection 5.3.6). As can be seen in figure 7.5, variation of diffusion coefficients in the Hybrid-Markov model

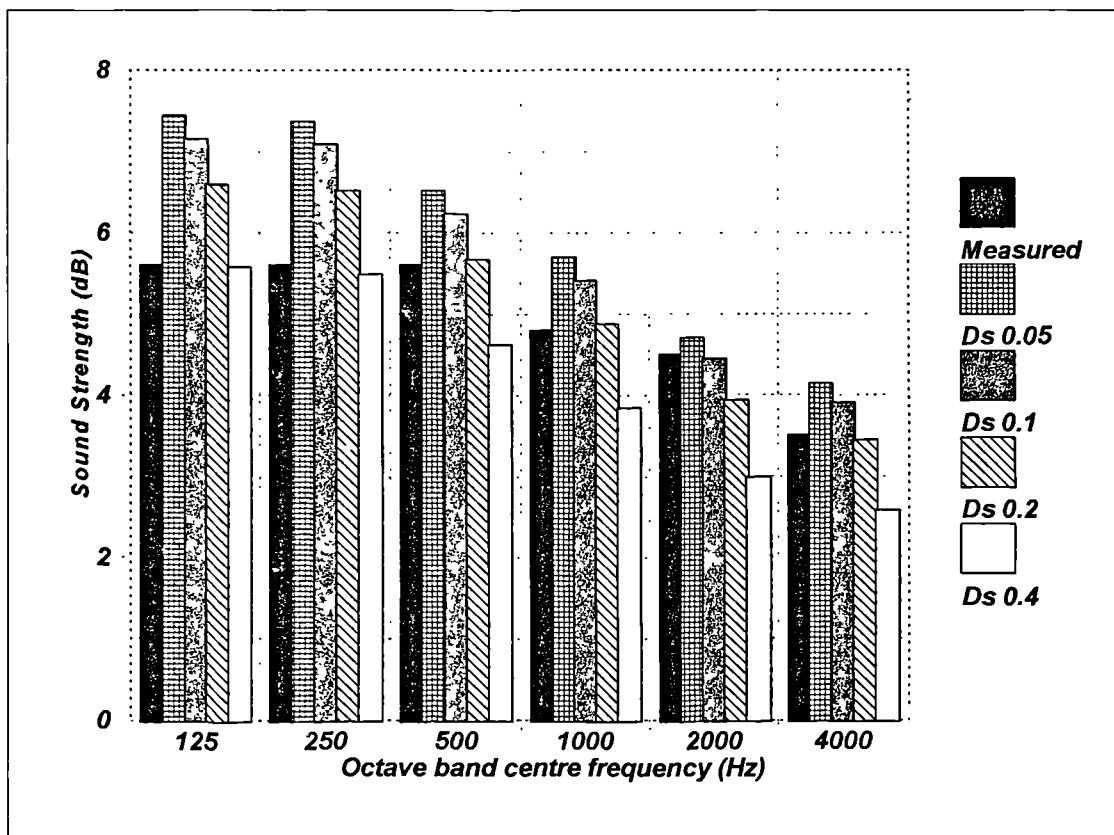


Figure 7.5 Effect of diffusion coefficient variation at receiver 9 in enclosure 5a ( $D_r = 0.7$ )

resulted in consistent variations in predicted sound strength, which will aid the optimization of diffusion coefficients for general use.

Since the Hybrid-Markov model allows the user to define diffusion coefficients in the frequency domain it would be possible to model the high frequencies using specular reflections and the low frequencies using the radiant-exchange process. Further work is therefore required to optimize the diffusion coefficients to give accurate predictions. For validity, this optimization would be best carried out by comparisons with measurements made in controlled rooms and is therefore beyond the scope of this study.

### 7.3.7 Modelling of barriers

Sound strength predictions in enclosure 6 are shown in figure 7.6. The hybrid model predictions, using a transition order of zero (TO 0) are discussed in subsection 5.3.5, where the drop in levels at receivers six to nine was attributed to the inaccurate modelling of balcony shielding effects. The Hybrid-Markov predictions still produced a drop in level at these positions but not to the same extent, errors therefore remained

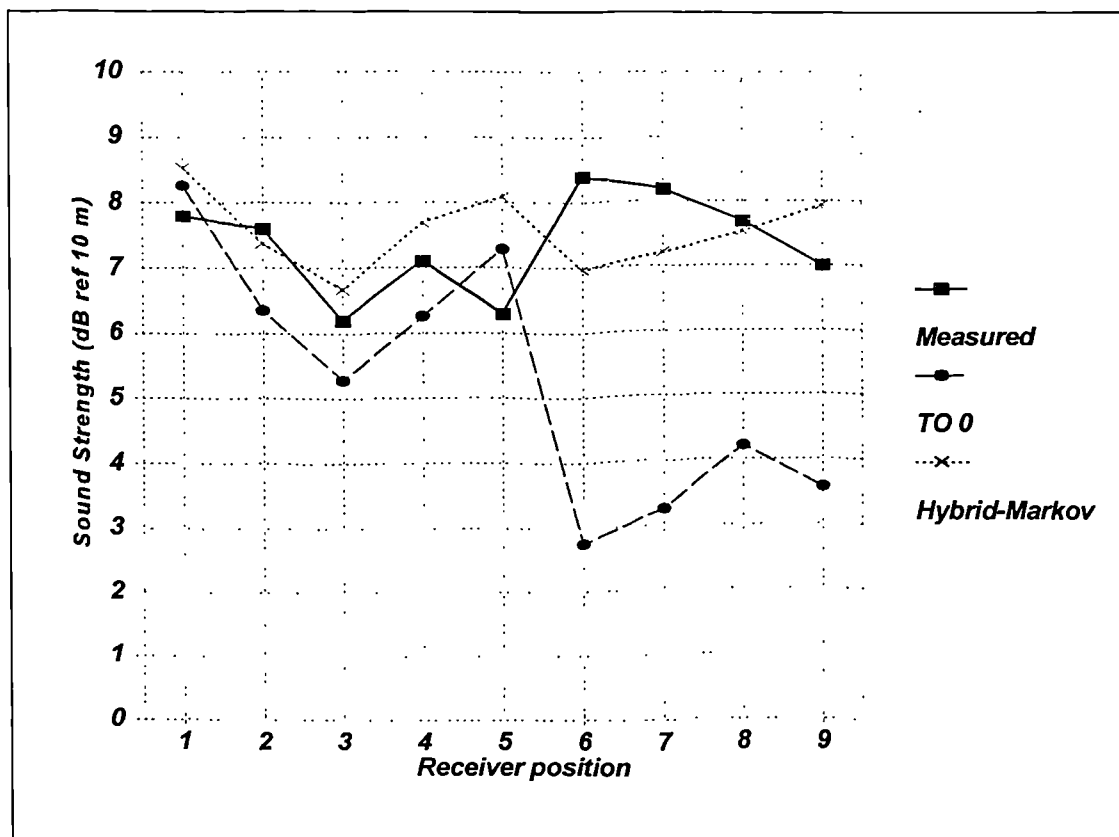


Figure 7.6 Comparison of sound strength predictions at 1000 Hz in enclosure 6 ( $D_s = 0.1$ ,  $D_r = 0.7$ )

within  $\pm 2$  dB. This is attributable to the way diffracted energy is accounted for in the radiant-exchange algorithm. A fraction of the energy incident on the balcony front (in this case 10 %) is transferred to the radiant-exchange process. In order to model energy diffracting over the balcony front, energy is radiated diffusely from the balcony front surface into  $4\pi$  space. This means that the modelled balcony front effectively becomes ‘translucent’ to diffuse sound. The theory behind this is explained in more detail in chapter 6.

### **7.3.8 Modelling of diffusion in the time domain**

Comparisons of predictions from specular and diffuse models with measured values indicated that for accurate predictions of reverberation time, early decay time, clarity index and deutlichkeit the modelling of surface diffusion should be present from the first reflection order. This has been achieved with the Hybrid-Markov model where the use of a parameter to control whether reflections are modelled specularly or diffusely according to reflection order has been removed. However, initial comparisons of average predictive errors from the Hybrid-Markov and diffuse secondary source models suggest that, because they have different calculation methods, further work is needed to determine optimum values for the diffusion coefficients and transition probabilities used.

## **7.4 Summary of Hybrid-Markov performance**

The Hybrid-Markov modelling technique was found to require more computer memory than the existing model investigated and because of software limitations could not be used to model two of the eight enclosures studied. This also meant that large data arrays used in the new modelling technique had to be stored on disk, which caused calculation times to be longer than with existing models. These practical problems would both be eliminated by use of more recent software.

Initial comparisons were made between the Hybrid-Markov model and the existing modelling techniques studied. For comparison purposes, the Hybrid-Markov model used the same diffusion coefficients as the existing models. As a result many of the average errors from the Hybrid-Markov model were found to be similar or slightly higher than

existing modelling techniques. However, the new technique is considered an improvement on existing techniques because it eliminates many of the weaknesses previously found and provides a flexible and robust framework for future development in the computer modelling of sound in enclosures. Of the eight weaknesses highlighted with existing modelling techniques, six were solved or partially-solved by the Hybrid-Markov method.

- Effects of the first three points were reduced by allowing specular and diffuse calculations to be combined to avoid reliance on a particular way of modelling reflections. This eliminated the use of a ‘transition order’ for the separation of specular and diffuse calculations. A ‘transition probability’ parameter was introduced to control directivities of diffuse energy radiating from surfaces.
- The new model does not directly allow reflection strength to be related to the dimensions of a reflecting surface. However, this would be possible through use of the transition probability parameter. This was not attempted because of time constraints.
- An existing program was used to model the geometry of enclosures. Curved surfaces were therefore still approximated by use of plane surfaces.
- Diffusion coefficients were defined in octave bands and assigned to each surface in a similar manner to absorption coefficients. The need for a random number generator in the modelling of diffusion was removed by transferring the modelling of surface diffusion into a radiant-exchange process. This is expected to improve the scope for optimizing diffusion parameters for use in a variety of enclosures.
- Modelling of edge diffraction around barriers was included by allowing diffuse energy to radiate ‘behind’ internal barriers. The method developed provides a framework for further refinement in the modelling of edge diffraction.

## Chapter 8

### Conclusions

Measurements of common room acoustic parameters were made in eight enclosures. Computer models of these enclosures were developed using existing software and effects of variations in the modelling of reflections were examined.

Comparisons of predictions with measurements highlighted weaknesses that can occur with existing modelling techniques. For prediction of reverberation time, early decay time, clarity index and deutlichkeit the modelling of diffuse reflections from the first reflection order was found to produce the smallest average errors. Apart from problems attributable to errors in input absorption coefficients, interference effects and to practical limitations of comparing point source predictions with measurements made using a sound source of finite dimensions, the remaining problems discovered were associated with the modelling of sound reflecting from surfaces. The following eight points were found to cause errors.

- i) Diffuse secondary sources over-scattered energy
- ii) Specular modelling of reflections did not provide enough scattering
- iii) Specular modelling produced over-strength reflections

- iv) Reflection strength was not related to the dimensions of a reflecting surface
- v) Curved surfaces were approximated by plane surfaces
- vi) Diffusion coefficients were not defined in the frequency domain
- vii) Modelling of diffraction around barriers was not included
- viii) Surface diffusion was not modelled correctly in the time domain

An improved modelling technique, referred to as a 'Hybrid-Markov' method, was developed to attempt to minimise the effects of these points. This method combined a conventional hybrid method with a radiant exchange procedure. Predictions from it were compared with measured values and previous predicted results.

Of the eight weaknesses highlighted with existing modelling techniques, six were solved or partially-solved by the Hybrid-Markov method.

- Effects of the first three points were reduced by allowing specular and diffuse calculations to be combined to avoid reliance on a particular way of modelling reflections. This eliminated the use of a 'transition order' for the separation of specular and diffuse calculations. A 'transition probability' parameter was introduced to control directivities of diffuse energy radiating from surfaces.
- The new model does not directly allow reflection strength to be related to the dimensions of a reflecting surface. However, this would be possible through use of the transition probability parameter. This was not attempted because of time constraints.
- An existing program was used to model the geometry of enclosures. Curved surfaces were therefore still approximated by use of plane surfaces.
- Diffusion coefficients were defined in octave bands and assigned to each surface in a similar manner to absorption coefficients. The need for a random number generator in the modelling of diffusion was removed by transferring the modelling of surface diffusion into a radiant-exchange process. This is expected to improve the scope for optimizing diffusion parameters for use in a variety of enclosures.

- Modelling of edge diffraction around barriers was included by allowing diffuse energy to radiate ‘behind’ internal barriers. The method developed provides a framework for further refinement in the modelling of edge diffraction.

Average errors of initial predictions from the Hybrid-Markov model were similar to those from existing models. However, the new modelling technique is an improvement on existing techniques because it provides a flexible and robust framework for future development by reducing random influences and unrealistic concepts. It can therefore be used to further improve the accuracy of acoustic predictions in enclosures.

## Chapter 9

### Further Work

The Hybrid-Markov modelling technique described in this text provides a new robust procedure for the further advancement of acoustic predictions in enclosures. Many of the unrealistic concepts present in previous procedures have been removed to allow further work to refine the modelling of surface reflections.

This refinement process would be enhanced by work in the following areas:

- Research on the optimization of diffusion coefficients of various surfaces could be undertaken by comparing predictions with measurements made in controlled enclosures. These diffusion coefficients could be defined in octave bands and could avoid coarse categorizations of 'smooth' and 'rough'.
- Research on scattering directivities and diffraction effects could be incorporated into the calculation of transition probabilities.
- Linkage of diffusion coefficients and transition probabilities with projects investigating the measurement and classification of diffusing surfaces may assist in improving the knowledge of diffuse surface behaviour.
- Transferring the modelling program to a programming language and computer

operating system that allows more flexible and efficient use of computer memory would enable larger, more complicated models to be generated and would speed up calculation procedures significantly.

- The modelling of curved surfaces could be developed, which would reduce the number of small plane surfaces required in models and would improve the prediction of focusing effects.

## References

1. Allred J C and Newhouse A, "Applications of the Monte Carlo method to architectural acoustics", J. Acoust. Soc America 30, p1, 1958
2. Vorländer M, "International round robin on room acoustical computer simulations." 15th ICA (II), p689, 1995
3. ISO 3382, "Measurement of the reverberation time of rooms with reference to other acoustical parameters.", International Standards Organization, 1997
4. Cremer L and Müller H A, "Principles and applications of room acoustics: Vol.1", Applied Science Publications, 1982
5. Polack J D, "Modifying the chambers to play billiards, or the foundations of reverberation theory", Acustica 76, p257, 1992
6. Eyring C F, "Reverberation time in 'dead' rooms", J. Acoust. Soc. Am. 1, p217, 1930
7. Knudsen V O and Harris C M, "Acoustical designing in architecture", John Wiley & sons, 1950
8. Rozenberg L D, "The method of calculation of sound fields formed by distributed systems of radiators working in enclosures", Zhurn. Tekhn. Fiz. 12, 1942
9. Mankovsky V S, "Acoustics of studios and auditoria", Focal Press, 1971
10. Gibbs B M and Jones D K, "A simple image method for calculating the distribution of sound pressure levels within an enclosure", Acustica 26, p24, 1972
11. Santon F, "Numerical prediction of echograms and the intelligibility of speech in rooms", J. Acoust. Soc. Am. 59, p1399, 1976
12. Allen J B and Berkley D A, "Image method for efficiently simulating small-room acoustics", J. Acoust. Soc. Am. 65, p943, 1979
13. Borish J, "Extension of the image model to arbitrary polyhedra", J. Acoust. Soc. Am. 75, p1827, 1984
14. Lee H and Lee B, "An efficient algorithm for the image model technique", Applied Acoustics 24, p87, 1988
15. Kristiansen U R, Krokstadt A and Follestad T, "Extending the image method to higher-order reflections", Applied Acoustics 38, p195, 1993

16. Krokstadt A, Strøm S and Sørdsal S, "Calculating the acoustical room response by the use of a ray tracing technique", *J Sound Vib.* 8, p118, 1968
17. Vorländer M, "Simulation of the transient and steady-state sound propagation in rooms using a new combined ray-tracing / image-source algorithm", *J. Acoust. Soc. Am.* 86, p172, 1989
18. Lehnert H, "Systematic errors of the ray-tracing algorithm", *Applied Acoustics* 38, p207, 1993
19. Krokstadt A, Strøm S and Sørdsal S, "Fifteen years experience with computerized ray tracing", *Applied Acoustics* 16, p291, 1983
20. Maercke D van, "Simulation of sound fields in time and frequency domain using a geometrical method", 12th ICA, pE11-7, 1986
21. Maercke D van and Martin J, "The prediction of echograms and impulse responses within the Epidaure software", *Applied Acoustics* 38, p93, 1993
22. Naylor G M, "ODEON - Another hybrid room acoustical model", *Applied Acoustics* 38, p131, 1993
23. Kuttruff H, "Room Acoustics", Second Edition, Applied Science Publishers Ltd, London, 1979
24. Schroeder M R, "Binaural dissimilarity and optimum ceilings for concert halls: more lateral sound diffusion", *J. Acoust. Soc. Am.* 65, p958, 1979
25. Hodgson M, "Evidence of diffuse surface reflections in rooms", *J. Acoust. Soc. Am.* 89, p765, 1991
26. Fricke F and Haan C H, "Musician and music critic responses to concert hall acoustics", 15th ICA (II), p457, 1995
27. Haan C H and Fricke F, "An evaluation of the importance of surface diffusivity in concert halls", *Applied Acoustics* 51, p53, 1997
28. Cox T J, "Designing curved diffusers for performance spaces", *J. Audio Eng. Soc.* 44, p354, 1996
29. Schroeder M R, "Diffuse sound reflection by maximum length sequences", *J. Acoust. Soc. Am.* 57, p149, 1975
30. Cox T J, "Optimization of profiled diffusers", *J. Acoust. Soc. Am.* 97, p2928, 1995
31. Beranek L L, "Concert hall acoustics - 1992", *J. Acoust. Soc. Am.* 92, p1, 1992
32. Ten Kate W R Th, "Analysis of the diffusor", 14th ICA, pF86, Beijing, 1992

33. Rindel J H, "Diffusion of sound in rooms - an overview", 15th ICA (II), p633, 1995
34. Lehnert H and Blauert J, "Principles of binaural room simulation", Applied Acoustics 36, p259, 1992
35. Kuttruff H and Stra en Th, "On the dependence of Reverberation Time on the 'wall diffusion' and on room shape", Acustica 45, p246, 1980
36. Heinz R, "Binaural room simulation based on an image source model with addition of statistical methods to include the diffuse sound scattering of walls and to predict the reverberant tail", Applied Acoustics 38, p145, 1993
37. Naylor G, "Treatment of early and late reflections in a hybrid computer model for room acoustics", J. Acoust. Soc. Am. 92 (Abstracts), p104, 1992
38. Lam Y W, "A comparison of three diffuse reflection modelling methods used in room acoustics computer models", J. Acoust. Soc. Am. 100, p2193, 1996
39. Gerlach R, "The reverberation process as markoff-chain - Theory and initial model experiments", Auditorium Acoustics, edited by Mackenzie R., Applied science publishers Ltd., London, 1975
40. Kruzins E and Fricke F, "The prediction of sound fields in non-diffuse spaces by a 'random walk' approach", J Sound Vib. 81, p549, 1982
41. Kr mer P, Alpei H, Kohlrausch A and P schel D, "Simulation von nachhallzeit und energieverlauf mit einem neuen nichtstatistischen computermodell", Acustica 75, p233, 1992
42. Lewers T, "A combined beam tracing and radiant exchange computer model of room acoustics", Applied Acoustics 38, p161, 1993
43. D'Antonio P, "The DISC project: Directional scattering coefficient determination and auralization of virtual environments", Noise-Con 93, p259, 1993
44. Dalenb ck B-I, Kleiner M and Svensson P, "A macroscopic view of diffuse reflection", J. Audio Eng. Soc. 42, p793, 1994
45. Dalenb ck B-I, "Room acoustic prediction and auralization based on a unified treatment of diffuse and specular reflection", 15th ICA (II), p425, 1995
46. Seraphim H P, "Untersuchungen  ber die unterschiedsschwelle exponentiellen abklingens von rauschbandimpulsen", Acustica 8, p280, 1958
47. Reichardt W and Schmidt W, "The audible steps of spatial impression in music performances", Acustica 17, p175, 1966

48. Reichardt W and Schmidt W, "The detectability of changes in sound field parameters for music", *Acustica* 18, p275, 1967
49. Cox T J, Davies W J and Lam Y W, "The sensitivity of listeners to early sound field changes in auditoria" *Acustica* 79, p27, 1993
50. Berntson A, "Comparisons between ray-tracing and reality", 15th ICA (II), p381, 1995
51. Farina A, "Verification of the accuracy of the pyramid tracing algorithm by comparisons with experimental measurements of objective acoustic parameters", 15th ICA (II), p445, 1995
52. Shearer K, "The acoustics of the Royal Albert Hall", *British kinematography sound and television*, February, p32, 1970
53. Schroeder M R, "New method of measuring reverberation time", *J. Acoust. Soc. Am.* 37, p409, 1965
54. Schroeder M R, "Integrated-impulse method measuring sound decay without using impulses", *J. Acoust. Soc. Am.* 66, p497, 1979
55. Golomb S W, "Shift register sequences", Aegean Park Press, 1982
56. Otshudi L, Guilhot J P and Charles J L, "Overview of techniques for measuring impulse response in room acoustics", *Proc. IOA* 10, p407, 1988
57. Rife D D and VanderKooy J, "Transfer-function measurement with Maximum-Length Sequences", *J. Audio Eng. Soc.* 37, p419, 1989
58. Davies W D T, "Generation and properties of Maximum-Length Sequences", *Control*, June, July, August, p53, 1966
59. Vorländer M and Bietz H, "Comparison of methods for measuring reverberation time", *Acustica* 80, p205, 1994
60. Bendat J S and Piersol A G, "Random data: analysis and measurement procedures", John Wiley and Sons, 1971
61. Naylor G and Rindel J H, "ODEON Room Acoustics Program version 2.5", User manual, Publication No. 49 from The Acoustics Laboratory, Technical University of Denmark, Lyngby, 1992
62. Rindel J H, Personal communication, 1995
63. BDP Acoustics Ltd, Sunlight House, PO Box 85, Quay Street, Manchester M60 3JA
64. Arup Acoustics, Parkin House, 8 St Thomas Street, Winchester, Hampshire SO23 9HE

65. Bies D A and Hansen C H, "Engineering noise control", Unwin Hyman, 1988
66. Kinsler L E, Frey A R, Coppens A B and Sanders J V, "Fundamentals of Acoustics", 3rd Edition, John Wiley & Sons, 1982
67. Sharland I, "Woods practical guide to noise control", Woods Acoustics, 1972
68. Beranek L L, "Acoustics", American Institute of Physics, 1986
69. "The Development of a Room Acoustic Diffusion Coefficient", A three year research project funded by the British Engineering and Physical Sciences Research Council (EPSRC), grant number GR/L13124, Commenced: 1 October 1996.
70. Howarth M J, Lin K and Lam Y W, "Predicting the acoustic influence of scale model modifications using a hybrid model", 15th ICA (II), p497, 1995
71. Lam Y W, "On the description of partially diffused reflections in a room acoustics computer model", 15th ICA (IV), p461, 1995
72. Bradley J S and Soulodre G A, "The acoustics of concert halls", Physics World, May 1997
73. Thiele R, "Richtungsverteilung und Zeitfolge der Schallrückwürfe in Räumen", Acustica 3, p291, 1953
74. Reichardt W and Lehman U, "Optimierung von Raumeindruck und Durchsichtigkeit von Musikdarbietung durch auswertung von Impulshalltests", Acustica 48 (3), p174, 1981
75. Barron M and Marshall A H, "Spatial impression due to early lateral reflections in concert halls: the derivation of a physical measure", J. Sound Vib. 77, p211, 1981
76. Tinsdeall N, "Sound insulation provided by windows", BRE Information Paper 6/94, 1994
77. Schultz T J and Watters B G, "Propagation of sound across audience seating", J. Acoust. Soc. Am. 36, p885, 1964
78. Sessler G M and West J E, "Sound transmission over theatre seats", J. Acoust. Soc. Am. 36, p1725, 1964
79. Davies W J and Lam Y W, "New attributes of seat dip attenuation", Applied Acoustics 41, p1, 1994

# Appendix A: Common acoustic parameters for rooms

## Reverberation Time, $T30$ (s)

Is a measure of the rate of decay of sound energy in an enclosure after a sound source has been switched off. It is defined as the time that would be required for the sound pressure level to decrease by 60 dB, at a rate of decay given by the linear least-squares regression of the measured decay curve from a level 5 dB below the initial level to 35 dB below.

## Sound Strength, $G$ (dB)

Is a sound pressure level produced by an omni-directional source normalized to the level that the same source would produce at a distance of 10 m in a free field. It is defined by

$$G = 10 \log \frac{\int_0^{\infty} p^2(t) dt}{\int_0^{\infty} p_{10}^2(t) dt}$$

where  $p(t)$  is the instantaneous sound pressure of the impulse response measured at the measurement point,  $p_{10}(t)$  is that measured at a distance of 10 m in a free field.

## Early Decay Time, $EDT$ (s)

Is similar to reverberation time but is measured over the initial 10 dB of the decay.

## Deutlichkeit, $D_{50}$

Is a measure of the balance between early and late arriving energy. It is normally used to determine whether conditions are suitable for speech. It is defined by

$$D_{50} = \frac{\int_0^{50ms} p^2(t) dt}{\int_0^{\infty} p^2(t) dt}$$

where  $p(t)$  is the instantaneous sound pressure of the impulse response measured at the measurement point.

### **Clarity Index, $C_{80}$ (dB)**

Is a measure of the balance between early and late arriving energy. It is normally used to determine whether conditions are suitable for music. It is defined by

$$C_{80} = 10 \log \frac{\int_0^{80ms} p^2(t) dt}{\int_{80ms}^{\infty} p^2(t) dt}$$

where  $p(t)$  is the instantaneous sound pressure of the impulse response measured at the measurement point.

### **Centre Time, $T_s$ (ms)**

Is a measure of the balance between early and late arriving energy. It is the time of the centre of gravity of the squared impulse response and is defined by

$$T_s = \frac{\int_0^{\infty} t.p^2(t) dt}{\int_0^{\infty} p^2(t) dt}$$

where  $p(t)$  is the instantaneous sound pressure of the impulse response measured at the measurement point.

### **Lateral Energy Fraction, $LF$**

Is a measure of the perceived width of the sound source and describes the fraction of the energy, arriving within the first 80 ms, that arrives from lateral directions. It is defined by

$$LF = \frac{\int_{5ms}^{80ms} p_L^2(t) dt}{\int_0^{80ms} p^2(t) dt}$$

where  $p_L(t)$  and  $p(t)$  are the instantaneous sound pressures of impulse responses measured at the measurement point using figure-of-eight and omni-directional microphones respectively.

# Appendix B: Hybrid-Markov program listing

## Visibility Check Unit

UNIT VisCheck;

(\* holds calcs for surface to surface and surface to receiver checks \*)

INTERFACE

USES tp crt, dos, graph, printer, CBBasis, MenuDec, MenuBas,  
Menu2, RayGlobals, GetBasic, Graph2D, PrRelPar, RayProcs, Response,  
Markoff;

VAR SurfToRecSolidAngle : CoefArray;  
DistToRecArr : CoefArray;  
AvPtOfSurf : PtOfSurfArray; (\* average point on each surface \*)

PROCEDURE CalcSurfToRecSolidAngles;  
PROCEDURE CalcSurfToSurfSolidAngles;  
PROCEDURE CalcAvPtsOfSurfaces;

IMPLEMENTATION

CONST NumOfCheckRays = 5460; (\* number of rays emitted from check  
source \*)  
(\* this is max no. available due to  
memory limits \*)

TYPE SpherVect = RECORD  
R, Elev, Azi : SINGLE;  
END;  
CartRayArray = ARRAY[ 1..NumOfCheckRays] OF SPT3D;  
SpherRayArray = ARRAY[ 1..NumOfCheckRays] OF SpherVect;

VAR ActualRaysUsed : INTEGER;  
PtrCartRayDir : ^CartRayArray;  
tempangf : TEXT;

PROCEDURE TransSpherToCartesian( r, theta, phi : DOUBLE; VAR CartVect :  
SPT3D);  
(\* transforms spherical coordinates to cartesian \*)  
BEGIN  
CartVect.x := r \* cos( theta ) \* cos( phi );  
CartVect.y := r \* cos( theta ) \* sin( phi );  
CartVect.z := r \* sin( theta );  
END; (\* procedure transsphertocartesian \*)

PROCEDURE CalcRayDistribution;

```

(* calculates ray directions from visibility check source *)

CONST SourceRelRayRadius1 = 1.7; (* re-stated for independence *)
  MaxRayRings1 = 200; (* max no of rings on check-source *)
  AzimuthLowest = -180;
  AzimuthHighest = 180; (* source radiation limits - degrees *)
  ElevationLowest = -90;
  ElevationHighest = 90;

VAR ChSourceHorizLower : Double; { Source radiation limits - radians }
  ChSourceHorizUpper : Double;
  ChSourceVertLower : Double;
  ChSourceVertUpper : Double;
  AvRaySeparation : Double;
  ChSourceVertAngle : Double;
  ChSourceNVertSteps : Integer;
  Ring : Integer;
  NoOfRings : Integer;
  ChRayNo : INTEGER;
  ChSourceVertStep : Double; { Vert. angle between rings of rays }
  ChSourceNHorizSteps : Array[ 1..MaxRayRings1] of Integer;

PROCEDURE GetRayDirections;
(* calculates ray directions from checksource *)

VAR AzStepNo : INTEGER;
  i : INTEGER;
  ChSourceHorizAngle : DOUBLE;
  ChSourceHorizStep : DOUBLE;
  TempStr2 : STRING[50];

BEGIN (* getraydirections *)
  ChSourceVertAngle := ChSourceVertLower - ChSourceVertStep * 0.5;
  ChRayNo := 0;
  FOR i := 1 TO NoOfRings DO
  BEGIN
    ChSourceVertAngle := ChSourceVertAngle + ChSourceVertStep;
    (* calc change in angle between adjacent rays on ring *)
    ChSourceHorizStep := Round( ChSourceHorizUpper -
ChSourceHorizLower)
    / ChSourceNHorizSteps[ i];
    ChSourceHorizAngle := ChSourceHorizLower - ChSourceHorizStep * 0.5; (*
start angle *)
    FOR AzStepNo := 1 TO ChSourceNHorizSteps[ i] DO
    BEGIN
      ChRayNo := ChRayNo + 1;
      ChSourceHorizAngle := ChSourceHorizAngle + ChSourceHorizStep;
      TransSpherToCartesian( 1, ChSourceVertAngle, ChSourceHorizAngle,
PtrCartRayDir^[ ChRayNo]);

      END; (* for horizstep *)
    END; (* for ring *)
  END; (* proc getraydirections *)

BEGIN (* calcraydistribution *)

```

```

FOR ChRayNo := 1 TO NumOfCheckRays DO
BEGIN
  PtrCartRayDir^[ ChRayNo].x := 0;
  PtrCartRayDir^[ ChRayNo].y := 0;
  PtrCartRayDir^[ ChRayNo].z := 0;
END; (* for *)
ChSourceHorizLower := AzimuthLowest * pih / 180;
ChSourceHorizUpper := AzimuthHighest * pih / 180;
ChSourceVertLower := ElevationLowest * pih / 180;
ChSourceVertUpper := ElevationHighest * pih / 180;
(* Set up array SourceNHorizSteps with no. of rays for each ring *)
AvRaySeparation := (Sin(ChSourceVertUpper) - Sin(ChSourceVertLower))
  * (ChSourceHorizUpper - ChSourceHorizLower) /
NumOfCheckRays;
AvRaySeparation := Sqrt(AvRaySeparation);
ChSourceNVertSteps := Round( ( ChSourceVertUpper - ChSourceVertLower)
  / AvRaySeparation);
IF ChSourceNVertSteps = 0 THEN ChSourceNVertSteps := 1;
ChSourceVertStep := (ChSourceVertUpper - ChSourceVertLower) /
ChSourceNVertSteps;
ChSourceVertAngle := ChSourceVertLower + ChSourceVertStep * 0.5;
ActualRaysUsed := 0;
Ring := 1;
WHILE ChSourceVertAngle <= ChSourceVertUpper DO
BEGIN
  ChSourceNHorizSteps[ Ring] := Round( ( ChSourceHorizUpper -
ChSourceHorizLower)
  * Cos( ChSourceVertAngle) / AvRaySeparation);
  IF ChSourceNHorizSteps[ Ring] = 0 THEN ChSourceNHorizSteps[ Ring] := 1;
  ChSourceVertAngle := ChSourceVertAngle + ChSourceVertStep;
  ActualRaysUsed := ActualRaysUsed + ChSourceNHorizSteps[ Ring];
  Ring := Ring + 1;
END;
NoOfRings := Ring - 1;
GetRayDirections;
END; (* proc calcraydistribution *)

```

```

PROCEDURE CalcSurfToRecSolidAngles;
(* calculates solid angles between visible surfaces and receiver *)

```

```

TYPE TallyArray = ARRAY[ 1..MaxNoWalls] OF INTEGER;

```

```

VAR i_Ray          : INTEGER;
    i_Surf         : INTEGER;
    TallyOfHits    : TallyArray;
    ChRDirection   : Pt3D;
    ChHitPt        : ReflPath;
    CosInc         : DOUBLE;
    ChSrceToHitLength : DOUBLE;
    ChSourcePt     : Pt3D;
    Stri_Ray       : STRING[6];

```

```

BEGIN

```

```

if writefileopened ( tempangf, 'srfrecsa.txt') then
begin
GETMEM ( PtrCartRayDir, SizeOf ( CartRayArray));
GW (23,20,80+Yellow,'Calculating Visibilities. ');
ChSourcePt.x := RunParams.Response.RelReceiverPosition.x;
ChSourcePt.y := RunParams.Response.RelReceiverPosition.y;
ChSourcePt.z := RunParams.Response.RelReceiverPosition.z;
CalcRayDistribution;
FOR i_Surf := 1 TO RunParams.Room.WallsInRoom DO
BEGIN
  TallyOfHits[ i_Surf] := 0;
END;
FOR i_Ray := 1 TO ActualRaysUsed DO
BEGIN
  STR( i_Ray, Stri_Ray);
  gw (23,21,80+Yellow, 'Ray No '+Stri_Ray);
  ChRDirection.x := PtrCartRayDir^[ i_Ray].x; (* convert to double *)
  ChRDirection.y := PtrCartRayDir^[ i_Ray].y;
  ChRDirection.z := PtrCartRayDir^[ i_Ray].z;
  IF FindWallHitByRay ( 0, ChSourcePt, ChRDirection, ChHitPt
    , CosInc, ChSrceToHitLength) THEN
  BEGIN
    FOR i_Surf := 1 TO RunParams.Room.WallsInRoom DO
    BEGIN
      IF i_Surf = ChHitPt.EndSurface THEN
      BEGIN
        TallyOfHits[ i_Surf] := TallyOfHits[i_Surf] + 1;
      END;
    END; (* for i_surf *)
  END; (* if findwallhitbyray *)
END; (* for i_ray *)
(* next calc solid angles *)
FOR i_surf := 1 TO RunParams.Room.WallsInRoom DO
BEGIN
  SurfToRecSolidAngle[ i_Surf] := TallyOfHits[ i_Surf] * 4 * Pih /
ActualRaysUsed;
  writeln(tempangf, 'Surface ', i_surf, 'Solid Angle ', SurfToRecSolidAngle[
i_Surf]);
END; (* for *)
FREEMEM ( PtrCartRayDir, SizeOf ( CartRayArray));
close(tempangf);
end; (* if tempang file opened *)
END; (* procedure CalcSurfToRecSolidAngles *)

```

```

PROCEDURE CalcAvPtsOfSurfaces;
(* calcs average point of each surface using corners *)

```

```

FUNCTION DistToRec ( EPx, EPy, EPz : DOUBLE) : DOUBLE;
(* calcs distance from refl endpoint to receiver *)
VAR Rx, Ry, Rz : DOUBLE;
BEGIN
  Rx := RunParams.Response.RelReceiverPosition.x;
  Ry := RunParams.Response.RelReceiverPosition.y;

```

```

    Rz := RunParams.Response.RelReceiverPosition.z;
    DistToRec := SQRT ( SQR(EPx-Rx) + SQR(EPy-Ry) + SQR(EPz-Rz));
END;

VAR SurfCorns      : CornerArr;
    i, j, NumOfCorns : INTEGER;
    SumX           : DOUBLE;
    SumY           : DOUBLE;
    SumZ           : DOUBLE;

BEGIN
    FOR i := 1 TO RunParams.Room.WallsInRoom DO
    BEGIN
        SumX := 0;
        SumY := 0;
        SumZ := 0;
        GetCorners ( i, SurfCorns, NumOfCorns);
        FOR j := 1 TO NumOfCorns DO
        BEGIN
            SumX := SumX + SurfCorns[ j].x;
            SumY := SumY + SurfCorns[ j].y;
            SumZ := SumZ + SurfCorns[ j].z;
        END; (* for j *)
        AvPtOfSurf[ i].x := SumX / NumOfCorns;
        AvPtOfSurf[ i].y := SumY / NumOfCorns;
        AvPtOfSurf[ i].z := SumZ / NumOfCorns;
        DistToRecArr[ i] := DistToRec( AvPtOfSurf[ i].x, AvPtOfSurf[ i].y, AvPtOfSurf[
i].z);
    END; (* for i *)
END; (* proc calcavptsofsurfaces *)

PROCEDURE CalcSurfToSurfSolidAngles;
(* calculates solid angles from surfaces to surfaces      *)
(*if a surface is not visible to the check-source      *)
(* it is not considered visible - ie solidangle = 0     *)

LABEL 111;

TYPE TallyArray = ARRAY[ 1..MaxNoWalls] OF INTEGER;

VAR i_Ray      : INTEGER;
    i_Surf     : INTEGER;
    SourceSurf : INTEGER;
    TallyOfHits : TallyArray;
    ChRDirection : Pt3D;
    ChHitPt     : ReflPath;
    CosInc      : DOUBLE;
    ChSrceToHitLength : DOUBLE;
    ChSourcePt  : Pt3D;
    Str_Surf    : STRING[3];
    Str_WallsInRoom : STRING[3];
    SurfToSurfSolidAngle : CoefArray;
    SToSfName   : STRING;

```

```

SToSFile      : CoefFile;
NoFileExists  : BOOLEAN;

PROCEDURE CheckIfFileExists(FName:string);
VAR DirInfo: SearchRec;
BEGIN
  NoFileExists := TRUE;
  FINDFIRST ( FName, Archive, DirInfo);
  IF DosError = 0 THEN NoFileExists := FALSE;
  writeln (tempangf, 'doserror ',DosError);
END; (* proc checkiffileexists *)

BEGIN
  if writefileopened ( tempangf, 'solangle.txt') then
  begin
    SToS FName := FileName+'.ang';
    writeln (tempangf, SToS FName);
    CheckIfFileExists ( SToS FName);
111:
    IF NoFileExists THEN
    BEGIN
      IF FMade ( SToSFile, SToS FName) THEN
      BEGIN
        GETMEM ( PtrCartRayDir, SizeOf ( CartRayArray));
        GW (20,20,80+Yellow,'Calculating Surface to Surface Visibilities');
        CalcAvPtsOfSurfaces;
        STR ( RunParams.Room.WallsInRoom, Str_WallsInRoom);
        FOR SourceSurf := 1 TO RunParams.Room.WallsInRoom DO
        BEGIN
          FOR i_Surf := 1 TO RunParams.Room.WallsInRoom DO
            SurfToSurfSolidAngle[ i_Surf] := 0;
          STR ( SourceSurf, Str_Surf);
          GW (23,21,80+Yellow, 'Surface '+Str_Surf+' of '+Str_WallsInRoom);
          ChSourcePt.x := AvPtOfSurf[ SourceSurf].x;
          ChSourcePt.y := AvPtOfSurf[ SourceSurf].y;
          ChSourcePt.z := AvPtOfSurf[ SourceSurf].z;
          CalcRayDistribution;
          FOR i_Surf := 1 TO RunParams.Room.WallsInRoom DO
          BEGIN
            TallyOfHits[ i_Surf] := 0;
          END;
          FOR i_Ray := 1 TO ActualRaysUsed DO
          BEGIN
            ChRDirection.x := PtrCartRayDir^[ i_Ray].x;
            ChRDirection.y := PtrCartRayDir^[ i_Ray].y;
            ChRDirection.z := PtrCartRayDir^[ i_Ray].z;
            IF FindWallHitByRay ( SourceSurf, ChSourcePt, ChRDirection, ChHitPt
              , CosInc, ChSrceToHitLength) THEN
            BEGIN
              FOR i_Surf := 1 TO RunParams.Room.WallsInRoom DO
              BEGIN
                IF i_Surf = ChHitPt.EndSurface THEN
                BEGIN
                  TallyOfHits[ i_Surf] := TallyOfHits[i_Surf] + 1;

```

```

        END;
        END; (* for i_surf *)
        END; (* if findwallhitbyray *)
        END; (* for i_ray *)
        (* next calc solid angles *)
        FOR i_surf := 1 TO RunParams.Room.WallsInRoom DO
        BEGIN
            SurfToSurfSolidAngle[ i_Surf] := TallyOfHits[ i_Surf] * 4 * Pih /
ActualRaysUsed;
            writeln ( tempangf, 'Surface ', SourceSurf,' to Surface ',i_surf
                , 'Solid Angle = ', SurfToSurfSolidAngle[ i_Surf]:8 :2);
            END; (* for *)
            WRITE ( SToSFile, SurfToSurfSolidAngle);
            END; (* for sourceSurf *)
            FREEMEM ( PtrCartRayDir, SizeOf ( CartRayArray));
            CLOSE ( SToSFile);
            END; (* if fmade *)
        END
    ELSE
        BEGIN
            WriteAndWait1(99,12,White,16*Blue,White,
                Answer,AnswerSC, 'File already exists. Re-calculate? ( Y/N)');
            IF Answer = 'Y' THEN
                BEGIN
                    NoFileExists := TRUE;
                    GOTO 111;
                END;
            END; (* if nofileexists *)
            GW (20,20,Blue,' ');
            close(tempangf);
            end; (* if tempang file opened *)
        END; (* procedure CalcSurfToSurfSolidAngles *)
    END.

```

## Radiant-exchange Unit

UNIT MarkOff;

INTERFACE

USES tpcrt, dos, graph, printer, CBBasis, MenuDec, MenuBas,  
Menu2, RayGlobals, GetBasic, Graph2D, PrRelPar, RayProcs, Response;

CONST MaxNoWalls = 161; (\* gives max number of walls for this method \*)  
(\* ODEON's previous max was 500 \*)  
DiffEnergyDecayFName = 'diffdec.arr'; (\* used in response.pas \*)

TYPE CoefArray = Array[ 1..MaxNoWalls] OF SINGLE;  
(\* is used to write to typed file \*)  
CoefFile = FILE OF CoefArray;  
FileNameString = STRING[ 12];  
EnergyArray = ARRAY[ 1..MaxNoWalls] OF SFreqArr;  
EnergyDecayFile = FILE OF SFreqArr;  
SFreqArrList = ARRAY [ 1..MaxNoWalls] OF SFreqArr;  
PtOfSurfArray = ARRAY[ 1..MaxNoWalls] OF Pt3D;

VAR DImpF : EnergyDecayFile; (\* diffuse energy decay file \*)  
PtrMrkoffEnHistogram : ^EnergyHistogram;  
MrkoffEnBefore50, MrkoffEnBefore80, MrkoffEnAfter80 : SFreqArr;  
MrkoffFig8En : SFreqArr;  
DMFarr : SFreqArrList; (\* contains diff coefs for each surface \*)  
MaxNoSteps : INTEGER; (\* number of steps in diffuse decay \*)  
TempStr : STRING;  
TempF, Temp2F : TEXT;

PROCEDURE RunMarkoff;  
PROCEDURE DispCoefFile ( MqFName : FileNameString;  
NoOfRows : INTEGER);  
PROCEDURE WatchOnScreen ( TxtToShow : STRING);  
FUNCTION WriteFileOpened ( VAR ProgName : TEXT;  
DosName : STRING) : BOOLEAN;  
FUNCTION EnergyDecayFOpened ( VAR TheFile : EnergyDecayFile;  
FName : STRING) : BOOLEAN;  
FUNCTION FMade ( VAR TheFile : CoefFile;  
FName : STRING) : BOOLEAN;

IMPLEMENTATION

USES VisCheck;

CONST DiffMatLibFName = 'diffmat.lib';  
DiffEnFName = 'diffuse.ene';  
DiffEnSteppedFName = 'diffstep.arr';  
TransProbFName = 'tranprob.arr';  
ReflCoefFName = 'reflcoef.arr';  
ProdMatFName = 'prodmatr.arr';  
CopyMatFName = 'copymatr.arr';

```

TransposeMatFName = 'transpos.arr'; (* used in proc transposematrix *)
MultMatFName = 'multiply.arr';
SingleBandProdMatFName = 'sb_prod.arr';
DiffEnergyMatFName = 'diffener.arr';

```

```

TYPE NumOfHitArr = ARRAY[ 0..MaxWallsInRoom] OF SINGLE;
  SurfDiffMatIndexRec = RECORD
    Index : BYTE;
    MatRef : LONGINT;
    MatName : String[100];
    DiffCoeff: SFreqArr;
  END;
  DiffEnergyRec = RECORD
    ReflTime : SINGLE;
    SurfaceNo : INTEGER;
    DiffEnergy: FreqArr;
  END;
  SurfDiffMatIndex = ARRAY[ 0..MaxDifMatRefs] of SurfDiffMatIndexRec;
  FreqCoefArr = ARRAY[ 1..NFreqBands] OF CoefArray;
  MatFile = FILE OF MatFileRecord;
  HisFileType = FILE OF SingleReflPath;
  DiffEnFileType = FILE OF DiffEnergyRec;

```

```

VAR StepTimeLength : Single;
  DiffMatFile : FILE OF SurfDiffMatIndexRec;
  SurfDiffMaterial : SurfDiffMatIndex;
  Material : MatFileRecord;
  AMFArr : SFreqArrList; (* contains abs coefs for each surface *)
  Refl : SingleReflPath; (* to read from HIS file *)
  RayEn : FreqArr; (* energy in ray *)
  RayEnWithAir : FreqArr; (* energy hitting surface *)
  DiffEn : FreqArr; (* diffuse energy from refl, calc'd in calcnewrayen *)
  MatF : MatFile;
  HisF : HisFileType;
  DiffEnF : DiffEnFileType;
  DiffLibF : TEXT;
  DiffEnSteppedF : CoefFile; (* energy is summed into each step - to be *)
                          (* added to markoff steps *)
  AngleFact : CoefArray;
  ReceiverTransform2 : Mat3D;
  TransProbData : CoefArray; (* 1 row of trans prob matrix *)
  CData : CoefArray; (* 1 row of refl coef matrices *)
  StartEnergy : EnergyArray; (* energy at each wall *)
  ProdData : CoefArray; (* 1 row of multiplied matrix *)
  TPF : CoefFile; (* file for trans prob matrix *)
  CF : CoefFile; (* file for refl coef matrices *)
  PF : CoefFile; (* file for product matrices *)
  TF : CoefFile; (* transposed matrix file *)
  DEF : CoefFile; (* each row gives surface energies at nstep *)
  SBPF : CoefFile; (* single matrix taken from pf *)
  PtrFig8MrkoffEnHis : ^EnergyHistogram;
  CosTheta : CoefArray;
  StrMaxNoSteps : STRING [ 4];

```

DirectSoundTime : SINGLE;

```
FUNCTION ReadFileOpened ( VAR ProgName : TEXT;
                          DosName : STRING) : BOOLEAN;
(* used to check text file has opened for reading *)
BEGIN
  ASSIGN ( ProgName, DosName);
  {$I-}      (* turns off auto check *)
  RESET ( ProgName);  (* opens file for reading only *)
  {$I+}
  IF IOResult = 0 THEN
    ReadFileOpened := TRUE
  ELSE
    ReadFileOpened := FALSE;
END; (* func readfileopened *)
```

```
FUNCTION MatFileOpened ( VAR ProgName : MatFile;
                          DosName : STRING) : BOOLEAN;
(* used to check text file has opened for reading *)
BEGIN
  ASSIGN ( ProgName, DosName);
  {$I-}      (* turns off auto check *)
  RESET ( ProgName);  (* opens file for reading only *)
  {$I+}
  IF IOResult = 0 THEN
    MatFileOpened := TRUE
  ELSE
    MatFileOpened := FALSE;
END; (* func matfileopened *)
```

```
FUNCTION HisFileOpened ( VAR ProgName : HisFileType;
                          DosName : STRING) : BOOLEAN;
(* used to check his file has opened for reading *)
BEGIN
  ASSIGN ( ProgName, DosName);
  {$I-}      (* turns off auto check *)
  RESET ( ProgName);  (* opens file for reading only *)
  {$I+}
  IF IOResult = 0 THEN
    HisFileOpened := TRUE
  ELSE
    HisFileOpened := FALSE;
END; (* func readfileopened *)
```

```
FUNCTION DiffEnFileCreated ( VAR ProgName : DiffEnFileType;
                              DosName : STRING) : BOOLEAN;
(* used to check diffenfile file has opened for writing*)
BEGIN
  ASSIGN ( ProgName, DosName);
  {$I-}      (* turns off auto check *)
```

```

REWRITE ( ProgName);    (* opens file for writing only *)
{$I+}
IF IOResult = 0 THEN
    DiffEnFileCreated := TRUE
ELSE
    DiffEnFileCreated := FALSE;
END; (* func diffenfilecreated *)

```

```

FUNCTION DiffEnFileOpened ( VAR ProgName : DiffEnFileType;
                             DosName : STRING) : BOOLEAN;
(* used to check diffenfile file has opened for reading *)
BEGIN
    ASSIGN ( ProgName, DosName);
    {$I-}          (* turns off auto check *)
    RESET ( ProgName);    (* opens file for reading only *)
    {$I+}
    IF IOResult = 0 THEN
        DiffEnFileOpened := TRUE
    ELSE
        DiffEnFileOpened := FALSE;
END; (* func diffenfilecreated *)

```

```

FUNCTION WriteFileOpened ( VAR ProgName : TEXT;
                            DosName : STRING) : BOOLEAN;
(* used to check text file has opened for writing*)
BEGIN
    ASSIGN ( ProgName, DosName);
    {$I-}          (* turns off auto check *)
    REWRITE ( ProgName);    (* opens file for writing only *)
    {$I+}
    IF IOResult = 0 THEN
        WriteFileOpened := TRUE
    ELSE
        WriteFileOpened := FALSE;
END; (* func writefileopened *)

```

```

FUNCTION FMade ( VAR TheFile : CoefFile;
                 FName : STRING) : BOOLEAN;
(* used to check coef typed file has opened for writing *)
BEGIN
    ASSIGN ( TheFile, FName);
    {$I-}          (* turns off auto check *)
    REWRITE ( TheFile);
    {$I+}
    IF IOResult = 0 THEN
        FMade := TRUE
    ELSE
        FMade := FALSE;
END; (* func FMade *)

```

```

FUNCTION EnergyDecayFileMade ( VAR TheFile : EnergyDecayFile;
                               FName : STRING) : BOOLEAN;
(* used to check energydecayfile has opened for writing*)
BEGIN
  ASSIGN ( TheFile, FName);
  {$I-}          (* turns off auto check *)
  REWRITE ( TheFile);
  {$I+}
  IF IOResult = 0 THEN
    EnergyDecayFileMade := TRUE
  ELSE
    EnergyDecayFileMade := FALSE;
END; (* func EnergydecayfileMade *)

```

```

FUNCTION FOpened ( VAR TheFile : CoefFile;
                  FName : STRING) : BOOLEAN;
(* used to check coef typed file has opened for reading*)
BEGIN
  ASSIGN ( TheFile, FName);
  {$I-}          (* turns off auto check *)
  RESET ( TheFile);
  {$I+}
  IF IOResult = 0 THEN
    FOpened := TRUE
  ELSE
    FOpened := FALSE;
END; (* func FOpened *)

```

```

FUNCTION EnergyDecayFOpened ( VAR TheFile : EnergyDecayFile;
                              FName : STRING) : BOOLEAN;
(* used to check coef typed file has opened for reading*)
BEGIN
  ASSIGN ( TheFile, FName);
  {$I-}          (* turns off auto check *)
  RESET ( TheFile);
  {$I+}
  IF IOResult = 0 THEN
    EnergyDecayFOpened := TRUE
  ELSE
    EnergyDecayFOpened := FALSE;
END; (* func FOpened *)

```

```

FUNCTION Log10 ( Sing1 : SINGLE) : SINGLE;
(* calcs log10 of single number *)
BEGIN
  IF ( Sing1 > 0) THEN
    BEGIN
      Log10 := LN ( Sing1) / LN ( 10);
    END
  ELSE
    BEGIN

```

```

    Log10 := -99;
END;
END; (* func sing1 *)

```

```

PROCEDURE EndBeep;
BEGIN
    SOUND ( 440);
    DELAY ( 200);
    NOSOUND;
END; (* proc endbeep *)

```

```

PROCEDURE CalcStepTimeLength;
(* calcs steptimelength and maxnosteps *)
BEGIN
    StepTimeLength := RunParams.Room.EstimatedMeanFreePath /
        RunParams.Room.SpeedOfSound;
    MaxNoSteps := TRUNC( RunParams.CTrace.MaxPathDuration * 0.001/
        StepTimeLength) + 1;
END; (* proc calcsteptimelength *)

```

```

PROCEDURE CreateDiffEnSteps;
(* puts diffuse refls into steps for use in markoff unit *)

```

```

VAR DiffRefIData : DiffEnergyRec; (* to read from diffenfile *)
    StepStartTime, StepEndTime : SINGLE;
    StepEnArr : FreqCoefArr;
    StepNo : INTEGER;
    StrStepNo : STRING [ 4];

```

```

BEGIN
    IF DiffEnFileOpened ( DiffEnF, DiffEnFName) THEN
        BEGIN
            IF FMade ( DiffEnSteppedF, DiffEnSteppedFName) THEN
                BEGIN
                    CalcStepTimeLength;
                    StepEndTime := 0.0;
                    STR ( MaxNoSteps, StrMaxNoSteps);
                    FOR StepNo := 1 TO MaxNoSteps DO
                        BEGIN
                            STR ( StepNo, StrStepNo);
                            gw (20,21,80+Yellow, 'Placing diffuse reflections into step '
                                +StrStepNo+' of '+StrMaxNoSteps);
                            FOR i := 1 TO MaxNoWalls DO (* initialise stepenarr *)
                                FOR Band := 1 TO NFreqBands DO
                                    StepEnArr [ Band, i] := 0;
                            StepStartTime := StepEndTime;
                            StepEndTime := StepStartTime + StepTimeLength;
                            WHILE NOT EOF ( DiffEnF) DO
                                (* loops through entire file for each step *)
                                BEGIN
                                    READ ( DiffEnF, DiffRefIData);

```

```

IF ( DiffRefIData.ReflTime >= StepStartTime) AND
    ( DiffRefIData.ReflTime < StepEndTime) THEN
BEGIN
    FOR Band := 1 TO NFreqBands DO
    BEGIN
        StepEnArr [ Band, DiffRefIData.SurfaceNo] :=
            StepEnArr [ Band, DiffRefIData.SurfaceNo] +
            DiffRefIData.DiffEnergy [ Band];
        END; (* for band *)
    END; (* if *)
    END; (* while loop *)
    (* next write all bands (1 band per line) of step to diffensteppedf *)
    FOR Band := 1 TO NFreqBands DO
        WRITE ( DiffEnSteppedF, StepEnArr [ Band]);
        RESET ( DiffEnF);
    END; (* for stepno *)
    CLOSE ( DiffEnSteppedF);
END
ELSE
BEGIN
    WRITELN ( 'Unable to create diffenstep file in proc CreateDiffEnSteps. ');
    WRITELN;
END;
CLOSE ( DiffEnF);
END
ELSE
BEGIN
    WRITELN ( 'Unable to open diffen file in proc CreateDiffEnSteps. ');
    WRITELN;
END; (* if diffenfilecreated *)
END; (* proc creatediffensteps *)

```

```

PROCEDURE CalcDiffuseRefls;
(* calc diffusion from a reflection and adds energy to *)
(* appropriate wall and step in diffuse decay      *)

```

```

VAR OnePathLength : SINGLE; (* path length between 2 refls *)
    SumOfPrevLengths : SINGLE;
    LastRayNum : INTEGER;
    SRayNum, StrRaysUsed : STRING[ 6];

```

```

FUNCTION DiffEnIsSignificant( D_En : FreqArr ) : BOOLEAN;
VAR MaxDVal : DOUBLE;
BEGIN
    MaxDVal := 0;
    FOR Band := 1 TO NFreqBands DO
        IF (D_En[ Band] > MaxDVal) THEN MaxDVal := D_En[ Band];
    IF (MaxDVal < 0.0000000001) THEN
        DiffEnIsSignificant := FALSE
    ELSE
        DiffEnIsSignificant := TRUE;
    END; (* function diffenissignificant *)

```

```

PROCEDURE CreateDMF;
(* creates dmf array *)
(* giving easy reference to diff coefs for each surface *)
(* each element in the array is the sfreqarr coefs for a surface *)
TYPE DiffLibRec = RECORD (* used to read data from diffmat.lib *)
    MatRef : LONGINT;
    MatName : STRING[ 100];
    DiffCoef : SFreqArr;
END;
VAR DiffLibData : DiffLibRec;
    Count1 : INTEGER;
BEGIN (* proc createDMF *)
    IF MatFileOpened( MatF, FileName+FileExtensions[MAT]) THEN
    BEGIN
        IF ReadFileOpened( DiffLibF, DiffMatLibFName) THEN
        BEGIN
            READ ( MatF, Material);
            FOR Count1 := 1 TO RunParams.Room.WallsInRoom DO
            BEGIN
                RESET ( DiffLibF);
                i := 0;
                WHILE NOT ( EOF( DiffLibF)) DO
                (* looks through all difflibf for each count1 *)
                BEGIN
                    INC ( i);
                    READLN ( DiffLibF, DiffLibData.MatRef, DiffLibData.MatName);
                    FOR Band := 1 TO NFreqBands DO
                        READ ( DiffLibF, DiffLibData.DiffCoef [ Band]);
                    READLN ( DiffLibF);
                    IF DiffLibData.MatRef = Material.SurfMatIndexArr[ Count1].MatRef
THEN
                        BEGIN
                            DMFarr[ Count1] := DiffLibData.DiffCoef;
                            END; (* if difflibdata.matref... *)
                        END; (* while not(eof) *)
                    END; (* for count1 *)
                    CLOSE ( DiffLibF);
                END
            ELSE
            BEGIN
                WRITELN ( 'Unable to open diffmat.lib in proc. CreateDMF. ');
                END; (* if readfileopened *)
                CLOSE ( MatF);
            END
            ELSE
            BEGIN
                WRITELN ( 'Unable to open MAT file in proc. CreateDMF. ');
                END; (* if matfileopened *)
            END; (* proc createdmf *)
        END
    END
    PROCEDURE CreateAMF;
(* creates amf array *)
(* giving easy reference to abs coefs for each surface *)
(* each element in the array is the sfreqarr coefs for a surface *)

```

```

(* same format as dmf array *)
BEGIN (* proc createamf *)
  IF MatFileOpened( MatF, FileName+FileExtensions[MAT]) THEN
  BEGIN
    READ ( MatF, Material);
    FOR i := 1 TO RunParams.Room.WallsInRoom DO
    BEGIN
      AMFArr [ i ] :=
        Material.AbsCoeffArr[ Material.SurfMatIndexArr[ i].Index];
    END; (* for i *)
    CLOSE ( MatF);
  END
  ELSE
  BEGIN
    WRITELN ( 'Unable to open MAT file in proc. CreateAMF. ');
  END; (* if matfileopened *)
END; (* proc createamf *)

PROCEDURE InitRayEnergy;
VAR SourceRefLevel : SFreqArr; (* these are defined and used in *)
    SourceRefDistance : REAL; (* response.pas but can't access *)
    SourceGain : DOUBLE; (* them. *)
    SourceStrength : FreqArr;
BEGIN
  SourceRefDistance := 10.0; (* these values lead to a strength *)
  SourceGain := 1.0; (* of 1 or 0dB at 10m *)
  FOR Band := 1 TO NFreqBands DO
  BEGIN
    SourceRefLevel [ Band ] := 0.01;
    SourceStrength [ Band ] := SourceRefLevel [ Band ] *
      SQR( SourceRefDistance ) * SourceGain;
    RayEn [ Band ] := SourceStrength [ Band ]; (* /
RunParams.CTrace.RaysUsed; *)
  END; (* for loop *)
END; (* proc initrayenergy *)

PROCEDURE CalcNewRayEn ( OPLength : SINGLE);
VAR AirAbs : SFreqArr;
    WallAbs : SFreqArr;
BEGIN
  FOR Band := 1 TO NFreqBands DO
  BEGIN
    AirAbs [ Band ] :=
      Pow ( 10.0, RunParams.Room.AirAttenuation[ Band ] * OPLength);
    (* distance attenuation is not required due to spread of finite number of rays
*)
    RayEnWithAir [ Band ] := RayEn[ Band ] * AirAbs[ Band ];
    WallAbs [ Band ] := AMFArr [ Refl.EndSurface, Band ] * RayEnWithAir [
Band];
    DiffEn [ Band ] := DMFArr [ Refl.EndSurface, Band ] *
      ( 1 - AMFArr [ Refl.EndSurface, Band ]) * RayEnWithAir [ Band ];
    RayEn[ Band ] := RayEnWithAir[ Band ] - WallAbs[ Band ] - DiffEn[ Band ];
    IF ( RayEn[ Band ] <= 0 ) THEN RayEn[ Band ] := 0;
  END;

```

```

END; (* proc calcnewrayen *)

PROCEDURE WriteToDiffEnFile;
(* writes refl time, wall and diffuse energy *)
VAR ReflDiffData : DiffEnergyRec; (* to write to diffenfile *)
BEGIN
  ReflDiffData.ReflTime := Refl.PathToEnd /
RunParams.Room.SpeedOfSound;
  ReflDiffData.SurfaceNo := Refl.EndSurface;
  ReflDiffData.DiffEnergy := DiffEn;
  WRITE ( DiffEnF, ReflDiffData);
END; (* proc writetodiffenfile *)

BEGIN (* proc calcdiffuserefls *)
IF HisFileOpened ( HisF, FileName+FileExtensions[HIS]) THEN
BEGIN
  CreateDMF;
  CreateAMF;
  IF DiffEnFileCreated ( DiffEnF, DiffEnFName) THEN
  BEGIN
    Refl.RayNum := 0;
    LastRayNum := Refl.RayNum;
    i := 0;
    REPEAT
      READ ( HisF, Refl); (* reads one refl of ray *)
      INC( i);
      STR( Refl.RayNum, SRayNum);
      STR( RunParams.CTrace.RaysUsed, StrRaysUsed);
      gw (20,21,80+Yellow, 'Calc Diff Refls:Ray '+SRayNum+' of
'+StrRaysUsed);
      IF Refl.RayNum <> LastRayNum THEN
      BEGIN
        i := 1;
        InitRayEnergy;
        SumOfPrevLengths := 0.0;
        END; (* if *)
        OnePathLength := Refl.PathToEnd - SumOfPrevLengths; (* length
between refls *)
        STR(OnePathLength, TempStr);
        CalcNewRayEn ( OnePathLength); (* energy in new refl *)
        IF (( DiskFree( 0) > 10000) AND ( DiffEnIsSignificant( DiffEn))) THEN
          WriteToDiffEnFile;
          SumOfPrevLengths := SumOfPrevLengths + OnePathLength;
          LastRayNum := Refl.RayNum;
        UNTIL EOF( HisF);
        CLOSE ( DiffEnF);
      END
    ELSE
      BEGIN
        WRITELN ( 'Unable to create diffen file in proc CalcDiffuseRefls. ');
        WRITELN;
      END; (* if diffenfilecreated *)
      CLOSE ( HisF);
    END
  END

```

```

ELSE
BEGIN
  WRITELN ('Unable to open his file in proc CalcDiffuseRefs. ');
  WRITELN;
  END; (* if hisfileopened *)
END; (* procedure calcdiffuserefls *)

```

```

PROCEDURE MsgToScreen ( MsgNo : INTEGER);
(* puts calcs in progress message on screen *)
BEGIN
  CASE MsgNo OF
    1: gw (20,20,80+Yellow,'Markov calculations in progress. ');
    2: gw (20,21,80+Yellow,'CreateReflCoefArr ');
    3: gw (20,21,80+Yellow,'MultAP ');
    4: gw (20,21,80+Yellow,'CalcDiffuseRefs ');
    5: gw (20,21,80+Yellow,'CreateDiffEnSteps ');
    6: gw (20,21,80+Yellow,'CreateDiffImpulse ');
    7: gw (20,21,80+Yellow,'SumWallEnergies ');
    8: gw (20,21,80+Yellow,'[CalcEnergiesForParameters ');
    9: gw (20,21,80+Yellow,'[| | | | | | | | ] ');
    3: gw (20,21,80+Yellow,'[| | ] ');
    4: gw (20,21,80+Yellow,'[| | | ] ');
    5: gw (20,21,80+Yellow,'[| | | | ] ');
    6: gw (20,21,80+Yellow,'[| | | | | ] ');
    7: gw (20,21,80+Yellow,'[| | | | | | ] ');
    8: gw (20,21,80+Yellow,'[| | | | | | | ] ');
    9: gw (20,21,80+Yellow,'[| | | | | | | | ] ');
  END; (* case *)
END; (* proc messagetoscreen *)

```

```

PROCEDURE CalcTransitionProb;
(* calcs prob of energy from one wall going to other walls *)
(* calculates probabilities according to the solid angles *)
(* stored in filename.ang *)

```

```

VAR Count1, Count2 : INTEGER;
  Omega : CoefArray; (* surface to surface solid angles *)
  SumOfOmegas : SINGLE;
  SToSFile : CoefFile;
  SToSFName : STRING;

```

```

BEGIN
  SToSFName := FileName+'.ang';
  IF FOpened ( SToSFile, SToSFName) THEN
  BEGIN
    IF FMade ( TPF, TransProbFName) THEN
    BEGIN
      FOR Count2 := 1 TO MaxNoWalls DO
        TransProbData [ Count2] := 0; (* initialize *)
      FOR Count2 := 1 TO RunParams.Room.WallsInRoom DO
      BEGIN
        SumOfOmegas := 0;

```

```

READ ( SToSFile, Omega);
FOR Count1 := 1 TO RunParams.Room.WallsInRoom DO
  SumOfOmegas := SumOfOmegas + Omega[ Count1];
IF (SumOfOmegas < TINY) THEN SumOfOmegas := HUGE;
  (* prevents division by zero *)
FOR Count1 := 1 TO RunParams.Room.WallsInRoom DO
BEGIN
  TransProbData[ Count1] := Omega[ Count1] / SumOfOmegas;
  (* this actually gives the transpose of the *)
  (* matrix in Gerlach's paper but is easier to *)
  (* use. row 1 here therefore corresponds to *)
  (* column 1 in Gerlach's matrix. *)
  END; (* for count1 *)
  WRITE( TPF, TransProbData);
  END; (* for count2 *)
CLOSE( TPF);
END
ELSE
BEGIN
  WRITELN ( 'Cannot open file to write transition probs. ');
  READLN;
  END; (* if fmade *)
CLOSE ( SToSFile);
END; (* if fopened *)
END; (* proc calctransitionprob *)

```

```

PROCEDURE CreateRefIcoefArr;
(* creates diagonal reflection coefficient matrix for each freq *)
(* these matrices are stored to a typed file. They are created *)
(* by successively sending one dimensional arrays as rows in the*)
(* typed file. The typed file therefore contains 6 two *)
(* dimensional matrices - one for each frequency. These follow *)
(* on sequentially, so the 125Hz matrix is followed by the 250Hz*)
(* matrix etc. *)

```

```

VAR Count1, Count2 : INTEGER;

```

```

BEGIN
  IF FMade ( CF, RefIcoefFName) THEN
  BEGIN
    FOR Band := 1 TO NFreqBands DO
    BEGIN
      FOR Count2 := 1 TO MaxNoWalls DO
      (* count2 counts rows of array in file *)
      BEGIN
        IF Count2 <= RunParams.Room.WallsInRoom THEN
        (* zero terms above actual no. of walls in room *)
        BEGIN
          FOR Count1 := 1 TO MaxNoWalls DO
          BEGIN
            IF ( Count1 <> Count2) OR
              ( Count1 > RunParams.Room.WallsInRoom) THEN
            BEGIN

```

```

        CData[ Count1] := 0;
    END
    ELSE
    BEGIN
        CData[ Count1] :=
            1 - PtrAbsCoeff^[ PtrWallMaterial^[ Count1], Band];
    END; (* end of if statement *)
    END; (* for count1 *)
END
ELSE
BEGIN
    (* set remaining matrix terms to zero *)
    FOR Count1 := 1 TO MaxNoWalls DO
        CData[ Count1] := 0;
    END; (* if count2 <= no of walls in room *)
    WRITE( CF, CData);
    (* writes one line of data to file *)
    END; (* for count2 *)
    END; (* for band *)
    CLOSE ( CF);
END
ELSE
BEGIN
    WRITELN ( 'Cannot open file to write refl. coefficients. ');
    READLN;
    END; (* if FMade *)
END; (* proc createreflcoefarr *)

```

```

PROCEDURE MultAP;
(* multiplies refl. coef matrices and trans prob matrix *)
(* resulting in product matrix *)
(* trans prob matrices are transpose of those by Gerlach *)
(* so rows are read instead of columns. *)

```

```

VAR Count1, Count2, Count3, Band : INTEGER;
    Sum1 : SINGLE;

```

```

BEGIN
    IF FOpened( CF, ReflCoefFName) THEN
    BEGIN
        IF FOpened( TPF, TransProbFName) THEN
        BEGIN
            IF FMade( PF, ProdMatFName) THEN
            BEGIN
                FOR Band := 1 TO NFreqBands DO
                BEGIN
                    FOR Count1 := 1 TO MaxNoWalls DO
                    (* steps through rows of refl coef matrix *)
                    BEGIN
                        IF NOT EOF ( CF) THEN
                        BEGIN
                            READ ( CF, CData);
                            (* reads full row from refl coef into CData *)

```

```

FOR Count2 := 1 TO MaxNoWalls DO
BEGIN
  IF NOT EOF ( TPF) THEN
  BEGIN
    READ ( TPF, TransProbData);
    (* reads full row from trans prob *)
    (* this would be a column in Gerlach's *)
    (* next calc one value of product matrix for each count1 *)
    Sum1 := 0;
    FOR Count3 := 1 TO MaxNoWalls DO
    BEGIN
      Sum1 := Sum1 + ( CData[ Count3] * TransProbData[ Count3]);
    END; (* for count3 *)
    ProdData [ Count2] := Sum1;
    END; (* if not eof(tpf) *)
    END; (* for count2 *)
    (* now write row to product file *)
    WRITE ( PF, ProdData);
    RESET ( TPF);
    END; (* if not eof(cf) *)
    END; (* for count1 *)
    END; (* for band *)
    CLOSE ( PF);
  END
  ELSE
  BEGIN
    WRITELN ( 'Cannot open prod mat file in procedure MultAP. ');
    READLN;
    END; (* if fmade pf *)
    CLOSE ( TPF);
  END
  ELSE
  BEGIN
    WRITELN ( 'Cannot open trans prob file in procedure MultAP. ');
    READLN;
    END; (* if fopened tpf *)
    CLOSE ( CF);
  END
  ELSE
  BEGIN
    WRITELN ( 'Cannot open refl coef file in procedure MultAP. ');
    READLN;
    END; (* if fopened cf *)
  END; (* proc multap *)

```

```

PROCEDURE TransposeMatrix( VAR MF : CoefFile);
(* transposes matrix and writes to file      *)
(* is used for squaring and multiplying matrices *)
(* mf is used so any matrix file can be transposed *)

```

```

VAR Count1, Count2 : INTEGER;
RowOfData : CoefArray; (* this is a row in the original matrix *)
ColOfData : CoefArray; (* this is a column in the original matrix *)

```

```

BEGIN
  IF FMade( TF, TransposeMatFName) THEN
    BEGIN
      FOR Count2 := 1 TO MaxNoWalls DO
        (* steps through columns of source matrix *)
        BEGIN
          FOR Count1 := 1 TO MaxNoWalls DO
            (* steps through rows of source matrix *)
            BEGIN
              READ ( MF, RowOfData);
              ColOfData [ Count1] := RowOfData [ Count2];
            END; (* for count1 *)
            WRITE ( TF, ColOfData);
            RESET ( MF);
          END; (* for count2 *)
        CLOSE ( TF);
      END
    ELSE
      BEGIN
        WRITELN ( 'Cannot create transpose file in procedure TransposeMatrix');
        READLN;
      END; (* if fmade tf *)
    END; (* proc transposematrix *)

```

```

PROCEDURE CreateSingleBandProdMatFile ( FreqBandNo : INTEGER);
(* opens prodmatfile and reads a product matrix *)
(* for a particular frequency *)

```

```

VAR Count1, FBand : INTEGER;
    RowOfProdData : CoefArray;

```

```

BEGIN
  IF FOpened( PF, ProdMatFName) THEN
    BEGIN
      IF FMade( SBPF, SingleBandProdMatFName) THEN
        BEGIN
          FOR FBand := 1 TO NFreqBands DO
            BEGIN
              FOR Count1 := 1 TO MaxNoWalls DO
                (* steps through rows of prod mat fname *)
                BEGIN
                  READ ( PF, RowOfProdData);
                  IF ( FBand = FreqBandNo) THEN
                    WRITE ( SBPF, RowOfProdData);
                  END; (* for count1 *)
                END; (* for fband *)
              CLOSE ( SBPF);
            END
          ELSE
            BEGIN
              WRITELN ( 'Cannot create single band prod file, proc CreateSingleBa...');
            END
          END
        END
      ELSE
        BEGIN
          WRITELN ( 'Cannot create single band prod file, proc CreateSingleBa...');
        END
      END
    END
  ELSE
    BEGIN
      WRITELN ( 'Cannot create single band prod file, proc CreateSingleBa...');
    END
  END

```

```

    READLN;
    END; (* if fmade xf *)
    CLOSE ( PF);
END
ELSE
BEGIN
    WRITELN ( 'Cannot open prod mat file in proc CreateSingleBa...');
    READLN;
    END; (* if fopened pf *)
END; (* procedure CreateSingleBandProdMatFile *)

```

```

PROCEDURE InitReceiver2;

```

```

var dx, dy, dz    : Double;
    CosE, SinE, CosA, SinA, CosR, SinR    : Double;

begin
with RunParams do
begin
    dx := Source.RelSourcePosition.x - Response.RelReceiverPosition.x;
    dy := Source.RelSourcePosition.y - Response.RelReceiverPosition.y;
    dz := Source.RelSourcePosition.z - Response.RelReceiverPosition.z;
    Response.ReceiverAzimuth := ArcTan2(dy, dx);
    Response.ReceiverElevation := ArcTan2(dz, Sqrt(Sqr(dx)+Sqr(dy)));
    CosA := Cos(Response.ReceiverAzimuth);
    SinA := Sin(Response.ReceiverAzimuth);
    CosE := Cos(Response.ReceiverElevation);
    SinE := Sin(Response.ReceiverElevation);
    CosR := 1; { no Rotation }
    SinR := 0;
end;
RunParams.Room.SRDistance := Sqrt( Sqr(dx) + Sqr(dy) + Sqr(dz));
{ coordinate transformation from room coords to receiver coords }
ReceiverTransform2[1][1] := CosE * CosA;
ReceiverTransform2[1][2] := CosE * SinA;
ReceiverTransform2[1][3] := SinE;
ReceiverTransform2[2][1] := -(CosR * SinA) - (SinR * SinE * CosA);
ReceiverTransform2[2][2] := (CosR * CosA) - (SinR * SinE * SinA);
ReceiverTransform2[2][3] := CosE * SinR;
ReceiverTransform2[3][1] := (SinR * SinA) - (CosR * SinE * CosA);
ReceiverTransform2[3][2] := -(SinR * CosA) - (CosR * SinE * SinA);
ReceiverTransform2[3][3] := CosR * CosE;
end;

```

```

PROCEDURE CoordTransform2(PSys1: Pt3D; VAR PSys2: Pt3D; TransMat:
Mat3D);

```

```

begin
    PSys2.x := TransMat[1][1] * PSys1.x
        + TransMat[1][2] * PSys1.y
        + TransMat[1][3] * PSys1.z;
    PSys2.y := TransMat[2][1] * PSys1.x

```

```

    + TransMat[2][2] * PSys1.y
    + TransMat[2][3] * PSys1.z;
PSys2.z := TransMat[3][1] * PSys1.x
    + TransMat[3][2] * PSys1.y
    + TransMat[3][3] * PSys1.z;
end; { CoordTransform }

```

```

PROCEDURE XYZToAzimuthElevation2(Pt: Pt3D; VAR Az, El: Single);

```

```

begin
  Az := ArcTan2(Pt.y, Pt.x);
  El := ArcTan2(Pt.z, Sqrt(Sqr(Pt.x) + Sqr(Pt.y)));
  while El > PihByTwo do
    El := El - PihByTwo;
  while El < -PihByTwo do
    El := El + PihByTwo;
end; { XYZToAzimuthElevation }

```

```

PROCEDURE CalcDirectSoundTime;

```

```

VAR Dx, Dy, Dz : SINGLE;

```

```

BEGIN

```

```

  WITH RunParams DO

```

```

    BEGIN

```

```

      Dx := Source.RelSourcePosition.x - Response.RelReceiverPosition.x;

```

```

      Dy := Source.RelSourcePosition.y - Response.RelReceiverPosition.y;

```

```

      Dz := Source.RelSourcePosition.z - Response.RelReceiverPosition.z;

```

```

    END;

```

```

      DirectSoundTime := Sqrt( Sqr(Dx) + Sqr(Dy) + Sqr(Dz) ) /

```

```

      RunParams.Room.SpeedOfSound;

```

```

    END;

```

```

PROCEDURE SumWallEnergies;

```

```

VAR RowOfDEData : CoefArray;

```

```

  SumOfRow, AirAbs : SFreqArr;

```

```

  StepCount, WallNo, NoOfRows, FirstMrkoffStep : INTEGER;

```

```

  FlightToRecTime, RecArrivTime : SINGLE;

```

```

  SCStr : STRING;

```

```

  RoomSurfRecDir : ^PtOfSurfArray; (* surface to receiver directions in room
coordinates *)

```

```

FUNCTION FindMrkoffStp ( Time1 : SINGLE ): INTEGER;

```

```

(* finds mrkoffstp containing time1 *)

```

```

VAR j1 : INTEGER;

```

```

  StrtTim, StpTim : SINGLE;

```

```

BEGIN

```

```

  FOR j1 := 1 TO MaxNoSteps DO

```

```

    BEGIN

```

```

      StrtTim := (j1 - 1) * StepTimeLength;

```

```

      StpTim := StrtTim + StepTimeLength;

```

```

    IF (Time1 >= StrtTim) AND (Time1 < StpTim) THEN
    BEGIN
        FindMrkoffStp := j1;
        EXIT;
    END; (* if *)
    END; (* for j1 *)
END; (* func findmrkoffstp *)

PROCEDURE CalcSurfAngleFactors;
(* calcs angle factors for fig8 response *)

VAR SurfRecAz, SurfRecEl : CoefArray;
    RecSurfRecDir : ^PtOfSurfArray; (* surface to receiver directions with
receiver as origin *)
    SurfNo : INTEGER;

BEGIN
    GETMEM ( RecSurfRecDir, SizeOf( PtOfSurfArray));
    FOR SurfNo := 1 TO RunParams.Room.WallsInRoom DO
    BEGIN
        (* incoming to receiver for use in proc coordtransform *)
        RoomSurfRecDir^[SurfNo].x := AvPtOfSurf[SurfNo].x -
RunParams.Response.RelReceiverPosition.x;
        RoomSurfRecDir^[SurfNo].y := AvPtOfSurf[SurfNo].y -
RunParams.Response.RelReceiverPosition.y;
        RoomSurfRecDir^[SurfNo].z := AvPtOfSurf[SurfNo].z -
RunParams.Response.RelReceiverPosition.z;
        InitReceiver2;
        CoordTransform2 ( RoomSurfRecDir^[SurfNo], RecSurfRecDir^[SurfNo],
ReceiverTransform2);
        XYZToAzimuthElevation2 ( RecSurfRecDir^[SurfNo], SurfRecAz[SurfNo],
SurfRecEl[SurfNo]);
        AngleFact [ SurfNo] := SQR( Sin( SurfRecAz[SurfNo]) * Cos(
SurfRecEl[SurfNo]));
        END; (* for surfno *)
        FREEMEM ( RecSurfRecDir, SizeOf( PtOfSurfArray));
    END; (* proc calcsurfanglefactors *)

PROCEDURE CalcCosThetas;
(* calcs cos of angle from surface av pts to receiver for Lambert diffusion *)
VAR SurfNo : INTEGER;
    DirVec : Pt3D;
    MagOfVec : SINGLE;
    SNStr : STRING;
BEGIN
    FOR SurfNo := 1 TO RunParams.Room.WallsInRoom DO
    BEGIN
        STR(SurfNo, SNStr);
        MagOfVec := SQRT( SQR(RoomSurfRecDir^[SurfNo].x)
+ SQR(RoomSurfRecDir^[SurfNo].y) +
SQR(RoomSurfRecDir^[SurfNo].z));
        DirVec.x := RoomSurfRecDir^[SurfNo].x / MagOfVec;
        DirVec.y := RoomSurfRecDir^[SurfNo].y / MagOfVec;

```

```

DirVec.z := RoomSurfRecDir^[SurfNo].z / MagOfVec;
CosTheta [ SurfNo] := PtrWallNorms^[ SurfNo, 1] * DirVec.x
+ PtrWallNorms^[ SurfNo, 2] * DirVec.y
+ PtrWallNorms^[ SurfNo, 3] * DirVec.z;
END; (* for surfno *)
END; (* proc calcceostheta *)

PROCEDURE PutMrkoffEnInHistogramFormat;
(* spreads the energy from mrkoff steps over relevant histogram buckets *)
VAR FirstHistBucket, EndHistBucket : INTEGER;
    NoOfBuckets : SINGLE;

    FUNCTION NewStepNo ( ArrivTim : SINGLE) : INTEGER;
    (* calcs step number in ptrmrkoffenhistogram *)
    (* this is bucket number *)
    VAR StpNo : INTEGER;
    BEGIN
    FOR StpNo := 0 TO ResponseHistogramLength DO
    BEGIN
    IF ArrivTim < ( ( StpNo +1) * RunParams.Response.HistogramTimeStep)
THEN
    BEGIN
    NewStepNo := StpNo; (* should jump out of function here *)
    EXIT;
    END; (* if *)
    END; (* for *)
    END; (* function newstepno *)

PROCEDURE SpreadMrkoffEnergy;
(* divides energy over noofbuckets at receiver *)
(* also does fig of 8 version *)
VAR BuckCount : INTEGER;
    BEGIN
gw (20,21,80+Yellow,'SpreadMrkoffEnergy 1 ');
    NoOfBuckets := INT ( EndHistBucket - FirstHistBucket + 1);
    FOR BuckCount := FirstHistBucket TO EndHistBucket DO
    BEGIN
    IF BuckCount <= ResponseHistogramLength THEN
    BEGIN
    PtrMrkoffEnHistogram^[ BuckCount, Band] :=
    PtrMrkoffEnHistogram^[ BuckCount, Band]
    + AirAbs[ Band] * RowOfDEData[ WallNo]
    * SurfToRecSolidAngle[ WallNo]
    / ( 4 * Pih * PtrWallArea^[ WallNo] * NoOfBuckets);
    IF ( ( BuckCount * RunParams.Response.HistogramTimeStep)
< ( DirectSoundTime + 0.08)) THEN
    BEGIN
    PtrFig8MrkoffEnHis^[ BuckCount, Band] :=
    PtrFig8MrkoffEnHis^[ BuckCount, Band]
    + AngleFact[ WallNo] * AirAbs[ Band] * RowOfDEData[ WallNo]
    * SurfToRecSolidAngle[ WallNo]
    / ( 4 * Pih * PtrWallArea^[ WallNo] * NoOfBuckets);
    END; (* if buckcount * runparams.... *)
    END; (* if buckcount <= response... *)

```

```

    END; (* for buckcount *)
    END; (* proc spreadmrkoffenergy *)

BEGIN (* proc putmrkoffeninhistogramformat *)
  IF (StepCount = FirstMrkoffStep) THEN
    (* spread energy from first bucket after direct sound *)
    (* to bucket nearest end of mrkoff timestep *)
    BEGIN
      FirstHistBucket := 1 + TRUNC ( DirectSoundTime /
                                     RunParams.Response.HistogramTimeStep);
      EndHistBucket := NewStepNo ( ( StepCount * StepTimeLength)
                                   + FlightToRecTime);

      SpreadMrkoffEnergy;
    END
  ELSE IF (StepCount > FirstMrkoffStep) THEN
    BEGIN
      FirstHistBucket := NewStepNo ( ((StepCount - 1) * StepTimeLength)
                                     + FlightToRecTime) + 1;
      EndHistBucket := NewStepNo ( ( StepCount * StepTimeLength)
                                   + FlightToRecTime);

      SpreadMrkoffEnergy;
    END
  ELSE
    BEGIN
      WRITELN ( 'Error in proc PutMrkOffEnInHistogramFormat');
      READLN;
    END; (* if *)
  END; (* proc putmrkoffeninhistogramformat *)

BEGIN (* procedure sumwallenergies *)
  IF FOpened ( DEF, DiffEnergyMatFName) THEN
    BEGIN
      IF EnergyDecayFileMade ( DImpF, DiffEnergyDecayFName) THEN
        BEGIN
          CalcAvPtsOfSurfaces;
          GETMEM ( RoomSurfRecDir, SizeOf( PtOfSurfArray));
          CalcSurfAngleFactors;
          CalcCosThetas;
          FREEMEM ( RoomSurfRecDir, SizeOf( PtOfSurfArray));
          FOR i := 0 TO ResponseHistogramLength DO (* initialise histograms *)
            BEGIN
              FOR Band := 1 TO NFreqBands DO
                BEGIN
                  PtrMrkoffEnHistogram^[ i, Band] := 0.0;
                  PtrFig8MrkoffEnHis^[ i, Band] := 0.0;
                END; (* for *)
              END; (* for i *)
              FirstMrkoffStep := FindMrkoffStp ( DirectSoundTime);
              FOR StepCount := 1 TO MaxNoSteps DO
                BEGIN
                  STR( StepCount, SCStr);
                  gw (20,21,80+Yellow,'SumWallEnergies: Step '+SCStr+' of
'+StrMaxNoSteps);
                  FOR Band := 1 TO NFreqBands DO

```

```

BEGIN
  READ ( DEF, RowOfDEData);
  IF (StepCount >= FirstMrkoffStep) THEN
    (* ensures mrkoff is not used before direct sound arrives *)
    BEGIN
      FOR WallNo := 1 TO RunParams.Room.WallsInRoom DO
        BEGIN
          FlightToRecTime := DistToRecArr[ WallNo] /
            RunParams.Room.SpeedOfSound;
          (* energy will now be put in different time step      *)
          (* according to time of arrival at the receiver      *)
          (* this stepped decay is the same format as that    *)
          (* in response.pas. This means there are now 2      *)
          (* different time step systems running, one        *)
          (* on the walls running the markoff chain, ie stepcount, *)
          (* and the other at the receiver - i or newstepno.  *)
          AirAbs [ Band] := Pow ( 10.0,
            RunParams.Room.AirAttenuation[ Band] * DistToRecArr[
WallNo]);
          PutMrkoffEnInHistogramFormat;
          gw (20,21,80+Yellow,'SumWallEnergies: Step '+SCStr+' E of
'+StrMaxNoSteps);
          END; (* if stepcount >= firstmrkoffstep *)
          END; (* for wallno *)
          END; (* for band *)
          END; (* for stepcount *)
          FOR i := 0 TO ResponseHistogramLength DO
            WRITE ( DImpF, PtrMrkoffEnHistogram^[ i]);
          CLOSE ( DImpF);
        END
      ELSE
        BEGIN
          WRITELN ( 'Cannot create DImpF in proc SumWallEnergies');
          READLN;
          END; (* if fopened dimpf *)
          CLOSE ( DEF);
        END
      ELSE
        BEGIN
          WRITELN ( 'Cannot open diffenergy mat file in proc SumWallEnergies');
          GW (20,21,80+Yellow,'Cannot open diffenergy mat file in proc
SumWallEnergies');
          READLN;
          END; (* if fopened def *)
        END; (* procedure sumwallenergies *)

PROCEDURE CreateDiffImpulse;
(* multiplies prodmat to the power nsteps      *)
(* writes each mult mat to diffusehismatfname *)

VAR NSteps : INTEGER;
    StrNSteps : STRING[ 4];
    EnOldPlusStepDiffEn : CoefArray;

```

EnNew, EnOld, StepDiffEn : FreqCoefArr;

```
PROCEDURE CalcEnNew ( XFName : FileNameString; EnCoefArr : CoefArray);  
(* multiplies matrix by enold coefarray *)  
(* this gives the energy at step n, this is written to *)  
(* def file opened in calling routine *)
```

```
VAR APNF : CoefFile;  
MEPCount1, Count3 : INTEGER;  
Sum1 : SINGLE;  
RowOfMultData, RowOfNData : CoefArray;  
(* rowofndata is energy at step n *)
```

```
BEGIN (* calcennew *)  
IF FOpened( APNF, XFName) THEN  
BEGIN  
TransposeMatrix( APNF);  
CLOSE ( APNF);  
END  
ELSE  
BEGIN  
WRITELN ( 'Cannot open ', XFName, ' in proc MultByStartEnergy');  
READLN;  
END; (* if fopened multf *)  
(* re-open tf for calculation *)  
IF FOpened( TF, TransposeMatFName) THEN  
BEGIN  
FOR MEPCount1 := 1 TO RunParams.Room.WallsInRoom DO  
(* counts through rows of tf *)  
(* effectively columns of multf *)  
BEGIN  
IF NOT EOF ( TF) THEN  
BEGIN  
READ ( TF, RowOfMultData);  
Sum1 := 0;  
FOR Count3 := 1 TO RunParams.Room.WallsInRoom DO  
BEGIN  
Sum1 := Sum1 + ( EnCoefArr [ Count3]  
* RowOfMultData [ Count3]);  
END; (* for count3 *)  
RowOfNData [ MEPCount1 ] := Sum1;  
END; (* if not eof(tf) *)  
END; (* for mepcount1 *)  
(* now write row to diffenergy file *)  
WRITE ( DEF, RowOfNData);  
EnNew[ Band ] := RowOfNData;  
CLOSE ( TF);  
END  
ELSE  
BEGIN  
WRITELN ( 'Cannot open transpose file in proc MultByStartEnergy');  
READLN;  
END; (* if fopened tf *)
```

```

END; (* procedure CalcEnNew *)

BEGIN (* proc creatediffimpulse *)
  IF FMade ( DEF, DiffEnergyMatFName) THEN
    BEGIN
      IF FOpened ( DiffEnSteppedF, DiffEnSteppedFName) THEN
        BEGIN
          FOR Band := 1 TO NFreqBands DO
            FOR i := 1 TO MaxNoWalls DO
              EnNew [ Band, i] := 0.0;
            FOR NSteps := 1 TO MaxNoSteps DO
              BEGIN
                STR ( NSteps, StrNSteps);
                gw (20,21,80+Yellow,'CreateDiffImpulse Step '+StrNSteps+' of
'+StrMaxNoSteps+'
                ');
                FOR Band := 1 TO NFreqBands DO
                  BEGIN
                    READ ( DiffEnSteppedF, StepDiffEn [ Band]);
                    CreateSingleBandProdMatFile ( Band);
                    EnOld := EnNew;
                    FOR i := 1 TO RunParams.Room.WallsInRoom DO
                      EnOldPlusStepDiffEn [ i] := EnOld [ Band, i] + StepDiffEn [ Band, i];
                    CalcEnNew ( SingleBandProdMatFName, EnOldPlusStepDiffEn); (*
calcs and writes energy to def *)
                    END; (* for band *)
                  END; (* for nsteps *)
                CLOSE ( DiffEnSteppedF);
              END
            ELSE
              BEGIN
                WRITELN ( 'Cannot open diffenstepped file in proc CreateDiffImpulse');
                READLN;
                END; (* if fopened diffensteppedf *)
              CLOSE ( DEF);
            END
          ELSE
            BEGIN
              WRITELN ( 'Cannot open diffenergy file in proc CreateDiffImpulse');
              READLN;
            END; (* if fmade def *)
          END; (* procedure CreateDiffImpulse *)

```

```

PROCEDURE CalcDiffEnForParams;
(* calcs diff energies before and after 50ms & 80ms *)
VAR t : SINGLE;

```

```

PROCEDURE CalcFig8En;
VAR t : SINGLE;
BEGIN
  FOR Band := 1 TO NFreqBands DO
    MrkoffFig8En[Band] := 0;
  FOR i := 0 TO ResponseHistogramLength DO

```

```

BEGIN
  t := i * RunParams.Response.HistogramTimeStep
        - DirectSoundTime;
  FOR Band := 1 TO NFreqBands DO
  BEGIN
    IF (t >= 0.005) AND (t < 0.08) THEN
    BEGIN
      MrkoffFig8En[Band] := MrkoffFig8En[Band]
        + PtrFig8MrkoffEnHis^[ i, Band];
    END; (* if *)
  END; (* for band *)
END; (* for i *)
END; (* proc calcfig8en *)

BEGIN (* proc calcdiffenforparams *)
(* first initialise energies *)
FOR i := 0 TO ResponseHistogramLength DO
BEGIN
  FOR Band := 1 TO NFreqBands DO
  BEGIN
    MrkoffEnBefore50[ Band] := 0;
    MrkoffEnBefore80[ Band] := 0;
    MrkoffEnAfter80[ Band] := 0;
  END; (* for band *)
END; (* for i *)
(* now calc energies *)
FOR i := 0 TO ResponseHistogramLength DO
BEGIN
  t := i * RunParams.Response.HistogramTimeStep
        - DirectSoundTime;
  FOR Band := 1 TO NFreqBands DO
  BEGIN
    IF t >= 0 THEN
    BEGIN
      IF t < 0.08 THEN
      BEGIN
        IF t < 0.05 THEN
        BEGIN
          MrkoffEnBefore50[ Band] := MrkoffEnBefore50[ Band]
            + PtrMrkoffEnHistogram^[ i, Band];
        END; (* if t < 0.05 *)
          MrkoffEnBefore80[ Band] := MrkoffEnBefore80[ Band]
            + PtrMrkoffEnHistogram^[ i, Band];
        END
      ELSE
      BEGIN
        MrkoffEnAfter80[ Band] := MrkoffEnAfter80[ Band]
          + PtrMrkoffEnHistogram^[ i, Band];
        END; (* if t < 0.08 *)
      END; (* if t >= 0 *)
    END; (* for band *)
  END; (* for i *)
  CalcFig8En;
END; (* proc calcdiffenforparams *)

```

```

PROCEDURE RunMarkoff;
(* controlling procedure *)
BEGIN
  GetMem ( PtrMrkoffEnHistogram, SizeOf ( EnergyHistogram));
  GetMem ( PtrFig8MrkoffEnHis, SizeOf ( EnergyHistogram));
  MsgToScreen ( 1);
  CalcTransitionProb;
  MsgToScreen ( 2);
  CreateReflCoefArr;
  MsgToScreen ( 3);
  MultAP;
  MsgToScreen ( 4);
  CalcDiffuseRefls;
  MsgToScreen ( 5);
  CreateDiffEnSteps;
  MsgToScreen ( 6);
  CreateDiffImpulse;
  MsgToScreen ( 7);
  CalcDirectSoundTime;
  SumWallEnergies;
  MsgToScreen ( 8);
  CalcDiffEnForParams;
  FreeMem ( PtrFig8MrkoffEnHis, SizeOf ( EnergyHistogram));
  FreeMem ( PtrMrkoffEnHistogram, SizeOf ( EnergyHistogram));
  MsgToScreen ( 9);
  EndBeep;
END; (* procedure runmarkoff *)

END.

```